

DAMAGE DETECTION IN BEAM-LIKE STRUCTURES VIA COMBINED
GENETIC ALGORITHM AND NON-LINEAR OPTIMISATION

A THESIS SUBMITTED TO
THE GRADUATE SCHOOL OF NATURAL AND APPLIED SCIENCES
OF
MIDDLE EAST TECHNICAL UNIVERSITY

BY

SEYFULLAH AKTAŞOĞLU

IN PARTIAL FULFILLMENT OF THE REQUIREMENTS
FOR
THE DEGREE OF MASTER OF SCIENCE
IN
AEROSPACE ENGINEERING

FEBRUARY 2012

Approval of the thesis:

**DAMAGE DETECTION IN BEAM-LIKE STRUCTURES VIA COMBINED
GENETIC ALGORITHM AND NON-LINEAR OPTIMISATION**

Submitted to **SEYFULLAH AKTAŞOĞLU** in partial fulfillment of the requirements for the degree of **Master of Science in Aerospace Engineering, Middle East Technical University** by,

Prof. Dr. Canan ÖZGEN

Dean, Graduate School of **Natural and Applied Sciences**

Prof. Dr. Ozan TEKİNALP

Head of Department, **Aerospace Engineering**

Assist. Prof. Dr. Melin ŞAHİN

Supervisor, **Aerospace Engineering Dept., METU**

Examining Committee Members

Prof. Dr. Yavuz YAMAN

Aerospace Engineering Dept., METU

Assist. Prof. Dr. Melin ŞAHİN

Aerospace Engineering Dept., METU

Prof. Dr. Altan KAYRAN

Aerospace Engineering Dept., METU

Assist. Prof. Dr. Ercan GÜRSES

Aerospace Engineering Dept., METU

Assist. Prof. Dr. Ender CİĞEROĞLU

Mechanical Engineering Dept., METU

Date: 09/02/2012

I hereby declare that all information in this document has been obtained and presented in accordance with academic rules and ethical conduct. I also declare that, as required by these rules and conduct, I have fully cited and referenced all material and results that are not original to this work.

Name, Last name : Seyfullah Aktařođlu

Signature :

ABSTRACT

DAMAGE DETECTION IN BEAM-LIKE STRUCTURES VIA COMBINED GENETIC ALGORITHM AND NON-LINEAR OPTIMISATION

Aktaşođlu, Seyfullah

M.Sc., Department of Aerospace Engineering

Supervisor: Assist. Prof. Dr. Melin Şahin

February 2012, 141 Pages

In this study, a combined genetic algorithm and non-linear optimisation system is designed and used in the identification of structural damage of a cantilever isotropic beam regarding its location and severity. The vibration-based features, both natural frequencies (i.e. eigenvalues) and displacement mode shapes (i.e. eigenvectors) of the structure in the first two out of plane bending modes, are selected as damage features for various types of damage comprising saw-cut and impact. For this purpose, commercial finite element modelling (FEM) and analysis software Msc. Patran/Nastran[®] is used to obtain the aforementioned features from intact and damaged structures. Various damage scenarios are obtained regarding saw-cut type damage which is modelled as change in the element thicknesses and impact type damage which is modelled as a reduction of the elastic modulus of the elements in the finite element models. These models are generated by using both 1-D bar elements and 2-D shell type elements in Msc. Patran[®] and then normal mode analyses are performed in order to extract element stiffness and mass matrices by using Msc. Nastran[®]. Sensitivity matrices

are then created by changing the related properties (i.e. reduction in elastic modulus and thickness) of the individual elements via successive normal mode analyses. The obtained sensitivity matrices are used as coefficients of element stiffness and/or mass matrices to construct global stiffness and/or mass matrices respectively. Following this, the residual force vectors obtained for different damage scenarios are minimised via a combined genetic algorithm and non-linear optimisation system to identify damage location and severity. This minimisation procedure is performed in two steps. First, the algorithm tries to minimise residual force vector (RFV) by only changing element stiffness matrices by aiming to detect impact type damage, as elastic modulus change is directly related to stiffness matrix. Secondly, it performs a minimisation over RFV by changing both element stiffness and mass matrices which aims to detect saw-cut type damage where thickness change is a function of both stiffness and mass matrices. The prediction of the damage type is then made by comparing the objective function value of these two steps. The lowest value (i.e. the fittest) indicates the damage type. The results of the minimisation also provide value of intactness where one representing intact and any value lower than one representing damage severity. The element related to that particular intactness value indicates the location of the damage on the structure. In case of having intactness values which are lower than one in value at various locations shows the existence of multi damage cases and provides their corresponding severities. The performance of the proposed combined genetic algorithm and non-linear optimisation system is tested on various damage scenarios created at different locations with different severities for both single and multi damage cases. The results indicate that the method used in this study is an effective one in the determination of type, severity and location of the damage in beam-like structures.

Keywords: Damage detection, genetic algorithm, non-linear optimisation, finite element analysis, residual force vector method, beam-like structures

ÖZ

KİRİŞ BENZERİ YAPILARDA BİRLEŞİK GENETİK ALGORİTMA VE LİNEER OLMAYAN OPTİMİZASYON İLE HASAR TESPİTİ

Aktaşođlu, Seyfullah

Yüksek Lisans, Havacılık ve Uzay Mühendisliđi Bölümü

Tez Yöneticisi: Yrd. Doç. Dr. Melin Şahin

Şubat 2012, 141 Sayfa

Bu çalışmada, genetik algoritma ile lineer olmayan eniyileme sistemi ankastre izotropik kiriş benzeri yapılarda hasar yerinin ve şiddetinin tespitinde kullanılmak üzere tasarlanmıştır. Titreşim tabanlı özellikler olan doğal frekanslar (yani eigen değerleri) ve yerdeğıştirme biçim şekilleri (yani eigen vektörleri) düzlem dışı ilk iki eğilme biçim şekilleri göz önüne alınarak testere kesiđi ve çarpma tipi hasar tespitleri için belirteç olarak kullanılmıştır. Bu amaca yönelik olarak söz konusu belirteçlerini elde etmek için sağlam ve hasarlı yapıların modelleme ve analizlerinde ticari sonlu elemanlar programı olan Msc. Patran/Nastran kullanılmıştır. Elastik modüldeki azalma olarak modellenen çarpma tipi hasarlar ve kalınlıktaki azalma olarak modellenen testere kesiđi tipi hasarlar için sonlu elemanlar modeli kullanılarak çeşitli hasar senaryoları oluşturulmuştur.

Bu modeller tek boyutlu bar tipi elemanlar ve iki boyutlu kabuk tipi elemanlar kullanarak Msc. Patran da modellenmiş, sonrasında eleman kütle ve esneklik

matrislerini elde etmek için ise Msc. Nastran da normal mod analizlerine tabi tutulmuştur. Duyarlılık matrisleri modellemedeki ilgili özelliklerde (elastik modülde ve eleman kalınlığında azalma) belirli oranlarda yapılan değişiklikler ve bunlara karşılık gelen normal mod analiz sonuçları sayesinde elde edilmiştir. Duyarlılık matrisleri genel kütle ve esneklik matrislerini oluşturmak için eleman kütle ve esneklik matrislerinin katsayısı olarak kullanılmış ve elde edilen bu matrisler yapının artık kuvvet matrislerinin oluşturması için birleştirilmiş, genetik algoritma ve lineer olmayan eniyileme birleşik sistemi ile yapıdaki hasarların yerini ve şiddetini bulmak için de minimize edilmişlerdir. Bu minimizasyon iki adımdan oluşur: birinci adımda çarpma tipi hasar yapının esneklik matrisi ile doğrudan ilgili olduğundan artık kuvvet vektörü eleman esneklik matrislerini değiştirerek bu tip hasarları bulma amaçlı minimize edilmiştir. İkinci adımda ise artık kuvvet vektörü üzerindeki minimizasyon testere kesiği tipi hasarı tespit amaçlı yapının kütle ve esneklik matrisleri üzerinden eş zamanlı olarak yapılmıştır. Bu iki adımın sonucunda elde edilen amaç fonksiyonunun sonuçları karşılaştırılarak hasar tipi tahmini gerçekleştirilmiştir. Amaç fonksiyonda en küçük değere sahip (yani en güçlü) olan hasar tipini belirlemektedir.

Minimizasyon ayrıca her eleman için sıfır ile bir arasında bir sağlamlık değeri vermektedir; bir değeri hasarsızlığı, birden küçük herhangi bir değer ise de hasarı varlığına delalet eder. Yapı üzerinde çeşitli yerlerde birden küçük olan değerler çoklu hasarların yerlerini ve karşılık gelen değerler de bu hasarların şiddetini göstermektedir. Önerilen genetik algoritma ve lineer olmayan birleşik eniyilemenin performansı farklı şiddette, farklı yerlerde tek veya çoklu olarak tasarlanmış hasar senaryoları ile test edilmiştir. Sonuçlar giriş benzeri yapıdaki hasarın yeri, şiddeti ve tipinin belirlenmesinde sunulan yöntemin etkin olduğunu göstermiştir.

Anahtar Kelimeler: Hasar tespiti, genetik algoritma, lineer olmayan eniyileme, sonlu eleman analizi, artık kuvvet vektör metodu, giriş benzeri yapılar

To my parents, especially, to my sister and my grandfather...

ACKNOWLEDGEMENTS

I would like to express my deepest gratitude and thanks to my supervisor Assist. Prof. Dr. Melin Şahin for his guidance, support and criticism. I will never forget his encouragement that motivated me to introduce this study.

My grateful thanks are for all my friends, the academic staff in the department, for their help, for giving their best for my academic education.

My special thanks are for my friends Sadettin Şen and Levent Ünlüsoy who always supported me and share their valuable experiences in helpful discussions.

I am grateful to my precious lady Işıl for her understanding and endless support before and during this study.

Finally, I would express my deepest thanks to my father for his encouragements and support throughout my whole life. I would like to thank my sister, Eda for her endless understanding and her endless warm motivation. And my greatest thanks go to my mother for her patience and love in all moments of my life. It would be never possible without her fondness and wishes.

TABLE OF CONTENTS

ABSTRACT	iv
ÖZ	vi
ACKNOWLEDGEMENTS.....	ix
TABLE OF CONTENTS	x
LIST OF TABLES	xiii
LIST OF FIGURES	xvi
CHAPTERS	
1. INTRODUCTION.....	1
1.1 Motivations of the study.....	1
1.2 Objectives of the study	2
1.3 Limitations of the study.....	3
1.4 Outline of the study.....	4
2. LITERATURE REVIEW	5
2.1 Introduction.....	5
2.2 Damage Detection Features	7
2.2.1 Natural Frequencies	7
2.2.2 Displacement Mode Shapes	8
2.2.3 Curvature Mode Shapes	10
2.2.4 Modal Strain Energy.....	12
2.2.5 Residual Force Vector Method.....	14
2.3 Optimisation Algorithms	17
2.3.1 Artificial Neural Networks	17
2.3.2 Genetic Algorithms.....	19
3. FINITE ELEMENT MODELLING AND ANALYSIS.....	22
3.1 Finite Element Modelling of Intact Structure.....	22
3.1.1 1-D Beam Element Approach for Intact Structure.....	23
3.1.2 2-D Shell Element Approach for Intact Structure	29
3.2 Finite Element Modelling of Damaged Structure	34
3.2.1 1-D Beam Element Approach for Damaged Structure	34
3.2.1.1 Impact Type Damage Modelling.....	34

3.2.1.1.1.	Single Impact Type Damage	35
3.2.1.1.2.	Multi Impact Type Damage	40
3.2.1.2	Saw-cut Type Damage Modelling	43
3.2.1.2.1.	Single Saw-cut Type Damage.....	43
3.2.1.2.2.	Multi Saw-cut Type Damage	47
3.2.2	2-D Shell Element Approach for Damaged Structure.....	49
3.2.2.1	Impact Type Damage Modelling.....	49
3.2.2.1.1.	Single Impact Type Damage	49
3.2.2.1.2.	Multi Impact Type Damage	55
3.2.2.2	Saw-cut Type Damage Modelling	59
3.2.2.2.1.	Single Saw-cut Type Damage.....	59
3.2.2.2.2.	Multi Saw-cut Type Damage	66
4.	DAMAGE IDENTIFICATION ALGORITHM.....	70
4.1	Damage Sensitive Features	70
4.2	Optimisation Problem.....	72
4.2.2	Genetic Algorithm	73
4.2.3	Constrained Non-Linear Optimisation	81
5.	DAMAGE IDENTIFICATION RESULTS	85
5.1	1-D Damage Detection.....	85
5.1.1	Impact Type Damage.....	85
5.1.1.1	Single Damage Scenarios	85
5.1.1.2	Multi Damage Scenarios	87
5.1.2	Saw-cut Type Damage	89
5.1.2.1	Single Damage Scenarios	89
5.1.2.2	Multi Damage Scenarios.....	91
5.1.3	Investigation of Damage Type in 1-D Approach	93
5.2	2-D Damage Detection.....	98
5.2.1	Impact Type Damage.....	98
5.2.1.1	Single Damage Scenarios	98
5.2.1.2	Multi Damage Scenarios	101
5.2.2	Saw-cut Type Damage	104
5.2.2.1	Single Damage Scenarios	104
5.2.2.2	Multi Damage Scenarios.....	108
5.2.3	Investigation of Damage Type in 2-D Approach	111
6.	CONCLUSIONS.....	122
6.1	General Conclusions	122
6.2	Recommendations for Future Work	123
REFERENCES	126

APPENDICES

A.1. Genetic Algorithm (GA) Performance Trials for the Saw-cut Type Damage created on the 6th Element with 30% Severity 133

A.2. Only FMINCON Performance for the Cases Including Initial Guesses from 0.4 to 0.8 by Increment of 0.1 136

A.3. Only FMINCON Performance for the Randomly Generated Initial Guesses Between [0.3-1]..... 139

LIST OF TABLES

Table 3.1.	Structural properties of the beam	23
Table 3.2.	First five natural frequencies (ω_n) of intact cantilever beam (Theoretical Solution)	24
Table 3.3.	First five natural frequencies of intact cantilever beam (FEA) with changing mesh densities.....	25
Table 3.4.	Comparison of natural frequencies of FEA [10] and 15 element-cantilever- beam model to analytical one	27
Table 3.5.	First five natural frequencies of intact cantilever beam (FEA) with changing mesh densities.....	29
Table 3.6.	First five natural frequencies of intact cantilever beam (FEA of Model-II)	32
Table 3.7.	First five natural frequencies of single impact type damaged cantilever beam; Damage on the 3 rd element with 40% severity	35
Table 3.8.	First five natural frequencies of single impact type damaged cantilever beam; Damage on the 8 th element with 60% severity	37
Table 3.9.	First five natural frequencies of single impact type damaged cantilever beam; Damage on the 13 th element with 20% severity	38
Table 3.10.	First five natural frequencies of multi impact damaged cantilever beam; Damage on the 3 rd element with 40% severity and the 12 th element with 20% severity	41
Table 3.11.	First five natural frequencies of multi impact damaged cantilever beam; Damage on the 7 th element with 30% severity and the 12 th element with 60% severity	42
Table 3.12.	First five natural frequencies of single saw-cut damaged cantilever beam; Damage on the 4 th element with 20% severity	43
Table 3.13.	First five natural frequencies of single saw-cut damaged cantilever beam; Damage on the 8 th element with 30% severity	44
Table 3.14.	First five natural frequencies of multi saw-cut damaged cantilever beam; Damage on the 2 nd element with 10% severity and the 14 th element with 10% severity	47

Table 3.15.	First five natural frequencies of multi saw-cut damaged cantilever beam; Damage on the 5 th element with 40% severity and the 7 th element with 60% severity	48
Table 3.16.	First five natural frequencies of single impact damaged cantilever beam; Damaged on the 6 th element with 40% severity.....	50
Table 3.17.	First five natural frequencies of single impact damaged cantilever beam; Damaged on the 15 th element with 20% severity.....	51
Table 3.18.	First five natural frequencies of single impact damaged cantilever beam; Damaged on the 13 th element with 20% severity.....	53
Table 3.19.	First five natural frequencies of single impact damaged cantilever beam; Damaged on the 20 th element with 40% severity.....	54
Table 3.20.	First five natural frequencies of multi impact damaged cantilever beam; Damaged on the 1 st element with 40% severity and the 14 th element with 50% severity	55
Table 3.21.	First five natural frequencies of multi impact damaged cantilever beam; Damaged on the 4 th element with 40% severity and the 9 th element with 10% severity	56
Table 3.22.	First five natural frequencies of multi impact damaged cantilever beam; Damaged on the 11 th element with 70% severity and the 22 nd element with 20% severity	57
Table 3.23.	First five natural frequencies of multi impact damaged cantilever beam; Damaged on the 14 th element with 50% severity and the 15 th element with 60% severity	58
Table 3.24.	First five natural frequencies of single saw-cut damaged cantilever beam; Damage on the 6 th element with 40% severity	59
Table 3.25.	First five natural frequencies of single saw-cut damaged cantilever beam; Damage on the 7 th element with 20% severity	60
Table 3.26.	First five natural frequencies of single saw-cut damaged cantilever beam; Damage on the 12 th element with 60% severity.....	60
Table 3.27.	First five natural frequencies of single saw-cut damaged cantilever beam; Damage on the 12 th element with 32% severity.....	61
Table 3.28.	First five natural frequencies of single saw-cut damaged cantilever beam; Damaged on the 5 th element with 10% severity.....	64
Table 3.29.	First five natural frequencies of single saw-cut damaged cantilever beam; Damaged on the 25 th element with 30% severity.....	65

Table 3.30.	First five natural frequencies of multi impact damaged cantilever beam; Damaged on the 5 th element with 50% severity and the 13 th element with 50% severity	66
Table 3.31.	First five natural frequencies of multi impact damaged cantilever beam; Damaged on the 8 th element with 20% severity and the 9 th element with 40% severity	67
Table 3.32.	First five natural frequencies of multi saw-cut damaged cantilever beam; Damage on the 10 th element with 10% severity and the 17 th element with 40% severity	68
Table 3.33.	First five natural frequencies of multi saw-cut damaged cantilever beam; Damage on the 4 th element with 20% severity and the 28 th element with 40% severity	69

LIST OF FIGURES

Figure 3.1.	Geometry of the cantilevered beam	23
Figure 3.2.	Cantilever beam bar2 element model (a) Isotropic view (b) Top view with element numbering*	26
Figure 3.3.	The first five out of plane bending mode shapes of the cantilevered beam obtained from FEA (1-D modelling).....	28
Figure 3.4.	Cantilever beam quad4 element model (Model-I) (a) Isometric view (b) Top view with element numbering	30
Figure 3.5.	The first five out of plane bending mode shapes of the cantilevered beam obtained from FEA (2-D modelling, Model-I).....	31
Figure 3.6.	2-D 2x15 Shell Element Model (Model-II) (a) Isotropic-view (b) Top-view with element numbering	32
Figure 3.7.	The first five out of plane bending mode shapes of the cantilevered beam obtained from FEA (2-D modelling, Model-II)	33
Figure 3.8.	Definition of damage location in bar2 elements.....	35
Figure 3.9.	Damage located on the 8 th element	36
Figure 3.10.	Damage located on the 13 th element	37
Figure 3.11.	Effects of changing damage location on natural frequencies (sample case for 10% damage), 1-D Modelling.....	39
Figure 3.12.	Damage at 50% location from the root with changing severities, 1-D Modelling	39
Figure 3.13.	Damage at 20% location from the root with changing severities, 1-D Modelling	40
Figure 3.14.	Damage located on the 3 rd and the 12 th elements	41
Figure 3.15.	Damage located on the 7 th and the 12 th elements	42
Figure 3.16.	Damage located on the 4 th element	43
Figure 3.17.	Damage located on the 8 th element	44
Figure 3.18.	Effects of changing damage location on natural frequency (sample case for 20% damage), 1-D Modelling.....	45
Figure 3.19.	Damage at 20% location from root with changing severities, 1-D Modelling	46

Figure 3.20.	Damage at 40% location from the root with changing severities, 1-D Modelling	46
Figure 3.21.	Damage located on the 2 nd and the 14 th elements.....	47
Figure 3.22.	Damage located on the 5 th and the 7 th elements.....	48
Figure 3.23.	Damage located on the 6 th element, 2-D Modelling, Model-I case.....	49
Figure 3.24.	Damage located on the 15 th element	50
Figure 3.25.	Effects of changing damage location on natural frequency (sample case for 60% damage), 2-D Modelling, Model-I case	51
Figure 3.26.	Damage at 20% location from the root with changing severities, 2-D Modelling, Model-I case.....	52
Figure 3.27.	Damage at 60% location from the root with changing severities, 2-D Modelling, Model-I case.....	52
Figure 3.28.	Damage located on the 13 th element, 2-D Modelling, Model-II case.....	53
Figure 3.29.	Damage located on the 20 th element	54
Figure 3.30.	Damage located on the 1 st and the 14 th elements	55
Figure 3.31.	Damage located on the 4 th and the 9 th elements.....	56
Figure 3.32.	Damage located on the 11 th and the 22 nd elements.....	57
Figure 3.33.	Damage located on the 14 th and the 15 th elements	58
Figure 3.34.	Damage located on the 12 th element	60
Figure 3.35.	Effects of changing damage location on natural frequency (sample case for 60% damage), 2-D Modelling, Model-I case	62
Figure 3.36.	Damage at 20% location from the root with changing severities, 2-D Modelling, Model-I case.....	62
Figure 3.37.	Damage at 60% location from the root with changing severities, 2-D Modelling, Model-I case.....	63
Figure 3.38.	Damage located on the 5 th element.....	63
Figure 3.39.	Damage located on 25 th element.....	64
Figure 3.40.	Damage located on the 5 th and the 13 th elements	66
Figure 3.41.	Damage located on the 8 th and the 9 th elements.....	67
Figure 3.42.	Damage located on the 10 th and the 17 th elements	68
Figure 3.43.	Damage located on the 4 th and the 28 th elements	69
Figure 4.1.	Schematic of the Damage Detection Procedure.....	73
Figure 4.2.	Effect of number of mode shapes in objective function on the optimisation procedure (a) Color-coded display of the best fitness values in each run (b) Means and standard deviations of the best fitness values (c) Number of iterations and its standard deviations	75

Figure 4.3.	GA results for 30% damage on the 6 th element (a) History of convergence (b) Identified damage location and severity (c) Numerical result of identified state	77
Figure 4.4.	Crossover Fraction Selection (a) Color-coded display of the best fitness values in each run (b) Means and standard deviations of the best fitness values (c) Number of iterations and its standard deviations	78
Figure 4.5.	GA results for 40% damaged on the 4 th element (a) History of convergence (b) Identified damage location and severity (c) Numerical result of identified state	80
Figure 4.6.	FMINCON results for 10% damage on the 6 th element (a) Identified damage location and severity (b) History of convergence (c) Numerical result of identified state	82
Figure 4.7.	GA results for 10% damage on the 6 th element (a) History of convergence (b) Identified damage location and severity (c) Numerical result of identified state	83
Figure 4.8.	FMINCON results as a part of the hybrid system for 10% damage on the 6 th element (a) Identified damage location and severity (b) History of Convergence (c) Numerical result of identified state	83
Figure 5.1.	GA results for 40% damage on the 3 rd element (a) History of Convergence (b) Identified damage location and severity (c) Numerical result of identified state	86
Figure 5.2.	FMINCON results as a part of the hybrid system for 40% damage on the 3 rd element (a) Identified damage location and severity (b) History of Convergence (c) Numerical result of identified state	87
Figure 5.3.	GA results for 40% damage on the 3 rd element and 20% damage on the 12 th element (a) History of Convergence (b) Identified damage location and severity (c) Numerical result of identified state.....	88
Figure 5.4.	FMINCON results as a part of the hybrid system for 40% damage on the 3 rd element and 20% damage on the 12 th element (a) Identified damage location and severity (b) History of Convergence (c) Numerical result of identified state	89
Figure 5.5.	GA results for 20% damage on the 4 th element (a) History of convergence (b) Identified damage location and severity (c) Numerical result of identified state	90

Figure 5.6.	FMINCON results as a part of the hybrid system for 20% damage on the 4 th element (a) Identified damage location and severity (b) History of Convergence (c) Numerical result of identified state	90
Figure 5.7.	GA results for 10% damage on the 2 nd element and 10% damage on the 14 th element (a) History of Convergence (b) Identified damage location and severity (c) Numerical result of identified state.....	91
Figure 5.8.	FMINCON results as a part of the hybrid system for 10% damage on the 2 nd element and 10% damage on the 14 th element (a) Identified damage location and severity (b) History of Convergence (c) Numerical result of identified state	92
Figure 5.9.	GA results for 20% damage on the 9 th element – Impact type damage simulation (a) History of Convergence (b) Identified damage location and severity (c) Numerical result of identified state	93
Figure 5.10.	FMINCON results as a part of the hybrid system for 20% damage on the 9 th element – Impact type damage simulation (a) Identified damage location and severity (b) History of Convergence (c) Numerical result of identified state	94
Figure 5.11.	GA Result for 20% damage on the 9 th element – Saw-cut type damage simulation (a) History of Convergence (b) Identified damage location and severity (c) Numerical result of identified state	94
Figure 5.12.	FMINCON results as a part of the hybrid system for 20% damage on the 9 th element – Saw-cut type damage simulation (a) Identified damage location and severity (b) History of Convergence (c) Numerical result of identified state	95
Figure 5.13.	GA results for 20% damage on the 9 th element – Impact type damage simulation (a) History of Convergence (b) Identified damage location and severity (c) Numerical result of identified state	96
Figure 5.14.	FMINCON results as a part of the hybrid system for 20% damage on 9 th element – Impact type damage simulation (a) Identified damage location and severity (b) History of Convergence (c) Numerical result of identified state	96
Figure 5.15.	GA results for 20% damage on the 9 th element – Saw-cut type damage simulation (a) History of Convergence (b) Identified damage location and severity (c) Numerical result of identified state	97

Figure 5.16.	FMINCON results as a part of the hybrid system for 20% damage on the 9 th element Saw-cut type damage simulation (a) Identified damage location and severity (b) History of Convergence (c) Numerical result of identified state	97
Figure 5.17.	GA Result for 20% damage on the 15 th element (a) History of Convergence (b) Identified damage location and severity (c) Numerical result of identified state	99
Figure 5.18.	FMINCON results as a part of the hybrid system for 20% damage on the 15 th element case (a) Identified damage location and severity (b) History of Convergence (c) Numerical result of identified state	99
Figure 5.19.	GA Result for 40% damage on the 20 th element (a) History of Convergence (b) Identified damage location and severity (c) Numerical result of identified state	100
Figure 5.20.	FMINCON results as a part of the hybrid system for 40% damage on the 20 th element (a) Identified damage location and severity (b) History of Convergence (c) Numerical result of identified state	101
Figure 5.21.	GA results for 40% damage on the 1 st element and 50% damage on the 14 th element (a) History of Convergence (b) Identified damage location and severity (c) Numerical result of identified state	102
Figure 5.22.	FMINCON results as a part of the hybrid system for 40% damage on the 1 st element and 50% damage on the 14 th element (a) Identified damage location and severity (b) History of Convergence (c) Numerical result of identified state	102
Figure 5.23.	GA results for 50% damage on the 14 th element and 60% damage on the 15 th element (a) History of convergence (b) Identified damage location and severity (c) Numerical result of identified state	103
Figure 5.24.	FMINCON results as a part of the hybrid system for 50% damage on 14 th element and 60% damage on the 15 th element (a) Identified damage location and severity (b) History of convergence (c) Numerical result of identified state	104
Figure 5.25.	GA results for 40% damage on the 6 th element (a) History of convergence (b) Identified damage location and severity (c) Numerical result of identified state	105
Figure 5.26.	FMINCON results as a part of the hybrid system for 40% damage on the 6 th element (a) Identified damage location and severity (b) History of Convergence (c) Numerical result of identified state	105

Figure 5.27.	GA results for 10% damage on the 5 th element (a) History of Convergence (b) Identified damage location and severity (c) Numerical result of identified state	106
Figure 5.28.	FMINCON results as a part of the hybrid system for 10% damage on the 5 th element (a) Identified damage location and severity (b) History of Convergence (c) Numerical result of identified state	107
Figure 5.29.	GA results for 50% damage on the 5 th element and 50% damage on the 13 th element (a) History of Convergence (b) Identified damage location and severity (c) Numerical result of identified state.....	108
Figure 5.30.	FMINCON results as a part of the hybrid system for 50% damage on the 5 th element and 50% damage on the 13 th element (a) Identified damage location and severity (b) History of Convergence (c) Numerical result of identified state	108
Figure 5.31.	GA results for 10% damage on the 10 th element and 40% damage on the 17 th element (a) History of Convergence (b) Identified damage location and severity (c) Numerical result of identified state.....	109
Figure 5.32.	FMINCON results as a part of the hybrid system for 10% damage on the 10 th element and 40% damage on the 17 th element (a) Identified damage location and severity (b) History of Convergence (c) Numerical result of identified state	110
Figure 5.33.	GA Result for 20% damage on the 9 th element – Impact type damage simulation, Model-I (a) History of Convergence (b) Identified damage location and severity (c) Numerical result of identified state.....	111
Figure 5.34.	FMINCON results as a part of the hybrid system for 20% damage on the 9 th element – Impact type damage simulation, Model-I (a) Identified damage location and severity (b) History of Convergence (c) Numerical result of identified state	112
Figure 5.35.	GA Result for 20% damage on the 9 th element – Saw-cut type damage simulation, Model-I (a) History of Convergence (b) Identified damage location and severity (c) Numerical result of identified state.....	112
Figure 5.36.	FMINCON results as a part of the hybrid system for 20% damage on the 9 th element – Saw-cut type damage simulation, Model-I (a) Identified damage location and severity (b) History of Convergence (c) Numerical result of identified state	113

Figure 5.37.	GA Result for 20% damage on the 9 th element – Impact type damage simulation, Model-I (a) History of Convergence (b) Identified damage location and severity (c) Numerical result of identified state.....	114
Figure 5.38.	FMINCON results as a part of the hybrid system for 20% damage on 9 th element – Impact type damage simulation, Model-I (a) Identified damage location and severity (b) History of Convergence (c) Numerical result of identified state	114
Figure 5.39.	GA Result for 20% damage on the 9 th element – Saw-cut type damage simulation, Model-I (a) History of Convergence (b) Identified damage location and severity (c) Numerical result of identified state.....	115
Figure 5.40.	FMINCON results as a part of the hybrid system for 20% damage on 9 th element – Saw-cut type damage simulation, Model-I (a) Identified damage location and severity (b) History of Convergence (c) Numerical result of identified state	115
Figure 5.41.	GA Result for 20% damage on both the 9 th element and 24 th element – Impact type damage simulation, Model-II (a) History of Convergence (b) Identified damage location and severity (c) Numerical result of identified state	116
Figure 5.42.	FMINCON results as a part of the hybrid system for 20% damage on both the 9 th element and 24 th element – Impact type damage simulation, Model-II (a) Identified damage location and severity (b) History of Convergence (c) Numerical result of identified state	117
Figure 5.43.	GA Result for 20% damage on both the 9 th element and 24 th element– Saw-cut type damage simulation, Model-II (a) History of Convergence (b) Identified damage location and severity (c) Numerical result of identified state	117
Figure 5.44.	FMINCON results as a part of the hybrid system for 20% damage on both the 9 th element and 24 th element – Saw-cut type damage simulation, Model-II (a) Identified damage location and severity (b) History of Convergence (c) Numerical result of identified state	118
Figure 5.45.	GA Result for 20% damage on both the 9 th element and 24 th element – Impact type damage simulation, Model-II (a) History of Convergence (b) Identified damage location and severity (c) Numerical result of identified state	119

Figure 5.46.	FMINCON results as a part of the hybrid system for 20% damage on both the 9 th element and 24 th element – Impact type damage simulation, Model-II (a) Identified damage location and severity (b) History of Convergence (c) Numerical result of identified state	119
Figure 5.47.	GA Result for 20% damage on both the 9 th element and 24 th element – Saw-cut type damage simulation, Model-II (a) History of Convergence (b) Identified damage location and severity (c) Numerical result of identified state	120
Figure 5.48.	FMINCON results as a part of the hybrid system for 20% damage on both the 9 th element and 24 th element – Saw-cut type damage simulation, Model-II (a) Identified damage location and severity (b) History of Convergence (c) Numerical result of identified state	120
Figure A.1.1	GA results for 30% damage on the 6 th element for Trial Run 1 (a) History of convergence (b) Identified damage location and severity (c) Numerical result of identified state.....	133
Figure A.1.2	GA results for 30% damage on the 6 th element for Trial Run 2 (a) History of convergence (b) Identified damage location and severity (c) Numerical result of identified state.....	134
Figure A.1.3	GA results for 30% damage on the 6 th element for Trial Run 3 (a) History of convergence (b) Identified damage location and severity (c) Numerical result of identified state.....	134
Figure A.1.4	GA results for 30% damage on the 6 th element for Trial Run 4 (a) History of convergence (b) Identified damage location and severity (c) Numerical result of identified state.....	135
Figure A.1.5	GA results for 30% damage on the 6 th element for Trial Run 5 (a) History of convergence (b) Identified damage location and severity (c) Numerical result of identified state.....	135
Figure A.2.1.1.	FMINCON results for 10% damage on the 6 th element (a) Initial guesses for the associated variable (b) Identified damage location and severity (c) History of Convergence (d) Numerical result of identified state.....	136
Figure A.2.1.2.	FMINCON results for 10% damage on the 6 th element (a) Initial guesses for the associated variable (b) Identified damage location and severity (c) History of Convergence (d) Numerical result of identified state.....	137
Figure A.2.1.3.	FMINCON results for 10% damage on the 6 th element (a) Initial guesses for the associated variable (b) Identified damage location and severity (c) History of Convergence (d) Numerical result of identified state.....	137

- Figure A.2.1.4.** FMINCON results for 10% damage on the 6th element (a) Initial guesses for the associated variable (b) Identified damage location and severity (c) History of Convergence (d) Numerical result of identified state.....138
- Figure A.2.1.5.** FMINCON results for 10% damage on the 6th element (a) Initial guesses for the associated variable (b) Identified damage location and severity (c)History of Convergence (d) Numerical result of identified state.....138
- Figure A.2.2.1.** FMINCON results for 10% damage on the 6th element (a) Initial guesses for the associated variable (b) Identified damage location and severity (c) History of Convergence (d) Numerical result of identified state.....139
- Figure A.2.2.2.** FMINCON results for 10% damage on the 6th element (a) Initial guesses for the associated variable (b) Identified damage location and severity (c) History of Convergence (d) Numerical result of identified state.....140
- Figure A.2.2.3.** FMINCON results for 10% damage on the 6th element (a) Initial guesses for the associated variable (b) Identified damage location and severity (c) History of Convergence (d) Numerical result of identified state.....140
- Figure A.2.2.4.** FMINCON results for 10% damage on the 6th element (a) Initial guesses for the associated variable (b) Identified damage location and severity (c) History of Convergence (d) Numerical result of identified state.....141
- Figure A.2.2.5.** FMINCON results for 10% damage on the 6th element (a) Initial guesses for the associated variable (b) Identified damage location and severity (c) History of Convergence (d) Numerical result of identified state.....141

CHAPTER 1

INTRODUCTION

1.1 Motivations of the study

Damage can be defined as degradation of any structural properties of a structure. This degradation results as a reduction on the limit load that the structure can carry or resist which increases the possibility of having a catastrophic failure. In order to avoid this, detecting damage before a catastrophic failure happens is vital especially in aerospace field. To decide whether a structure has damage or not, both the initial and the final states of the structure has to be compared. Investigation and quantification of the possible differences between those states forms the basis of the damage identification methods. One of the most used concepts in damage identification is Residual Force Vector (RFV) [1]. Residual force provides an objective function to be minimised for achieving the dynamic balance [2].

Many authors used this method via neural networks [3] and genetic algorithm (GA) [2], [4]. However, their investigations on the mentioned method are generally limited with truss members due to usage of classical beam theory [5].

Therefore, the aim of this thesis is to enhance the capability of FE modelling and analysis for the use of 1-D isotropic beam-like structures and design an applicable combined genetic algorithm and non-linear optimisation system for damage detection. In order to achieve this goal, first an interface between commercial code Msc. Patran/Nastran[®] is written to obtain mass and stiffness matrices of any shape of structure. This interface gives opportunity to model beam-like structure in 2-D and therefore identify damage on its entire surface. By using this interface, obtained matrices of any structure can be arranged to construct

residual force vectors (RFVs) which are then fed into optimisation algorithm as an objective function. This thesis also comprises a usage of an efficient optimization system that is able to deal with complex models. For this purpose hybrid-genetic algorithm is used to combine power of genetic algorithm (GA) throughout the solution space and the speed of the local optimiser [6]. These are detailed in section 4.2. The combination of mentioned interface and optimisation system is applied to isotropic beam-like structures having single or multi damage cases.

1.2 Objectives of the study

The objectives of this study can be listed as follows:

- Having finite element models (FEM) of both intact and damaged structures comprising 1-D and 2-D type elements,
- Validating the obtained FEM of the intact structure via finite element analysis (FEA) and making comparisons with modal data available in the literature,
- Creating different damage scenarios by modifying FEM of the intact structure
- Extracting element mass and stiffness matrices for individual element by changing Msc. Nastran[®] input file and performing normal mode dynamic analysis for each modification.
- Constructing sensitivity matrices and using them in the optimizations' objective function,
- Performing an optimisation process via GA for damage identification in beam-like structures
- Constructing tuned hybrid-GA system for the optimisation process to achieve better accuracy in the damage identification of beam-like structures

1.3 Limitations of the study

The main limitations of this study can be listed as follows:

- In FE modelling, only isotropic structures are examined due to the simplicity on obtaining stiffness and mass matrices.
- The FE software used in the analyses, Msc. Patran[®], has a variety of element types to mesh a model in 1-D or 2-D. Every element type has changing node numbers and degree of freedom. This affects element mass/stiffness matrices location in global mass/stiffness matrices. The main Matlab code generated in this study which is dealing with both the interface and optimization part of the system is only introduced by bar2 elements in 1-D and quad4 elements in 2-D. No other element types including 3-Ds can be interpreted for the optimisation of the study.
- The analyses consider only the first two out of plane bending modes of vibration and therefore no torsional modes are included as damage features.
- The method comprising the use of RFV is designed for only undamped systems and therefore the damping effects are not taken into account.
- As large number of elements in the FE models leads to larger matrix dimensions which brings some hardware limitations and slows the generated Matlab codes down, the FE models are kept small in size and meshed according without violating the mesh density requirements in convergence of modal solution.

1.4 Outline of the study

The organization of this thesis can be given as follows:

In Chapter 2, the literature survey about damage detection methods given briefly. The focus is especially on RFV concept and its application areas. The procedures of constructing the FEMs in order to obtain RFVs and the design of optimisation algorithms to minimise the obtained RFVs are also investigated in details in this chapter.

Chapter 3 presents the FEMs of beam-like intact structures regarding both 1-D and 2-D type modelling. The verification studies are then completed by performing modal analysis and comparing the obtained results with the ones in the literature. Having obtained and verified the FEM of the intact structure, different damage scenarios are then created regarding their types, locations and severities.

Chapter 4 is devoted to damage identification method and its applications. First, damage features are extracted. Then, optimisation system is detailed and finally, the implementation of the damage features into optimisation system is presented.

In Chapter 5, results of the damage identification procedure are presented in terms of different damage types, their locations and severities using the optimisation system constructed on damaged models.

Chapter 6 includes the general conclusions drawn from this study and provides recommendations for the future works.

CHAPTER 2

LITERATURE REVIEW

2.1 Introduction

Damage can be defined as degradation of any structural properties of a structure. This degradation result in a reduction on the limit load that can the structure can carry or resist which ultimately increases the possibility to have a catastrophic failure. To avoid this situation, detecting damage beforehand a failure is vital especially in the aerospace field. Additionally, in order to decide whether the structure has damage or not, both initial and final states of the structure have to be known and compared.

The effects of damage on a structure can be categorised as linear and non-linear. If the linear elastic structure remains linear elastic after damage then the damage is called as linear damage. For this case structural response can be modelled by using linear equations of motions. Linear methods can be further classified as model-based and non-model-based. Model-based methods assume that the monitored structure responds in some predetermined manner that can be accurately discretised by finite element analysis, such as the response described by Euler-Bernoulli beam theory. If linear elastic structure characteristics change into a non-linear manner after damage occurs than the damaged is called as a non-linear one. Fatigue crack is one of the examples for a non-linear type damage.

Another identification system is four levels of damage identification as represented by Rytter(1993) [7] , as follows:

- Level 1: Determination that damage is present in the structure
- Level 2: Determination of the geometric location of the damage

- Level 3: Quantification of the severity of the damage
- Level 4: Prediction of the remaining service life of the structure

Vibration-based damage identification methods indicate only the Level 1 and Level 2 damage identification. If the structural model is included in vibration-based analysis then Level 3 damage identification can be obtained. Level 4 prediction is generally associated with the fields of fracture mechanics, structural design assessment and fatigue-life analysis. To have Level 3 type damage identification method, as stated earlier, the structural model is needed. Structures can be modelled analytically or via finite element methods. The finite element methods are receiving an attention in recent years due to providing an opportunity of analysing even complex structures accurately and economically [8]. Additionally, FEA is designed for rapid engineering analyses which can be performed on powerful computers. It procures this speed increase in analysis due to the fact that FEA uses the known properties of standard geometric shapes, i.e. finite elements. Wide range of structural analysis can be performed by FEA, such as; static displacement and stress, natural frequencies and mode shapes, forced harmonic response amplitude and dynamic stress, etc. Therefore, FEA can provide dynamic properties of structures, including natural frequencies and corresponding mode shapes [8]. Most of the damage identification methods in literature use FEM extractions [9] or directly FEM updating for matrix updating methods [4]. Using FEM can also be divided into two main groups; researchers using their own in-house FE codes [10] and the researchers using commercial FEM tools [11]. If FEM updating is associated with researchers who are using their own codes, then it can be said that those codes are more applicable on multi damage cases [12] although they are limited with the shape of the structure, i.e. FE codes written on the basis of beam elements can only be applicable to 1-D beam-like structures.

The difficulty on damage detection is due to the fact that it is a non-unique and inverse problem as different damage types at various locations and with different severities may lead same changes on the dynamic behaviour of the structure [13]. Therefore, type sensitive algorithms may results in better location and severity predictions but the assumption of detecting the correct type of damage holds true. Different type of damage creates different physical properties on the

host structure. Due to the fact that modal parameters are functions of physical properties of the structure, changes on physical properties affects also modal parameters. For example, any deficiency due to an impact on structure can be modelled as percentage reduction in stiffness of the elements that are exposed on FE [4]. Furthermore, saw-cut on a structure [14] can be modelled as a percentage reduction in stiffness of elements or percentage reduction in thickness/cross-section of the model [15] .

2.2 Damage Detection Features

2.2.1 Natural Frequencies

A rich source of literature on damage detection is using shifts in natural frequencies. As stated in Section 2.1; modal parameters are functions of physical properties of the structure therefore changes on physical properties affects also modal parameters. Due to being easy to measure experimentally, damage can be detected from dynamic analysis aiming at natural frequencies. Therefore, methods using natural frequency changes as a damage signature are reviewed in this section.

Zak et al. [9] used finite element model to analyse single and closing delamination on vibrating laminated composite plate. Numerical calculations were performed for an eight-layer graphite/epoxy composite plate and accuracy of the model was supported by experimental results of harmonically excited mid plane delaminated composite plate. After having had compatible results from FEMs and experimental work, authors concluded that the both delamination length and its location affect the vibration modes and consequently the natural frequencies of the structure. Hu and Hwu [16] performs free vibration analysis on a sandwich plates with an across the width delamination located at the interface between the upper face and the core. One of the outcomes of this research was that the existence of the delamination lowers the natural frequency.

De Roeck et al. [17] monitored three span box bridge Z24 in Switzerland over one year and environmental effects such as; air temperature, humidity, rain,

wind speed and wind directions were also monitored to distinguish these effects on natural frequencies. Researchers demonstrated that if the environmental effects were eliminated than stiffness reduction could be detected. Zhichun Yang and Le Wang [18] applied natural frequency vector assurance criteria (NFVAC) on natural frequency data which was obtained from FEA of intact and damaged structure. To be able to apply this concept, a series of analyses had to be done on artificial damaged states of the structure to have a database. Application of the NFVAC concept on natural frequency vector (NFV) of damaged structure provided a method on damage identification. However, having limited database restrains this method to be exact. Hu et al. [19] developed identification methods for assessing structural damages using modal test data. The authors employed 10-bay planar truss structure to check these approaches numerically. Additionally, experimental data were provided via modal analysis of aluminium beam with both end fixed. The authors revealed that increase of the modal data was beneficial for having accurate results both on damage severity and location estimations.

2.2.2 Displacement Mode Shapes

Mode shape measurement of a structure can be done either single excitation point and many sensors or a roving exciter with one or more fixed sensors. For being easy to obtain and being physically connected to stiffness and mass changes, there is a large amount of literature on mode shape applications. Two commonly used methods are the Modal Assurance Criterion (MAC) [20] and Coordinate Modal Assurance Criterion (COMAC) [20].

Fox [21] increased sensitivity of MAC by determining the measurement points close to a nodal point for a particular mode. The author also applied relative scaling between changes of intact and damaged mode shapes for better identification of damage in terms of location [22]. It was concluded that comparison of relative changes in mode shapes were required to determine the location of damage accurately. Messina et al. [23] extended the approach to Multi Damage Location Assurance Criterion (MDLAC), which utilizes a correlation coefficient to

identify the damage. In this sense, MDLAC is similar to MAC in the comparison of mode shapes. An attractive feature of this method is that it requires only few numbers of the natural frequencies between the undamaged and damaged states. Numerical analysis part of this research consisted of application of MDLAC method on thirty-one bar truss and offshore platform structure. The results of the method were also validated experimentally using a three-beam test structure. The authors concluded that MDLAC provided reliable information about the location and the extent of damage.

Araújo dos Santos et al. [24] applied a method which was based on the orthogonality condition sensitivities of the mode shapes of the damaged and the undamaged structures. The damage was modelled as stiffness reduction on individual FEMs. Both the aforementioned method and the eigenvector sensitivities methods were applied on laminated rectangular plate which was free in space. The authors concluded that the orthogonality sensitivity based method was efficient, stable in detecting damage on more than one element. Also, the results of the orthogonality sensitivity based method were more accurate than that of eigenvector sensitivity based one.

Khan et al. [25] traced changes on mode shapes via scanning laser Doppler vibrometer (SLDV) on laboratory-scale structures. Three type of laboratory-scale test structures were evaluated: a metal cantilever beam with a saw-cut through 80% of its thickness, intact and damaged versions of a thin cantilever plate and reinforced concrete beams with and without cracks. The authors concluded that using continuously scanned laser Doppler vibrometer is an effective way in detecting and locating the damages on metal and concrete structures, however, the method worked in thick metal structures only if damage extended through more than half of the thickness. Waldron et al. [26] extended Khan et al.'s [25] method of mode shape comparison via SLDV. Waldron et al. [26] used operational deflection mode shapes (ODSs) while examining the mode shapes. The angle between the healthy and damaged normalised ODS vector was used as damage indicator. Two aluminium beams were tested in healthy and damage cases. At different boundary conditions, damage characteristics and force combinations were modelled on FEM to analyse damage detection characteristics of ODS. FE and experimental results

concluded that SLDV and ODS are effective ways on crack detection and at higher natural modes detection of damage was easier. The authors also concluded that rotational ODS gives more information about damage in terms of location and severity than the translational ones.

2.2.3 Curvature Mode Shapes

The curvature mode shapes were also used as damage features in literature due to the fact that they carry on local vibration information of the structure in order to localise the damage [13]. The curvature mode shapes are generally calculated by using central difference approximation from the displacement mode shapes which were obtained either experimentally or performing through modal analysis.

Roeck and Wahab [27] introduced curvature damage factor (CDF), aiming at to sum up cumulative effect of damage on all mode shapes summarised in one number. CDF was calculated by averaging the differences of the intact and damaged curvature mode shapes of the interest. The method was applied on Z24 bridge in Switzerland. Damages were simulated on FEM by a reduction in bending stiffness. The authors concluded that lower modes' modal curvatures were more accurate than those of the higher ones and CDF turned out to be an effective factor when the structure had several damages at different locations.

Wahab [28], on the other hand, used sensitivity based model updating algorithm for damage detection. The author included modal curvatures into algorithm in addition to eigenfrequencies and mode shapes as damage signature to investigate its effect on damage identification. For this purpose, a simply supported beam was modelled on FE. Damage on model was simulated as reduction in bending stiffness of elements. It was concluded that including the modal curvatures into account did not change convergence characteristics of the algorithm.

Zhang et al. [29] developed a simple method to extract structural mode shape squares (MOSS) approximately by using an approach in which acceleration of a passing vehicle and the structure of interest stand for a tapping device and a beam respectively. In order to increase the sensitivity to damage appearance, a

new damage index which was absolute difference of undamaged and damaged structure's MOSS vectors was used. The proposed method was then applied on two plates having single and double impact damages and was also simulated on a beam structure. It was concluded that the method was effective in terms of being robust in noisy environment.

Hamey et al. [30] applied four different methods of damage detection based on the curvature mode shapes and curvature frequency response functions (FRF). In contrary to other methods using curvature mode shapes obtained from second derivatives of displacement data, this research was based on measuring curvature mode shapes directly by roving piezoelectric film sensors through the structure. The damage detection algorithms used in this particular research were Curvature Damage Factor (CDF), Absolute Differences Method (ADM), Damage Index Method (DIM) and FRF Curvature Method (FCM). The methods were tested with three different type damage; delamination, impact and saw-cut type, on a cantilevered carbon/epoxy composite beam. It was concluded that DIM was better than the others in terms of detecting and isolating the damage. Additionally, the identification procedure gave better results for large delamination configuration than relatively localised damage cases, such as impact or saw-cut damages, when the sensors located opposite to the delamination side. The frequencies were inadequate to be used as a parameter in the damage severity prediction due to being widely changed from one test to another. And finally, the curvature mode shape methods could be used as a promising one in the damage detection.

Qiao et al. [14] applied curvature mode shape based damage detection method on two different testing systems; scanning laser vibrometer (SLV) with lead-zirconate-titanate (PZT) actuators (PZT-SLV) and polyvinylidene fluoride (PVDF) sensors with PZT actuators (PZT-PVDF) on e-glass/epoxy composite plate with embedded delamination. Numerical analysis also performed with FE method. Delamination was modelled on FE with special element named as Link10 which was designed as compression only element, meaning zero stiffness when element is under tension. Simplified gapped smoothing method (GSM), generalized fractal dimension (GFD) and strain energy method (SEM) were applied to analyse the experimental and numerical data and uniform load surface (ULS) curvatures. The

authors concluded that PZT-SLV was decided to be better, by correlation of FEM results, than PZT-PVDF system with refined scanning mesh ability. The use of ULS curvature based one was an effective way of determining delamination on composites due to being highly sensitive to damage and having reduced truncation and measurement errors.

2.2.4 Modal Strain Energy

On a particular structural load path, large amount of strain energy can be stored for a particular vibration mode. The frequency and mode shape of that mode are highly sensitive to changes in that load path [12]. The assumption is that damage will cause redistribution of strain energy and raise the beam curvature in the vicinity of damage. Therefore, it is feasible to select it as a damage feature.

The literature generally focussed on 1-D strain methods (except Cornwell et al. [31]), however, 2-D and 3-D structures' decomposed versions can also be interpreted by 1-D algorithm. Kim and Stubbs [32] applied a damage detection algorithm on a single cracked plate girder and accuracy of the algorithm was assessed in terms of model uncertainties. Damaged and intact elements' structural modal energy ratio was used as a damage signature. Cubic-spline functions were used to complete missing information about modal amplitudes by interpolation of mode shapes. Displacement function, which was used to obtain curvatures, was generated for the entire structure using third-order interpolation. By means of this procedure, necessary information, i.e. curvatures, was obtained in order to calculate modal energy. The authors concluded that while uncertainty on the selection of damage detection model (such as; Euler-Bernoulli or Timoshenko beam models) was less effective on damage localization and false-negative error (i.e., missing detection of true damage locations), model selection uncertainty had relatively great effect on severity estimation and false-positive error (i.e., prediction of locations that are not damaged). The detection accuracy was also affected by both quality and amount of modal information and the modifications in damage detection algorithm.

Kim and Stubbs [33] improved their own method by including mass and stiffness matrix information in their damage identification algorithm. This improvement increased the prediction accuracy of damage detection procedure and decreased the truncation error in computations and FEM error at the higher modes.

Shi and Law [34] proposed modal strain energy based damage locating technique and the proposed method benefited from the differences between elemental modal strain energy of intact and damage structures. The authors considered effect of random error in terms of measurement noise in the mode shapes and systematic error in terms of errors from incomplete measurements in several damage cases on a simulated structure. The damage localization method was simulated on eight element cantilever beam model, two dimensional truss structure consisting of seventy eight two dimensional beam elements and experimental localization studied on a two storey steel plane frame structure modelled with eighteen two dimensional beam elements. Research indicated that the method was efficient on both single and multi damaged structures. The authors also concluded that measurement noise and incompleteness of measured modes have a strong effect on damage location result.

Chen et al. [35] used a non-destructive evaluation method for damage identification of ceramic candle filters which were made of a porous ceramic material. Experiments consisted of impact hammer excitation, sensing and signal processing of a ceramic candle with free-free boundary conditions. Modal strain energy of the elements was calculated with the help of FEA which was correlated with experimental data obtained from both intact and damaged structures. Damage was identified, both in location and severity, by comparing the differences in the modal strain energy. It was concluded that the non-destructive evaluation method was useful in detecting a damage zone along the filter span and it was beneficial for the stiffness estimation of the used candle filters.

Many of the methods related to modal strain energy require correlated FEM with experimental data and mass normalised mode shapes. The method applied by Cornell et al. [31] requires only displacement mode shapes of the structure before and after the damage. The research extended 1-D strain energy method to 2-D plate-like structures. Experimental analyses were conducted on an aluminium plate

with two saw-cut damages. Results indicated that 2-D strain energy method showed high tendency for false-positive results when compared to 1-D strain energy method's historical performance.

2.2.5 Residual Force Vector Method

Natural frequencies and mode shapes information as well as the mass and stiffness matrices information of the structure can be formulated in a one function named Residual Force Vector (RFV).

The equations governing the dynamics of a multi degree of freedom undamped system can be written in matrix form as follows:

$$[M_h]\{\ddot{X}(t)\} + [K_h]\{X(t)\} = \{F(t)\} \quad (2.1)$$

where $[M_h]$ and $[K_h]$ are $n \times n$ mass and stiffness matrices of the healthy system respectively, $\{X(t)\}$ is the displacement vector and $\{F(t)\}$ is the applied load vector.

j^{th} eigenvalue equation associated with Eqn. 2.1 is given by:

$$[K_h]\{\phi_j\} - \lambda_j[M_h]\{\phi_j\} = 0 \quad (2.2)$$

where λ_j is eigenvalue and $\{\phi_j\}$ is the corresponding normalized eigenvector. When damage occurs in a structure, Eqn. 2.2 takes the following form,

$$[K_d]\{\phi_{jd}\} - \lambda_{jd}[M_d]\{\phi_{jd}\} = 0 \quad (2.3)$$

where $[K_d]$, $[M_d]$ are damaged global stiffness and mass matrices, respectively. Both can be defined as the following;

$$[K_d] = [K_h] + [\Delta K] \quad (2.4)$$

$$[M_d] = [M_h] + [\Delta M] \quad (2.5)$$

where ΔK and ΔM are changes in stiffness and mass matrices, respectively. However, the amount of change on healthy matrices is not known. If the healthy stiffness and mass matrices are known and substituted into Eqn. 2.3, it will provide a residual vector;

$$\{R_j\} = [K_h]\{\phi_{jd}\} - \lambda_{jd}[M_h]\{\phi_{jd}\} \quad (2.6)$$

Eqn. 2.6 is the RFV of the j^{th} mode as every mode has one. Right hand side of the Eqn. 2.6 is known. Each row of the RFV corresponds to a single degree of freedom of the structure. Damages cause unexpected increase in value on a vector. Location of the increase on vector corresponds to damage location in terms of structural degree of freedom. Damage extend can be found by performing further analyses on the vector. For this purpose, the stiffness matrix of the structure $[K_d]$ can be expressed as a sum of element stiffness matrices multiplied by reduction factors associated with the each of the 'm' elements $\beta_i (i = 1, 2, \dots, m)$, resulting from the damage, as in the following forms;

$$[K_d] = \sum_{i=1}^m \beta_i \cdot [k]_i \quad (2.7)$$

$$[M_d] = \sum_{i=1}^m \beta_i \cdot [m]_i \quad (2.8)$$

where $[k]_i, [m]_i$ are the healthy element stiffness and mass matrices of i^{th} element, respectively. Values of β_i range from 0 to 1. The value of 1 on reduction factor indicates that element is undamaged, that of 0 implies completely damaged element, any other values distance to 1 corresponds to the percentage reduction of the function of interest. When Eqn. 2.7 and Eqn. 2.8 are substituted into Eqn. 2.6, definition of the residual vector becomes,

$$\{R_j\} = \sum_{i=1}^m \beta_i \cdot [k]_i \{\phi_{jd}\} - \lambda_{jd} \sum_{i=1}^m \beta_i \cdot [m]_i \{\phi_{jd}\} \quad (2.9)$$

and it will be 0, if only a correct set of β_i are introduced under available damaged modal information λ_{jd} and $\{\phi_{jd}\}$ of a particular mode j .

Farhat and Hemez [36] applied sensitivity based algorithm for updating mass and stiffness parameters of the structure in order to minimise norm of the RFV. The algorithm was capable of zooming on the detected error locations to minimize errors individually. This made a dramatic advantage on computational saving (i.e. CPU

time per iteration). Algorithm was applied both on cantilever beam and 2-D plane truss structures. It was concluded that the methodology had a potential to detect structural damage and modelling errors. Brown et al. [37] extended the aforementioned method [36] to lightly damped structures. Although the algorithm was able to correct errors by simulating mass and stiffness matrices simultaneously as Farhat and Hemez [36] did, this was limited to only two or three elements. The matrices were sensitive to both elastic modulus and density. The method was applied to different two models of a cantilever beam having 10 elements and 10 degree-of freedom and a cantilever truss structure consisting of eight half meters bays, 36 joints, five 1-lb and three 5-lb masses. The method demonstrated good results on simulated examples and showed its potential on damped structures.

Chen and Bicanic [38] performed damage detection by using both minimisation of residual vector (MRF) and minimisation of residual energy (MRE). Gauss-Newton Least Squares technique was used for minimisation procedures so that damage identification could be done by limited amount of measurements of incomplete modal data. Both algorithms were sensitive to elastic modulus reduction on element stiffness matrices and applied cantilevered plate with three different damage scenarios (i.e. different locations). Two mode shape data was used in the minimisation procedure and incomplete modal data was completed via mode shape expansion technique. It was concluded that both procedures provided promising results not only location detection but only severity detection of the damage.

Yang and Liu [1] compared minimum-rank elemental update (MREU) method and natural frequency sensitivity method with residual force equation. The authors used mode shape expansion technique, as Chen and Bicanic [38] did, to overcome incomplete measurement data problem. The method was applied on simply supported plane truss structure consisted of 23 elements and 11 nodes. Modal data was used as if only the first five nodes' information gathered and the rest was completed by using mode shape expansion technique. Damage was modelled as 10% stiffness reduction on elements and two single damage and one multi damage scenarios were used to validate the method. It was concluded that residual force vector could locate damages for measured and unmeasured locations as a preliminary manner. On the other hand, the method struggled to identify damage

when the measured mode shapes included large measurement noises. It was also stated that natural frequency sensitivity method and node residual force vector method could be a practical couple for damage detection only if node residuals were used to determine probable damage locations.

Zhao and Zhang [39] developed residual force vector assurance criterion (RFVAC) to eliminate the errors caused from mode shape expansion method and to improve efficiency. Three damage scenarios consisting of single and multi damage scenarios were simulated on a simply supported beam in order to validate the methodology. Authors concluded that preliminary damage localisation and severity detection could be done by the proposed method.

2.3 Optimisation Algorithms

Damage detection is a process of somehow fitting, estimating, simulating the damage state of the structure. Researchers achieved this process either by iterative manners or writing their own optimisation codes. Most common optimisation algorithms used in damage detection in the literature are Neural Networks (NN) and Genetic Algorithms (GA).

2.3.1 Artificial Neural Networks

Artificial Neural Network (ANN) is a mathematical model that is inspired by biological neural networks. Group of interconnected artificial neurons constitutes a neural network (NN) which processes information by philosophy of biological neurons. In most cases, artificial neural networks changes its structure based on internal and external information that is feed into during its learning phase. For damage detection purposes, due to ANNs being non-linear statistical data modelling tools, a significant database of information (i.e. damage scenarios) is needed [40].

One of the researches focusing on using NNs learning ability was Wu et al. [41]. In their study, NNs were trained with frequency response of the undamaged and damaged structure. The method was then applied on a three story frame having three degree of freedom. Damage on model was defined as stiffness

reduction on individual member. It was concluded that NNs were capable of damage identification in terms of location and extend. In Bakhary et al.'s [42] study; ANN was used in a statistical manner to take into account effect of uncertainties. Statistics of stiffness parameters were estimated by Rosenbluet's point estimate method [43] verified by Monte Carlo simulation. The methodology was applied on concrete slab in laboratory and steel portal frame model. Damage was modelled as percentage stiffness reduction on FEM. In the analyses, both modelling error and measurement noise were assumed to have normal distribution and zero means. It was concluded that the method was an effective one to decide whether the structure had damage or not.

Yam et al. [44] applied wavelet transform for damage feature extraction and feed-forward multilayer ANN for damage detection. The methodology was applied on crack detection on PVC sandwich plates. Crack on FEM were expressed using nodal discontinuity of two adjacent eight-node quadrangular elements. Single crack four different damage scenarios were examined by the algorithm. Although the obtained results showed that the detection accuracy reduced with decreasing crack length, the study was successful in localisation and prediction of damage extent.

Marwala and Hunt [45] developed a method named committee of neural network, which employed frequency response functions and modal data simultaneously. The method was applied to a FEM of aluminium cantilever beam consisting of five substructures and fifty elements. The NNs trained to be sensitive to 1-10% reduction of cross sectional area. By comparing the committee NNs results to frequency response function and modal property based fault identification methods it was concluded that the committee gave less averaging error, less variance and was able to diagnose multi faults.

Şahin [13] also applied feed-forward multilayer ANN for damage identification on laminated cantilever composite, steel and sandwich beam structures. Damage on laminated composite beam was modelled as a reduction in stiffness, on steel beam as a local thickness reduction and on sandwich beam as removing of elements on FEM. FEA with different damage scenarios were conducted in order to train ANN. In his thesis, ANN was fed by features comprising reduction in natural frequencies, maximum absolute differences in curvature mode shapes and

their corresponding locations. It was concluded that feeding ANN with three features instead of one, made it to provide more accurate results both on noise free and noise-polluted cases.

2.3.2 Genetic Algorithms

Genetic Algorithm (GA) is a search method based on the idea of Darwin's theory of survival of the fittest. Natural selection according to Darwin's theory is that '...any being, if it vary slightly in any manner profitable to itself... will have a better chance of surviving'. His concept of survival affects '...not only the life of the individual, but success in leaving progeny' [46]. GA simulates Darwin's theory numerically, either binary coded or real. Binary-coded GA decodes the binary variables prior to each iteration. Real-coded GA does not spend time for decoding, makes it faster. Binary-coded GA has limit of precision, while real-coded GA works with the machine precision.

To make analogy between genetics and GA;

- Each gene in genetics corresponds to a variable in GA,
- Chromosome in genetics is a group of genes, so is in GA. Number of genes in chromosome is specified by a number of the variables in the optimisation problem. Each chromosome in GA also refers to a possible solution of the problem.
- Population in GA which is a set of chromosomes and dimension of which is pre-defined by the user in the algorithm.

Generation of population and searching for a solution in GA is determined by characteristic parameters, such as selection, genetic operators and evolve [6]. GA starts with random initial population. Chromosomes in population are evaluated based on the objective function, so the following population is created by a selection process, meaning that chromosomes with higher fitness have a higher probability to survive. There are three main selection processes namely; roulette wheel [47], tournament [48] and normalized geometric [6]. Randomly paired chromosomes created by selection process. Each paired of chromosomes are named as parents. For the second level of GA process; these pairs are processed by GA operators;

crossover and mutation. Crossover and mutation are applied to a certain extent of chromosomes with individual probability ratios. As a result, new pairs of children are created [49]. Crossover function mainly affects the performance of the GAs and some of the crossover functions are namely; single point, two point [49], arithmetic and heuristic [50]. The mutation operation makes random changes in a chromosome in order to create a child. Mutation avoids losing whole information coming from the heritage, however, increases randomness while tracing the solution space. Population generation procedure is repeated until the convergence criterion/criteria is/are succeeded.

Chou and Ghaboussi [51] used static measurements of displacements at few degrees of freedom and residual force in the system of equilibrium equations for objective function so as to formulate damage detection as an optimisation problem. Binary-coded GA was selected as a solver for the problem. The method was applied on statically indeterminate and determinate truss bridges for validation. Damage was modelled as axial stiffness reduction in FEM. It was concluded that the method was capable of damage identification in terms of location and extent.

One of the earliest researches using RFV as an objective function on binary-coded GA was performed by Marace and Surace [4]. In their study, GA was used in a model updating manner. RFV was formulated for a linear undamped structural dynamic system. The objective function was maximised via taking the RFV term in denominator and feeding the RFV equations with six numbers of modes. The method was applied on both truss structure and cantilever beam. Damage was modelled on FEM as bending stiffness reduction. It was concluded that the method provided promising results about damage location and extent with a reasonable degree of accuracy. Hao et al. [15] used real-coded GA also in a model updating manner. Frequency changes, mode shape changes and combination of two were used as an objective function to minimise. The method was applied on aluminium cantilever beam and one-span steel portal frame. Damages were modelled as stiffness reduction on FEM. The authors concluded that real-coded GA gave better damage detection results than the conventional optimisation method.

Ostachowicz et al. [52] proposed localisation of concentrated mass on isotropic plates by means of GA. First four natural frequency changes were used as features

and formulated as objective function to be minimized. It was concluded that the method was accurate for finding location and value of the concentrated mass. Meruane and Heylen [6] also used GA for identification of damage. Different objective functions were selected based on frequencies, mode shapes, strain energy and frequency response functions. To avoid false damage detection, a penalization term was added on objective functions. The method was applied on three-dimensional space frame structure and results were compared with Inverse Eigen sensitivity method (IESM) and Response function method (RFM). The FEM was conducted on Matlab with 3-D truss elements. The damage was modelled as percentage stiffness reduction on elements. Removing or replacing a bar was also considered as mass reduction. The authors concluded that GA provided more accurate results than conventional optimisation methods and GA was successful under experimental noise and numerical errors.

As a conclusion of the literature review, in this thesis, a combined genetic algorithm and non-linear optimisation system is designed in order to combine GA search capability in whole solution space and convergence efficiency of the local optimiser. In order to increase the effectiveness of using more than one feature such as; natural frequencies and corresponding mode shapes simultaneously, residual force vector is also used as an objective function of the optimisation system which is aiming at single or multi damage cases on beam-like structures modelled by using both 1-D and 2-D approaches.

CHAPTER 3

FINITE ELEMENT MODELLING AND ANALYSIS

Finite element analysis (FEA) is designed for rapid engineering analyses which can be performed on computers. It procures this speed increase in analysis due to the fact that FEA uses the known properties of standard geometric shapes, i.e., finite elements. Wide range of structural analysis can be performed by FEA, such as; static displacement and stress, natural frequencies and mode shapes, forced harmonic response amplitude and dynamic stress, etc. Therefore, FEA can provide dynamic properties of structures, including natural frequencies and corresponding mode shapes [8], which are the features for damage detection algorithm where RFV was used. In this chapter, since model-dependent vibration-based analyses are performed and considered in this thesis, FEMs are validated and damage modelling style on FEM will be explained considering both intact and damaged structures.

3.1 Finite Element Modelling of Intact Structure

This part consists of the validation of the FEMs by comparison to both classical beam theory and a benchmark article results in 1-D modelling and its extension to 2-D.

3.1.1 1-D Beam Element Approach for Intact Structure

Due to having closed form solution of modal analysis and having an application [10] of it in the literature, uniform isotropic cantilever steel beam (Figure 3.1) with dimensions 1000mm × 50mm × 25mm is chosen as an intact model to analyse with FEs. Structural properties of the beam are also given in Table 3.1.

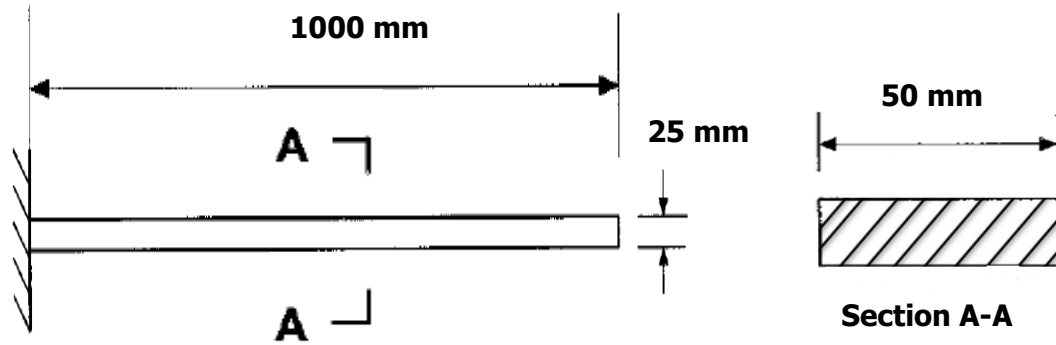


Figure 3.1. Geometry of the cantilevered beam

Table 3.1. Structural properties of the beam

Steel		
Density (ρ)	7827	kg/m^3
Young's Modulus (E)	2.06×10^{11}	Pa
Length (L)	1.00	m
Moment of Inertia (I)	6.51×10^{-8}	$kg.m^2$
Cross-sectional Area (A)	1.25×10^{-3}	m^2
Mass per unit length (m)	9.78	kg/m

The first five out of plane bending natural frequencies of the cantilever beam is calculated theoretically by using Eqn. 3.1 [53]. Results are also tabulated in Table 3.2.

$$\omega_n = \frac{\lambda_i^2}{2\pi L^2} \left(\frac{EI}{m} \right)^{1/2} \quad m = \rho A \quad (3.1)$$

where λ_i and ω_n are boundary condition dependent parameter and natural frequency of the structure, respectively.

Table 3.2. First five natural frequencies (ω_n) of intact cantilever beam (Theoretical Solution)

Mode No	λ_i [rad/s]	ω_n [Hz]
1	1.88	20.72
2	4.69	129.84
3	7.85	363.56
4	11.00	712.42
5	14.14	1177.69

Package software, MSC[®]/PATRAN, is used for modelling of the structure [54]. The model is created with Bar2 elements. Cantilever boundary condition is obtained by fixing six degrees of freedom of the related node. Different mesh densities are studied in order to select the optimum one, i.e. minimum computational source with reasonable accuracy. And the criterion for the accuracy is of percentage difference from the analytical data and it is given in Eqn. 3.2.

$$\text{Percentage Difference} = \frac{FEA - \text{Analytical Data}}{FEA} \cdot 100 \quad (3.2)$$

Table 3.3. First five natural frequencies of intact cantilever beam (FEA) with changing mesh densities

FEM		FEM		FEM	
(BAR2 10 Elements)		(BAR2 15 Elements)		(BAR2 100 Elements)	
ω_{n_h} [Hz]	%Difference	ω_{n_h} [Hz]	%Difference	ω_{n_h} [Hz]	%Difference
20.62	-0.50	20.67	-0.24	20.71	-0.04
127.47	-1.86	128.58	-0.98	129.47	-0.28
352.04	-3.27	357.09	-1.81	361.15	-0.67
678.79	-4.95	692.69	-2.85	703.85	-1.22
1100.75	-6.99	1131.27	-4.10	1155.43	-1.93

[Difference is calculated with Eqn. 3.2 and ω_{n_h} represents the natural frequencies of the healthy beam.]

Beam model with 15 elements and 16 nodes is selected due to providing results with reasonable degree of accuracy and to correlate with number of elements with Friswell's study [10] which is chosen as a benchmark. Figure 3.2 (a) shows the cantilever beam FEM isotropic view with beam elements and Figure 3.2 (b) shows the element numbering of FE and top view of the model. Msc. Nastran[®] uses 3-D beam element model which has 6 degrees of freedoms per node. Therefore, model consists of 90 degrees of freedoms with 16 nodes in total.

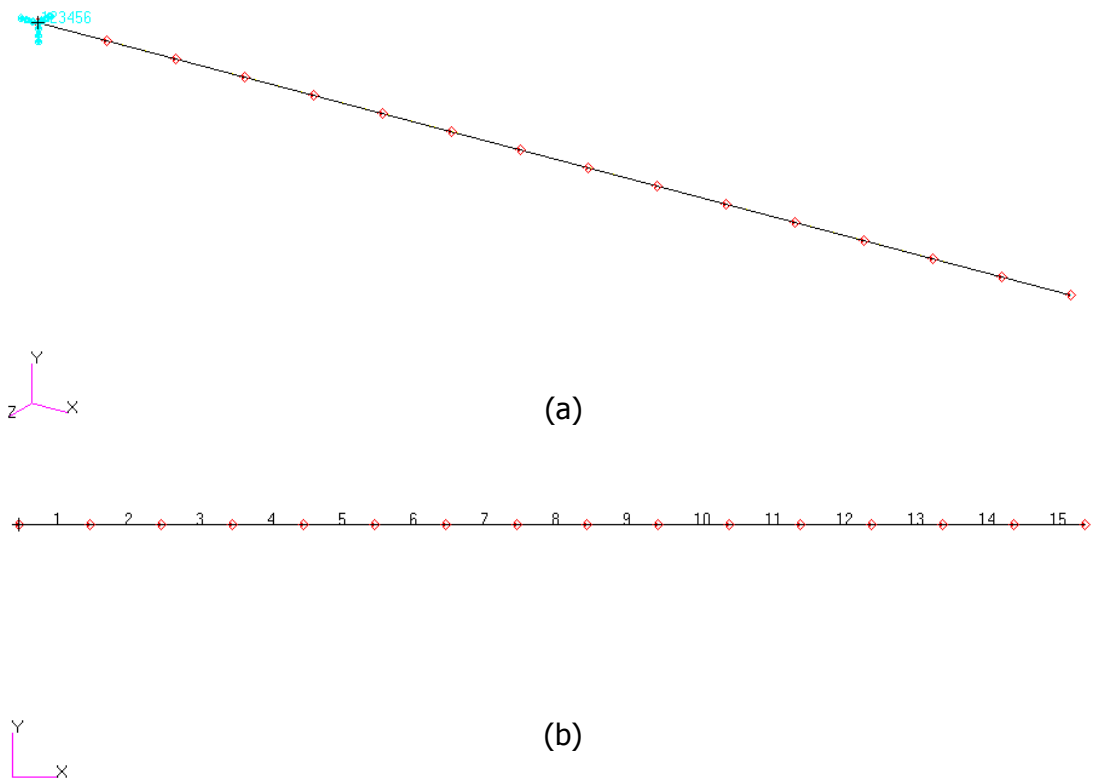


Figure 3.2. Cantilever beam bar2 element model (a) Isotropic view (b) Top view with element numbering*

*Boundary conditions are not shown on Figure 3.2 (b) to avoid confusion with the element numbering, the root of the beam is the outer most left hand side of the Figure 3.2 (b) which is closer to the Element Number 1.

If the Friswell's [10] FEA data is compared with the 15 elements cantilever beam model's modal analysis data, the following results in Table 3.4 are obtained.

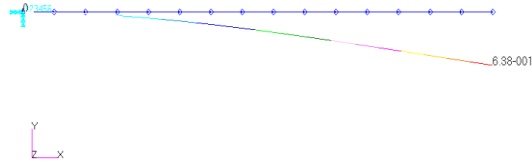
Table 3.4. Comparison of natural frequencies of FEA [10] and 15 element-cantilever-beam model to analytical one

FEA data [10]		15 beam elements	
ω_{n_h} [Hz]	% Difference	ω_{n_h} [Hz]	% Difference
21.00	1.34	20.67	-0.24
131.30	1.11	128.58	-0.98
367.70	1.13	357.09	-1.81
720.70	1.15	692.69	-2.85
1191.70	1.18	1131.27	-4.10

[Difference is calculated with Eqn. 3.2]

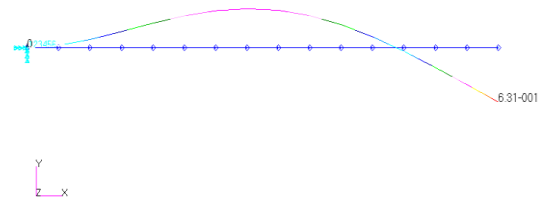
The first five out of plane bending modes (Figure 3.3) are used as damage feature in the preliminary analyses. The obtained mode shapes are identified with mode numbers, i.e. the way and the order they appear in FE software, and the corresponding out of plane bending mode number which are also given in parenthesis. Out of plane bending modes are used due to ease of measuring them experimentally and comparing by literature examples [10]. The corresponding five mode shapes show different sensitivities to damages that are at different locations with different severities. Although the first five modes are considered at the beginning of the study, the aim is to detect damage by using minimum possible information coming from vibration-based analysis data.

Fringe: Default, A1 Mode 1 : Freq. = 20.668, Eigenvectors, Translational, Magnitude, (NON-LAYERED)
Deform: Default, A1 Mode 1 : Freq. = 20.668, Eigenvectors, Translational.



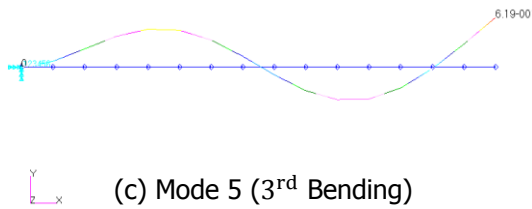
(a) Mode 1 (1st Bending)

Fringe: Default, A1 Mode 3 : Freq. = 128.58, Eigenvectors, Translational, Magnitude, (NON-LAYERED)
Deform: Default, A1 Mode 3 : Freq. = 128.58, Eigenvectors, Translational.



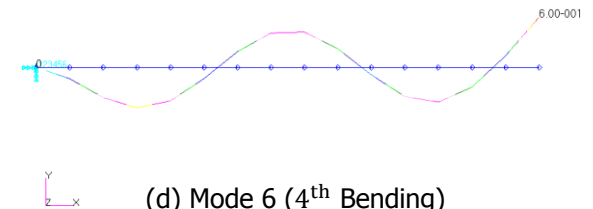
(b) Mode 3 (2nd Bending)

Fringe: Default, A1 Mode 5 : Freq. = 357.09, Eigenvectors, Translational, Magnitude, (NON-LAYERED)
Deform: Default, A1 Mode 5 : Freq. = 357.09, Eigenvectors, Translational.



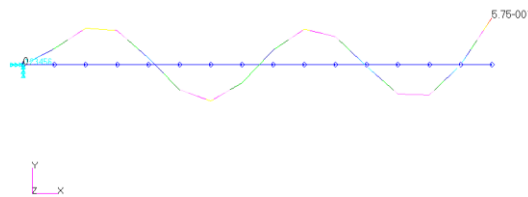
(c) Mode 5 (3rd Bending)

Fringe: Default, A1 Mode 6 : Freq. = 692.69, Eigenvectors, Translational, Magnitude, (NON-LAYERED)
Deform: Default, A1 Mode 6 : Freq. = 692.69, Eigenvectors, Translational.



(d) Mode 6 (4th Bending)

Fringe: Default, A1 Mode 8 : Freq. = 1131.3, Eigenvectors, Translational, Magnitude, (NON-LAYERED)
Deform: Default, A1 Mode 8 : Freq. = 1131.3, Eigenvectors, Translational.



(e) Mode 8 (5th Bending)

Figure 3.3. The first five out of plane bending mode shapes of the cantilevered beam obtained from FEA (1-D modelling)

3.1.2 2-D Shell Element Approach for Intact Structure

In order to show 1-D modelling extension to 2-D and to correlate it, 15×1 (Model-I) element configuration is selected for preliminary 2-D analysis. Later, this model will be the basis for 2-D beam-like structures with multi damage cases. The mesh density checks were also performed for this model as well and showed in Table 3.5.

Table 3.5. First five natural frequencies of intact cantilever beam (FEA) with changing mesh densities

FEM		FEM		FEM	
(QUAD4 10x1)		(QUAD4 15x1)		(QUAD4 100x6)	
ω_{n_h} [Hz]	%Difference	ω_{n_h} [Hz]	%Difference	ω_{n_h} [Hz]	%Difference
20.74	0.13	20.75	0.15	20.76	0.18
128.42	-1.10	129.19	-0.50	129.76	-0.06
355.65	-2.22	359.23	-1.20	362.00	-0.43
688.84	-3.42	698.23	-2.03	705.69	-0.95
1123.78	-4.80	1143.41	-3.00	1158.81	-1.63

[Difference is calculated with Eqn. 3.2]

The selected model's isometric view and the top view with element numberings are presented in Figure 3.4 (a) and Figure 3.4 (b) respectively. This element identification is also identical with the damage location labelling.

Quad4 elements are also specified as 6 degrees of freedom per node. Cantilever boundary condition is obtained by fixing 6 degrees of freedom at root, which can be seen on Figure 3.4 (a-b). The model consists of 32 nodes and therefore, both structure's mass and stiffness matrices have 180 degrees of freedom.

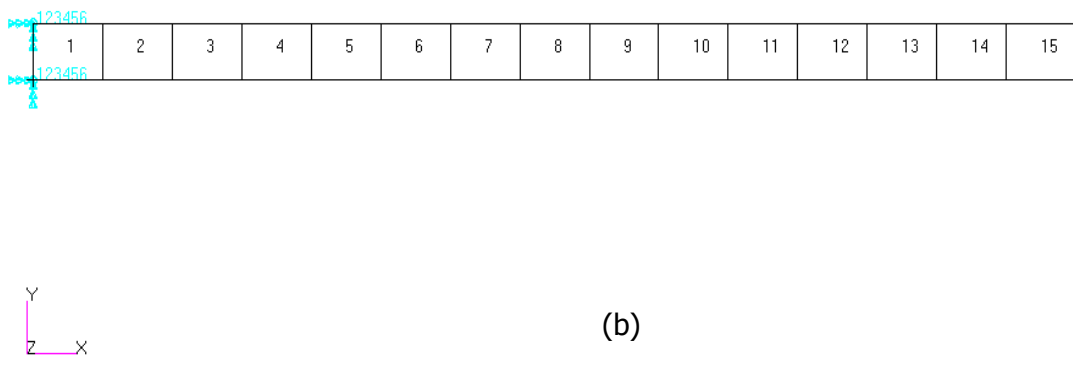
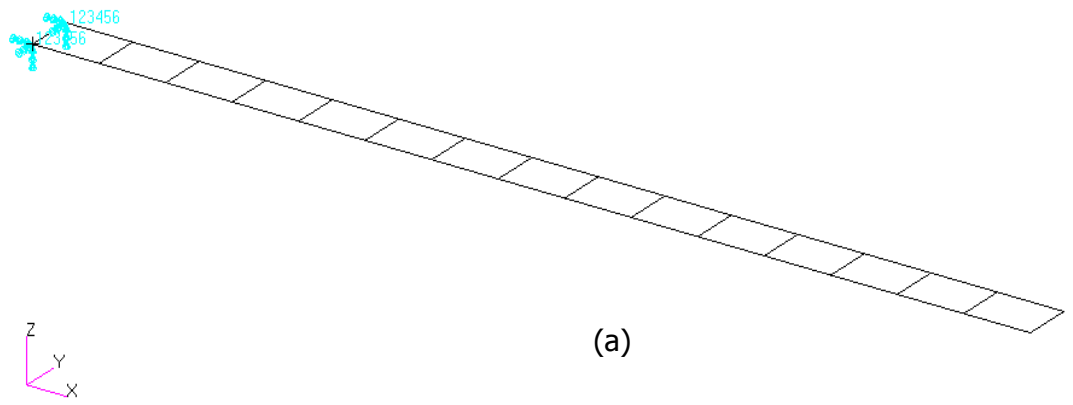


Figure 3.4. Cantilever beam quad4 element model (Model-I) (a) Isometric view
 (b) Top view with element numbering

Mode shapes that are used in analysis are obtained and plotted in Figure 3.6. The obtained mode shapes are identified with mode numbers, i.e. the way and the order they appear in FE software, and the corresponding out of plane bending mode number which are also given in parenthesis.

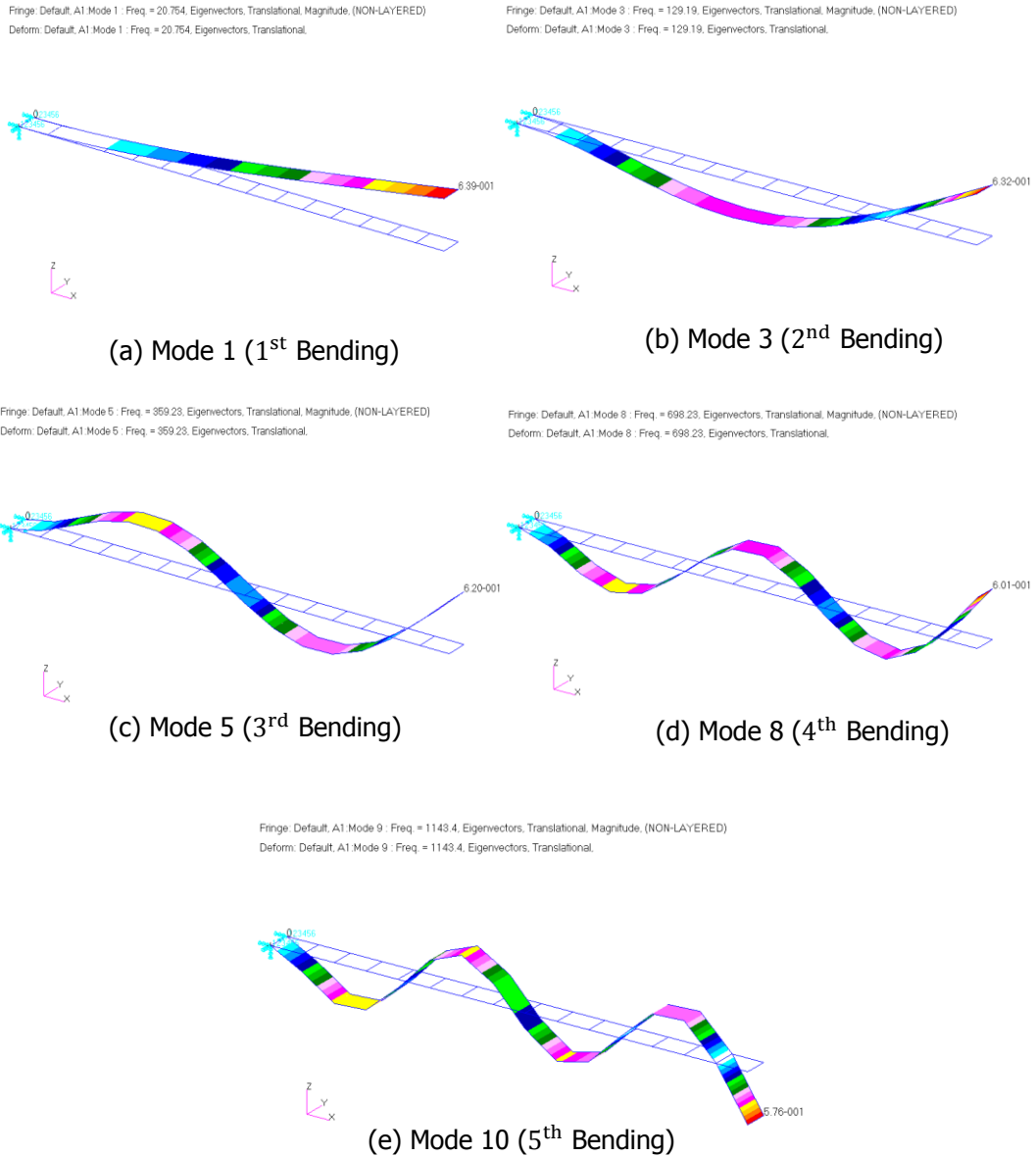
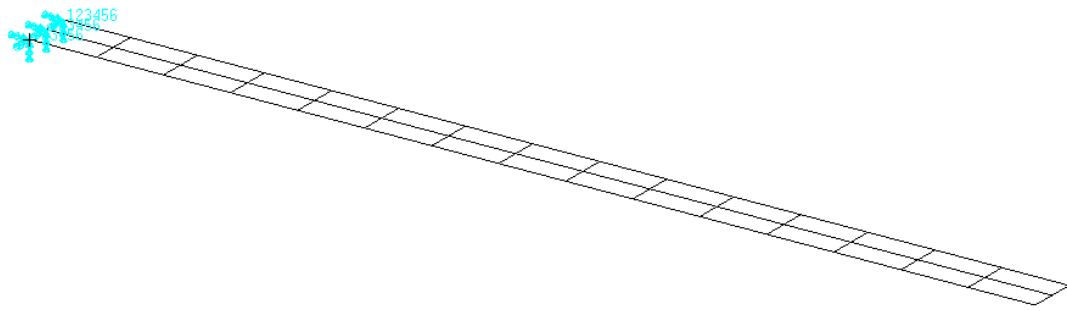
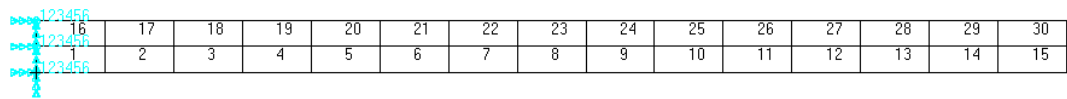


Figure 3.5. The first five out of plane bending mode shapes of the cantilevered beam obtained from FEA (2-D modelling, Model-I)

In order to verify the extension of the model to 2-D, Model-I is taken one step further and 15x2 quad4 element configuration is used in the modelling (Figure 3.6). After performing modal analysis with Model-II, the results are obtained (Figure 3.7) and tabulated in Table 3.6.



(a)



(b)

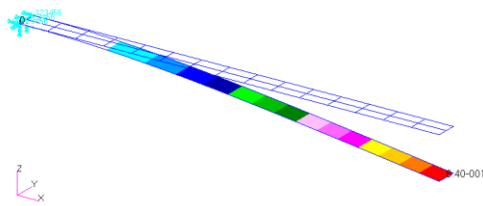
Figure 3.6. 2-D 2x15 Shell Element Model (Model-II) (a) Isotropic-view
(b) Top-view with element numbering

Table 3.6. First five natural frequencies of intact cantilever beam
(FEA of Model-II)

Theoretical ω_{n_h} [Hz]	FEM (QUAD4 15x2 Elements) ω_{n_h} [Hz]	% Difference
20.72	20.77	0.22
129.84	129.26	-0.45
363.56	359.45	-1.14
712.42	698.78	-1.95
1177.69	1144.54	-2.90

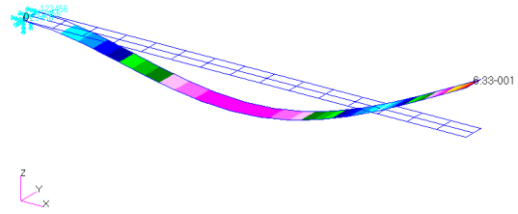
[Difference is calculated with Eqn. 3.2]

Fringe: Default, A1 Mode 1 : Freq. = 20.865, Eigenvectors, Translational, Magnitude, (NON-LAYERED)
Deform: Default, A1 Mode 1 : Freq. = 20.865, Eigenvectors, Translational.



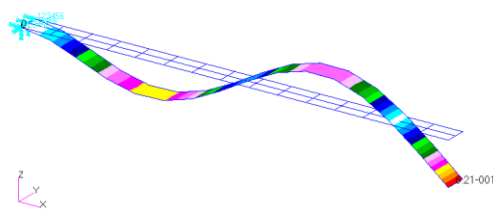
(a) Mode 1 (1st Bending)

Fringe: Default, A1 Mode 3 : Freq. = 129.93, Eigenvectors, Translational, Magnitude, (NON-LAYERED)
Deform: Default, A1 Mode 3 : Freq. = 129.93, Eigenvectors, Translational.



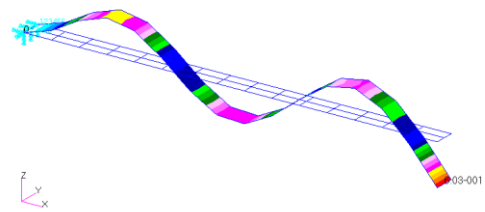
(b) Mode 3 (2nd Bending)

Fringe: Default, A1 Mode 5 : Freq. = 361.71, Eigenvectors, Translational, Magnitude, (NON-LAYERED)
Deform: Default, A1 Mode 5 : Freq. = 361.71, Eigenvectors, Translational.



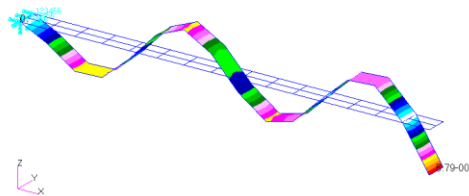
(c) Mode 5 (3rd Bending)

Fringe: Default, A1 Mode 7 : Freq. = 704.4, Eigenvectors, Translational, Magnitude, (NON-LAYERED)
Deform: Default, A1 Mode 7 : Freq. = 704.4, Eigenvectors, Translational.



(d) Mode 7 (4th Bending)

Fringe: Default, A1 Mode 9 : Freq. = 1156.5, Eigenvectors, Translational, Magnitude, (NON-LAYERED)
Deform: Default, A1 Mode 9 : Freq. = 1156.5, Eigenvectors, Translational.



(e) Mode 9 (5th Bending)

Figure 3.7. The first five out of plane bending mode shapes of the cantilevered beam obtained from FEA (2-D modelling, Model-II)

3.2 Finite Element Modelling of Damaged Structure

Two different damage types are modelled in this thesis, namely; impact and saw-cut types. While impact damage in FEM is defined as percentage reduction of elastic modulus, saw-cut type is defined as a percentage reduction of thickness of the selected elements of the structure. The effects of changing damage locations and severities on natural frequencies of the structure are also examined in this section. While performing these analyses, mode order changes due to effect of damage is also taken into account and related graphs are plotted accordingly.

3.2.1 1-D Beam Element Approach for Damaged Structure

In this study, location of the damage is defined in terms of the corresponding element location. Element identification for the damaged structure is defined as it is given in Figure 3.2 (b) for 1-D modelling. To apply damage conditions on individual elements, element properties in FEM are assigned separately. The "damage" is defined as the percentage reduction on predefined (i.e. either elastic modulus or thickness) properties of FEM.

3.2.1.1 Impact Type Damage Modelling

Impact type damage is modelled as percentage reduction of elastic modulus of an individual element in FEM. To test the damage detection algorithm; this damage modelling procedure is followed for all elements with various damage severities. Damage severities are covered from 10% reduction of predefined properties as minimum to 70% reduction as maximum by 10% increments. Therefore, seven different damage severities on number of elements (i.e. 15 different elements along the span of the beam) provide 105 different damage scenarios in total to check the damage detection system. However, for multi damage cases, a random damage creation routine is written in order to create damage scenarios which are twice the number of elements and every individual element involves scenarios with two different damage severity cases. In this section, these damage scenarios will be exemplified.

3.2.1.1.1. Single Impact Type Damage

Damage assigned on an individual element is named as single damage. Figure 3.8 is an example of single impact damage, by showing damage assigned on the 3rd element of the model.

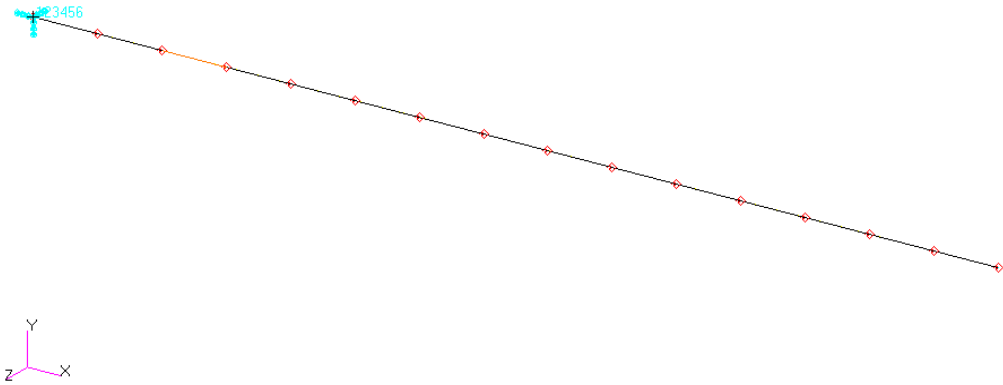


Figure 3.8. Definition of damage location in bar2 elements

On above figure, damage is introduced to the 3rd element of the model by reducing its elastic modulus by 40% of its intact value. As all the other elements' properties are separately defined, they are not affected from this reduction. After performing the modal analysis, the natural frequencies and the corresponding first five out of plane bending modes of the new structures are tabulated in Table 3.7.

Table 3.7. First five natural frequencies of single impact type damaged cantilever beam; Damage on the 3rd element with 40% severity

Intact Beam	Damaged Beam	% Difference
$\omega_{n_h} [Hz]$	$\omega_{n_d} [Hz]$	
20.67	19.66	4.90
128.58	127.98	0.47
357.09	355.27	0.51
692.69	677.92	2.13
1131.27	1100.14	2.75

Percentage differences are calculated by using Equation 3.3 as;

$$\text{Percentage Difference in FEA} = \frac{FEA_h - FEA_d}{FEA_h} \cdot 100 \quad (3.3)$$

where subscripts h and d stand for healthy and damaged respectively. In other words, and ω_{n_h} represents the natural frequencies of the healthy structure and ω_{n_d} stands for the damaged structure's natural frequencies.

If the same procedure which was conducted on the 3rd element is chased for the 8th element (Figure 3.9) with a 60% reduction of elastic modulus and for the 13th element (Figure 3.10) with a 20% reduction of elastic modulus, the following results are obtained after performing a modal analysis on the damaged models and tabulated in Table 3.8 and Table 3.9 respectively.

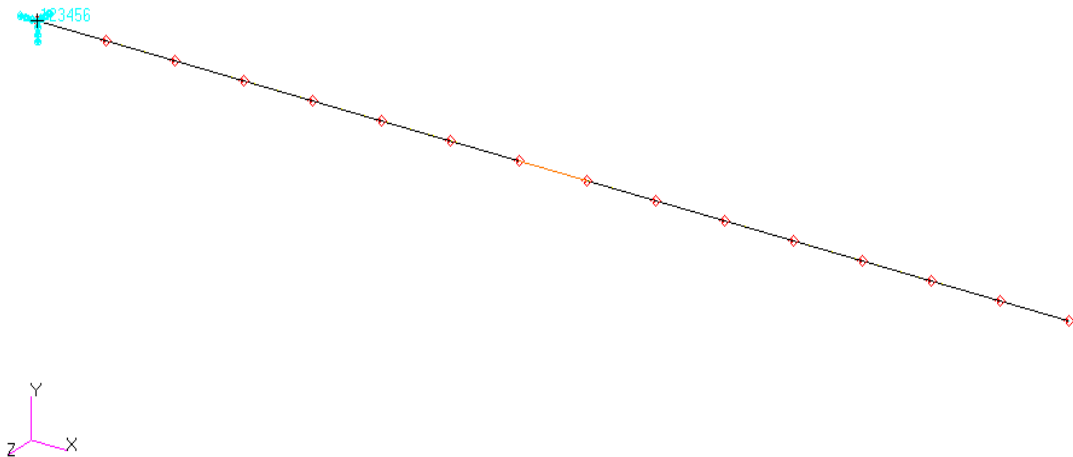


Figure 3.9. Damage located on the 8th element

Table 3.8. First five natural frequencies of single impact type damaged cantilever beam; Damage on the 8th element with 60% severity

Intact Beam	Damaged Beam	% Difference
ω_{n_h} [Hz]	ω_{n_d} [Hz]	
20.67	20.20	2.27
128.58	117.77	8.41
357.09	355.92	0.33
692.69	645.68	6.79
1131.27	1118.89	1.09

[Difference is calculated with Eqn. 3.3]

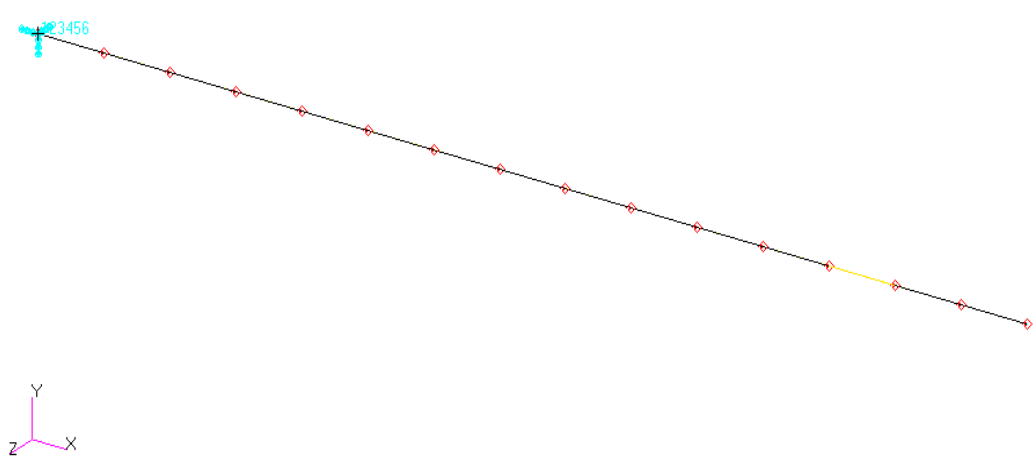


Figure 3.10. Damage located on the 13th element

Table 3.9. First five natural frequencies of single impact type damaged cantilever beam; Damage on the 13th element with 20% severity

Intact Beam	Damaged Beam	% Difference
ω_{n_h} [Hz]	ω_{n_d} [Hz]	
20.67	20.67	0.01
128.58	128.34	0.19
357.09	354.00	0.87
692.69	681.90	1.56
1131.27	1113.76	1.55

[Difference is calculated with Eqn. 3.3]

By comparing the results given in Table 3.8 and Table 3.9, it is found that all the modes are affected up to different extents regarding both the location and the severity of the damage. In case of examining one of the parameters, either damage severity or damage location, Figure 3.11 can be obtained in order to show the effects of changing in damage location on natural frequencies in the first five out of plane bending modes. In this particular case, the damage severity is modelled as 10% and its location is then changed to four different spatial locations along the span of the beam as 20%, 30%, 50% and 80% of the length of the beam which are measured from the root (i.e. cantilever end).

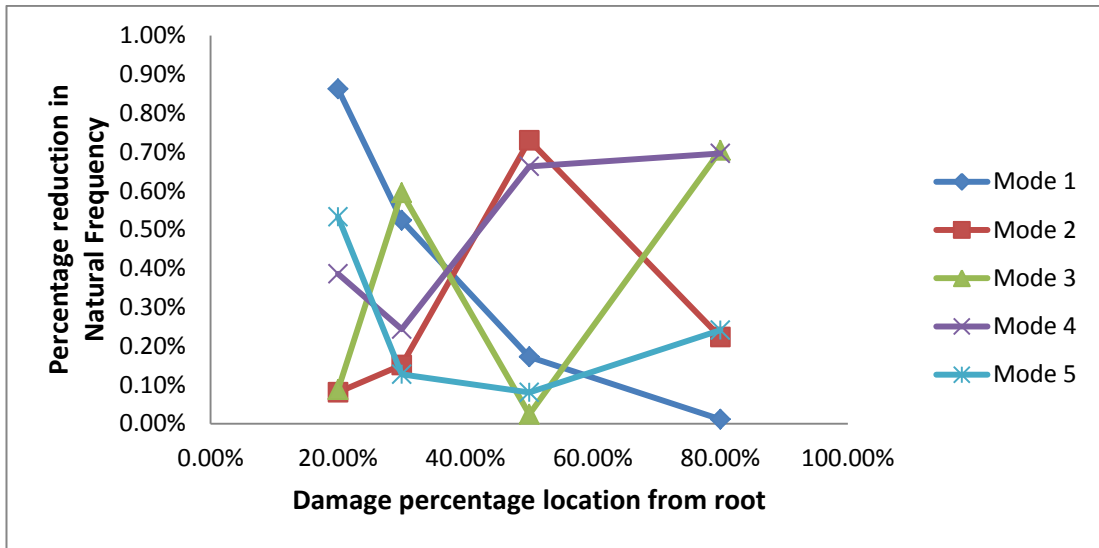


Figure 3.11. Effects of changing damage location on natural frequencies (sample case for 10% damage), 1-D Modelling

As it can be seen from the Figure 3.11 that the change in damage location affects natural frequencies in a different and varying manner regarding the mode of interest. If the damage location is kept constant as 50% and 20% and the effect of the damage severity is examined, Figure 3.12 and Figure 3.13 are then obtained. It can be interpreted from these two figures that different modes are sensitive to damages with different extents at different locations.

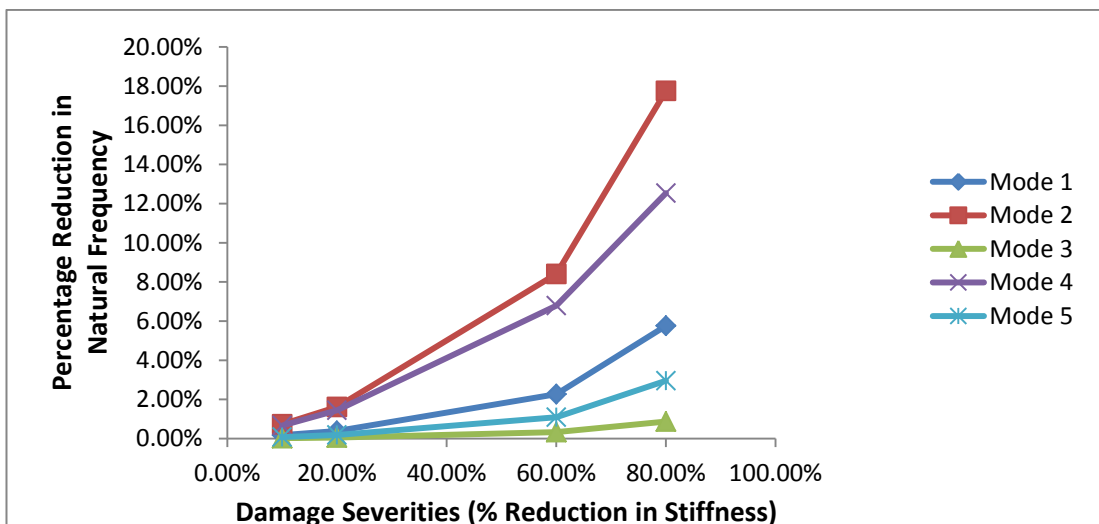


Figure 3.12. Damage at 50% location from the root with changing severities, 1-D Modelling

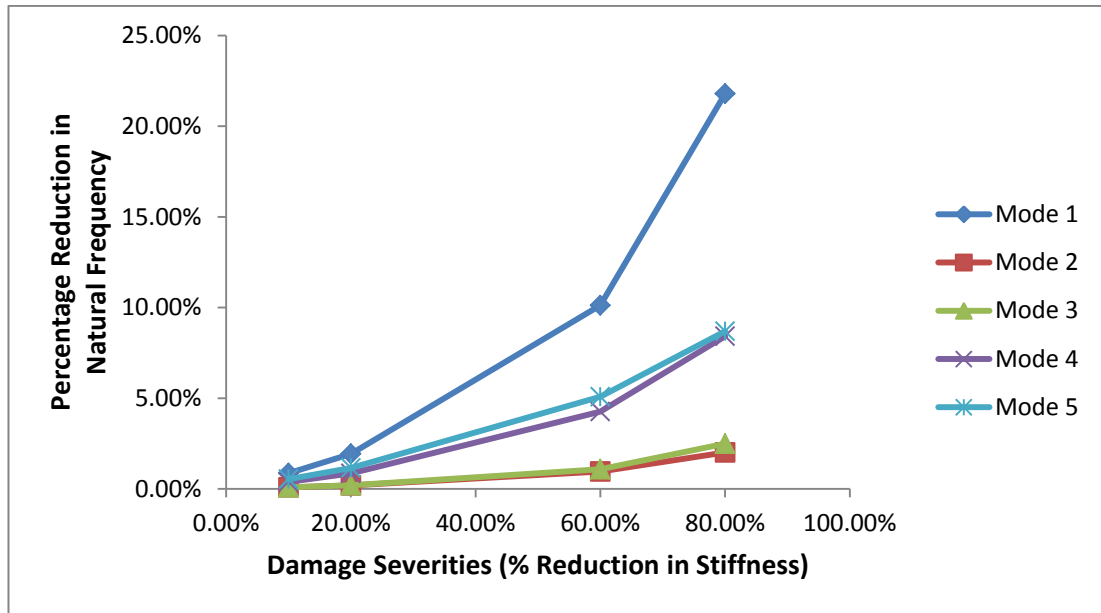


Figure 3.13. Damage at 20% location from the root with changing severities, 1-D Modelling

It can be concluded from above two figures that the percentage reduction effect on natural frequencies varies with changing damage location and severities. Any damage case on specific location and severity may have similar effects on natural frequencies to any other damage case at different location and different damage severity by making the damage detection problem a non-unique and inverse problem.

3.2.1.1.2. Multi Impact Type Damage

In order to test whether the damage detection algorithm works on multi damage cases or not, multi damage modelling on FEMs is then performed. This section is exemplification of some of these damage cases. The below is an example of a multi damage case where damages are created on both 3rd element with 50% severity and 12th element with 20% severity (Figure 3.14). After performing modal analysis on this damaged model, the results are obtained and tabulated in Table 3.10. Then another example of multi impact damaged scenario (Figure 3.15) is obtained where the damages are created on 7th and 12th elements with 30% severity and 60% severity, respectively. As it can be seen from Figure 3.15 that by

setting one damage location fixed with the case presented on Figure 3.14 and by letting the other free can change the effects of the damage on the structure's modal data remarkably (Table 3.11).

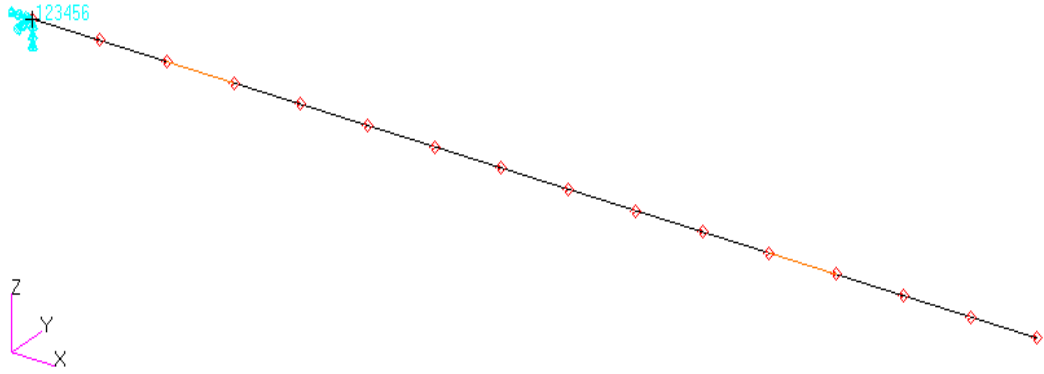


Figure 3.14. Damage located on the 3rd and the 12th elements

Table 3.10. First five natural frequencies of multi impact damaged cantilever beam; Damage on the 3rd element with 40% severity and the 12th element with 20% severity

Intact Beam $\omega_{n_h} [Hz]$	Damaged Beam $\omega_{n_d} [Hz]$	% Difference
20.67	19.65	4.92
128.58	127.34	0.97
357.09	349.83	2.03
692.69	667.87	3.58
1131.27	1093.86	3.31

[Difference is calculated with Eqn. 3.3]

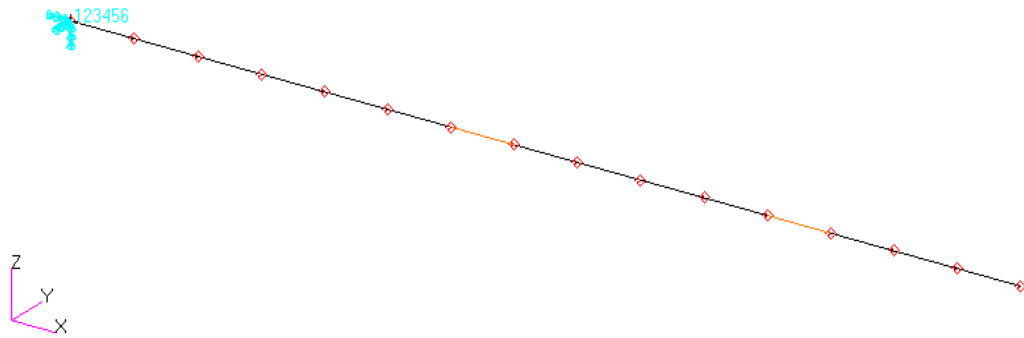


Figure 3.15. Damage located on the 7th and the 12th elements

Table 3.11. First five natural frequencies of multi impact damaged cantilever beam; Damage on the 7th element with 30% severity and the 12th element with 60% severity

Intact Beam $\omega_{n_h} [Hz]$	Damaged Beam $\omega_{n_d} [Hz]$	% Difference
20.67	20.43	1.15
128.58	122.23	4.94
357.09	324.37	9.16
701.01	638.77	8.88
1131.27	1083.43	4.23

[Difference is calculated with Eqn. 3.3]

Even if the multi damage case has two damaged elements, there might be plenty of damage scenarios that may reveal similar effects on the structure. Therefore, multi damage cases are also considered as the proof of the non-uniqueness of the damage detection problem. This brings the necessity of using more than one damage feature for the damage identification, i.e. not only spatial location but also damage severity.

3.2.1.2 Saw-cut Type Damage Modelling

Saw-cut type damage is modelled as percentage reduction of thickness of an individual element on FEM. The damage scenarios used to test the damage detection algorithm are taken as the same that performed in impact type damage. Therefore, damage modelling procedures for saw-cut damage are the same as the ones defined in section 3.2.1.1.

3.2.1.2.1. Single Saw-cut Type Damage

In this section, single damage assignment as percentage thickness reduction resembling saw-cut type damage is examined. One of the examples given below is a damage which is created on the 4th element.

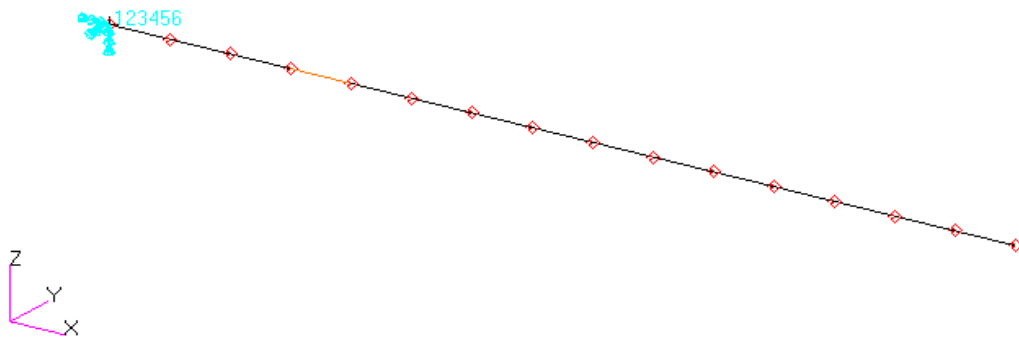


Figure 3.16. Damage located on the 4th element

Table 3.12. First five natural frequencies of single saw-cut damaged cantilever beam; Damage on the 4th element with 20% severity

Intact Beam $\omega_{n_i} [Hz]$	Damaged Beam $\omega_{n_d} [Hz]$	% Difference
20.67	19.55	5.40
128.58	128.93	-0.27
357.09	351.19	1.65
692.69	674.36	2.65
1131.27	1119.63	1.03

[Difference is calculated with Eqn. 3.3]

In Table 3.12, modal analysis results of the saw-cut damage scenario created on the 4th element with 20% severity are tabulated and it can be seen that there is barely any effect on the second natural frequency. If damage detection depends only on the 2nd out of plane bending mode than probably no damage would be identified. Figure 3.17 is an example of saw-cut damage, created on 8th element with 30% severity. For this case; as can be seen from Table 3.13, 3rd out of plane bending mode is barely affected from the damage and it is different from the one tabulated in Table 3.12.

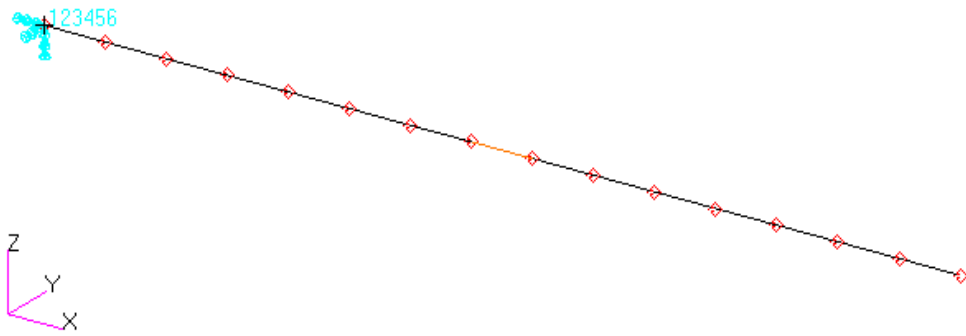


Figure 3.17. Damage located on the 8th element

Table 3.13. First five natural frequencies of single saw-cut damaged cantilever beam; Damage on the 8th element with 30% severity

Intact Beam $\omega_{n_h} [Hz]$	Damaged Beam $\omega_{n_d} [Hz]$	% Difference
20.67	20.16	2.45
128.58	118.03	8.21
357.09	356.47	0.17
692.69	650.08	6.15
1131.27	1124.68	0.58

[Difference is calculated with Eqn. 3.3]

Therefore, the damage effect on natural frequencies changes by varying damage locations and damage severities and the approach used in section 3.2.1.1.1 can also be used for the saw-cut damage types as well. For this purpose, the following figure (Figure 3.18) is obtained.

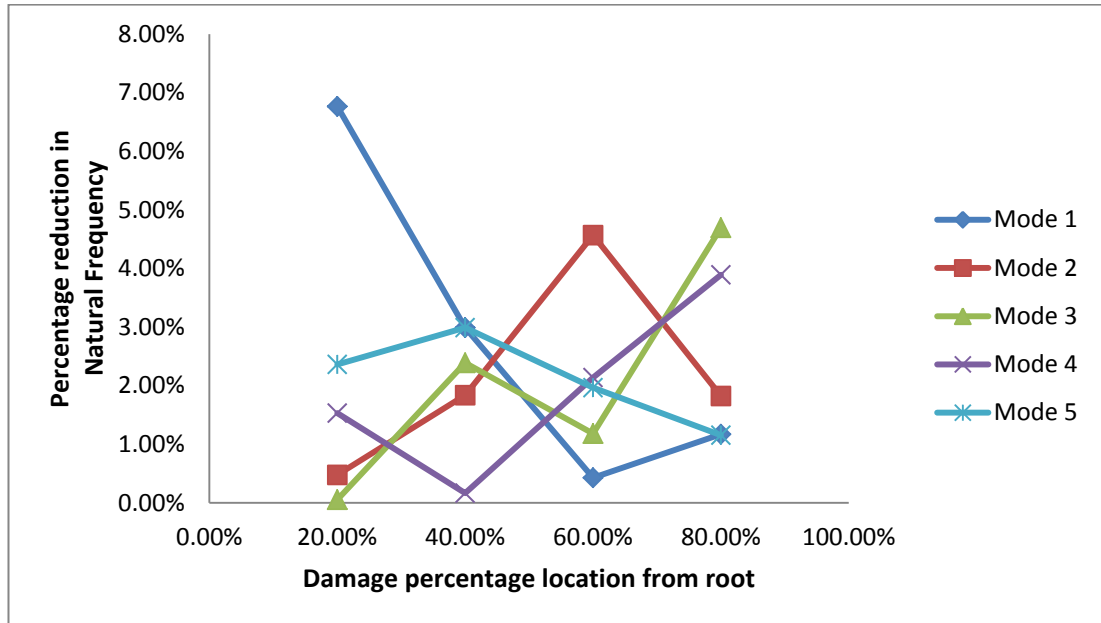


Figure 3.18. Effects of changing damage location on natural frequency (sample case for 20% damage), 1-D Modelling

Above figure is obtained by performing various numbers of modal analyses where the damage severity and the type are fixed as 20% and saw-cut type, respectively. As it can be seen from Figure 3.18 that all modes are affected in a varying manner for various damage locations. Following these, damage location is then fixed and changing damage severities are examined. Fixing damage location at 20% and 40% from the root provide results shown in the following two figures, Figure 3.19 and Figure 3.20.

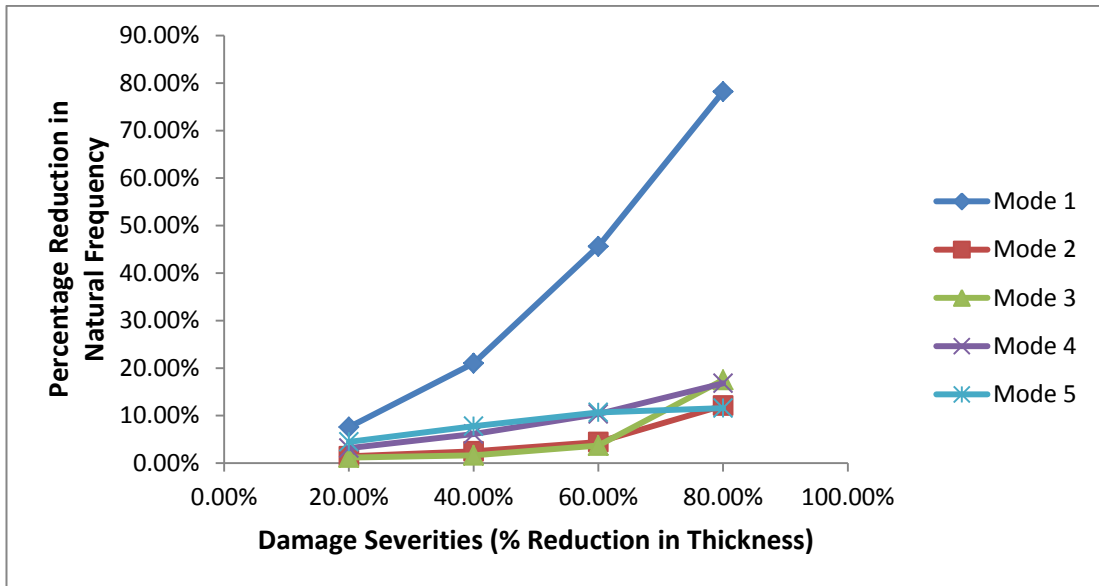


Figure 3.19. Damage at 20% location from root with changing severities, 1-D Modelling

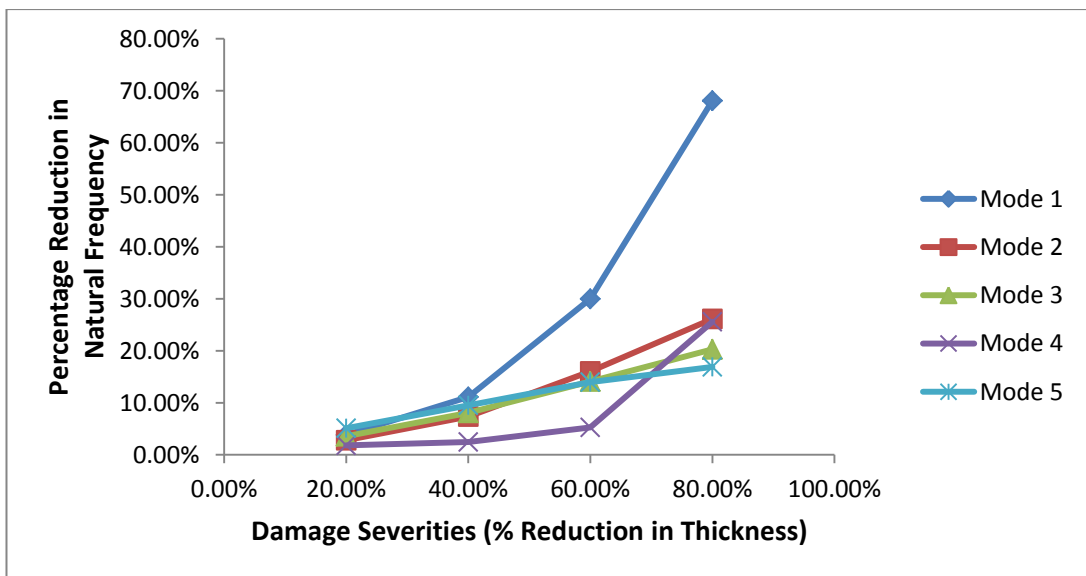


Figure 3.20. Damage at 40% location from the root with changing severities, 1-D Modelling

As it can be seen from the above two figures that in comparison with the figures obtained in Section 3.2.1.1.1 (i.e. for impact type damage analysis), same amount of saw-cut type damage makes an extreme effect on the reduction in natural frequencies.

3.2.1.2.2. Multi Saw-cut Type Damage

Damage for multi saw-cut type damage cases are created by following the same procedure in the single damage ones. Different from single damage case generation, two element properties are degraded in multi saw-cut type damages. Multi saw-cut damage scenarios are created by using the same algorithm which is used for multi impact type damages. One of the damage scenarios presented below is the one where damages are created on 2nd and 14th elements having the same severity as 10% (Figure 3.21). After performing the modal analysis for this damage case, the results are summarised in Table 3.14.

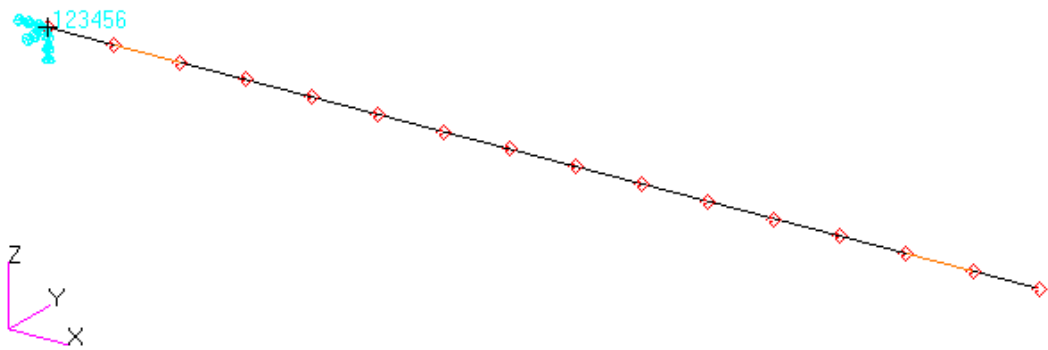


Figure 3.21. Damage located on the 2nd and the 14th elements

Table 3.14. First five natural frequencies of multi saw-cut damaged cantilever beam; Damage on the 2nd element with 10% severity and the 14th element with 10% severity

Intact Beam ω_{n_h} [Hz]	Damaged Beam ω_{n_d} [Hz]	% Difference
20.67	19.99	3.28
128.58	125.04	2.75
357.09	348.15	2.51
692.69	675.29	2.51
1131.27	1100.99	2.68

[Difference is calculated with Eqn. 3.3]

Further damage scenarios are also shown in Figure 3.22 where they can be created close to each other. The corresponding modal analysis aiming to find percentage reduction in natural frequencies is tabulated in Table 3.15. As it can be seen from the results tabulated in Table 3.15 that the damages nearly in middle of the span of the beam, such as on the 5th element and the 7th element with severe damages like 40% and 70% saw-cut type damages affect out of plane bending modes dramatically.

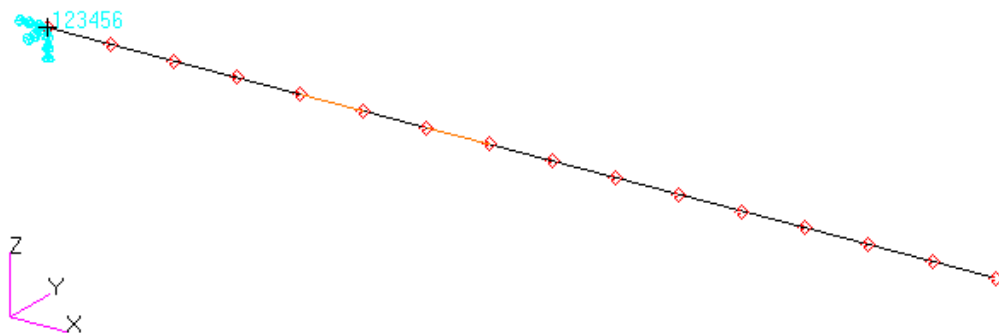


Figure 3.22. Damage located on the 5th and the 7th elements

Table 3.15. First five natural frequencies of multi saw-cut damaged cantilever beam; Damage on the 5th element with 40% severity and the 7th element with 60% severity

Intact Beam ω_{n_i} [Hz]	Damaged Beam ω_{n_d} [Hz]	% Difference
20.67	14.47	29.97
128.58	98.82	23.15
357.09	323.78	9.33
692.69	552.00	20.31
1131.27	1017.61	10.05

[Difference is calculated with Eqn. 3.3]

3.2.2 2-D Shell Element Approach for Damaged Structure

In this thesis, 2-D damages are created on two different models, which are namely Model-I (1x15 mesh density shown in Figure 3.4) and Model-II (2x15 mesh density shown in Figure 3.6). Single and multi damage scenario creation procedures/algorithms are the same as in 1-D case (see section 3.2.1.1) however due to being dependent on number of elements in the FEM, Model-II is tested twice the scenarios generated that of in the Model-I. Therefore, in this section, impact and saw-cut type damage samples are again categorised whether the damage is a single or a multi one.

3.2.2.1 Impact Type Damage Modelling

Impact type damage is created by following the same procedure as in 2-D FEM. Damage modelling is examined first as single and then multi damage cases in impact type damage modelling.

3.2.2.1.1. Single Impact Type Damage

As same procedure used in 1-D modelling is also followed here in 2-D models as well regarding the modelling of damage severities and their locations. Therefore, similar damage scenarios are created and in 2-D models for the damage detection analyses. In below figure (Figure 3.23), damage assignment on the 6th element in Model-I is presented. Damage is modelled as 40% reduction on elastic modulus of the corresponding element, i.e. the 6th element. After modal analysis is performed, the results are the obtained and then tabulated in Table 3.16.

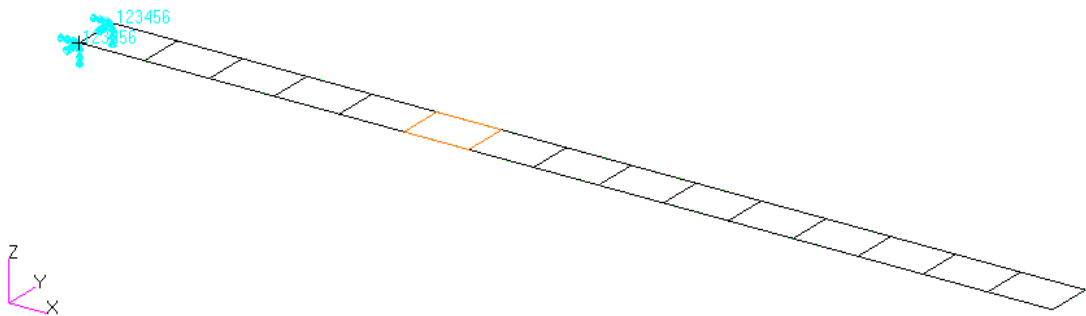


Figure 3.23. Damage located on the 6th element, 2-D Modelling, Model-I case

Table 3.16. First five natural frequencies of single impact damaged cantilever beam; Damaged on the 6th element with 40% severity

Intact Beam	Damaged Beam	% Difference
ω_{n_h} [Hz]	ω_{n_d} [Hz]	
20.75	20.30	2.17
129.19	126.49	2.09
359.23	350.04	2.56
698.23	696.14	0.30
1143.41	1109.85	2.93

[Difference is calculated with Eqn. 3.3]

Below (Figure 3.24) is an example of tip damaged beam with lightly impact damage (20% reduction) and after performing the modal analysis, the following results (Table 3.17) are obtained.

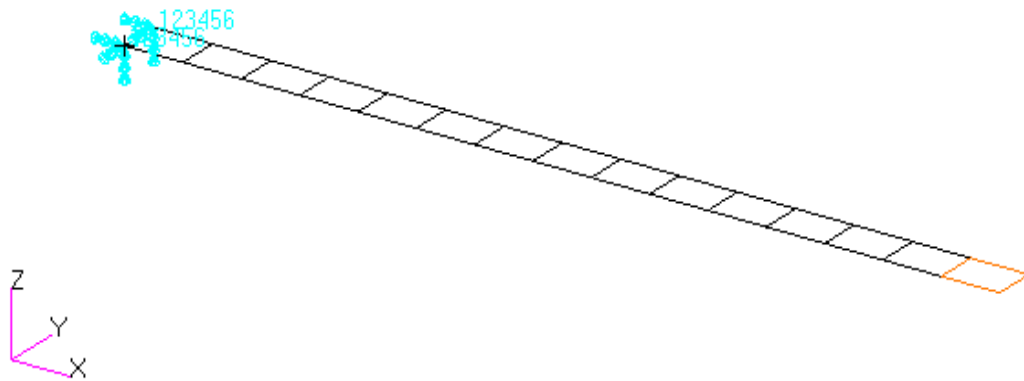


Figure 3.24. Damage located on the 15th element

Table 3.17. First five natural frequencies of single impact damaged cantilever beam; Damaged on the 15th element with 20% severity

Intact Beam	Damaged Beam	% Difference
ω_{n_h} [Hz]	ω_{n_d} [Hz]	
20.75	20.75	0.00
129.19	129.19	0.00
359.23	359.15	0.02
698.23	697.68	0.03
1143.41	1141.21	0.19

[Difference is calculated with Eqn. 3.3]

As it can be seen from Table 3.17, tip damage has no effect on both fundamental and the second natural frequencies. The higher modes are barely affected as well. If the natural frequency changes are examined by fixing the damage severity, as performed in 1-D modelling approach, the effects of changing damage location on the first five out of plane bending modes are obtained and presented in Figure 3.25 representing the case of 60% impact type damage. If the damage location is fixed on 20% and 60% from root and the effect of the change in severity of the damage on natural frequencies are examined, Figure 3.26 and Figure 3.27 are obtained.

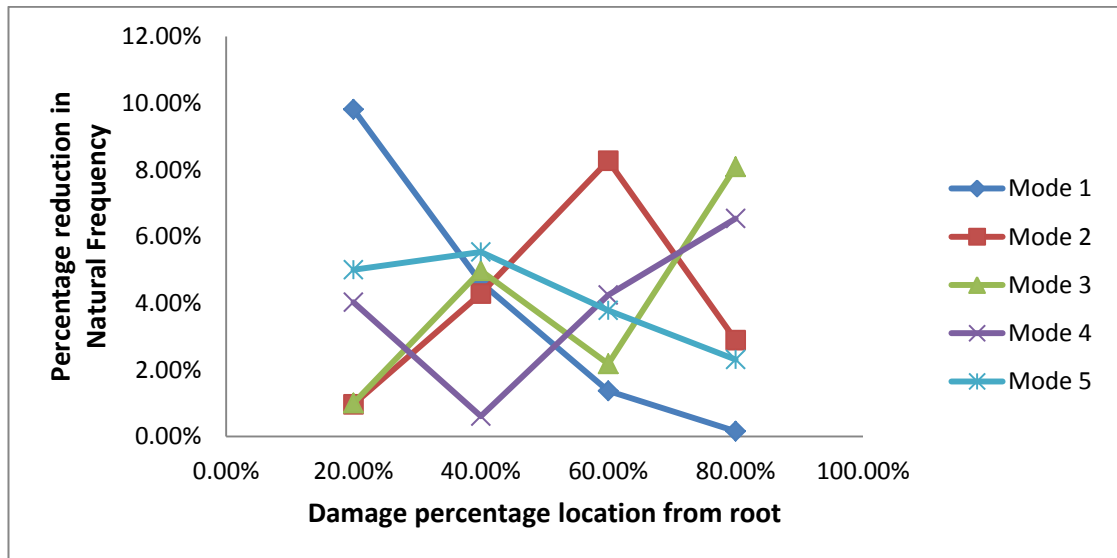


Figure 3.25. Effects of changing damage location on natural frequency (sample case for 60% damage), 2-D Modelling, Model-I case

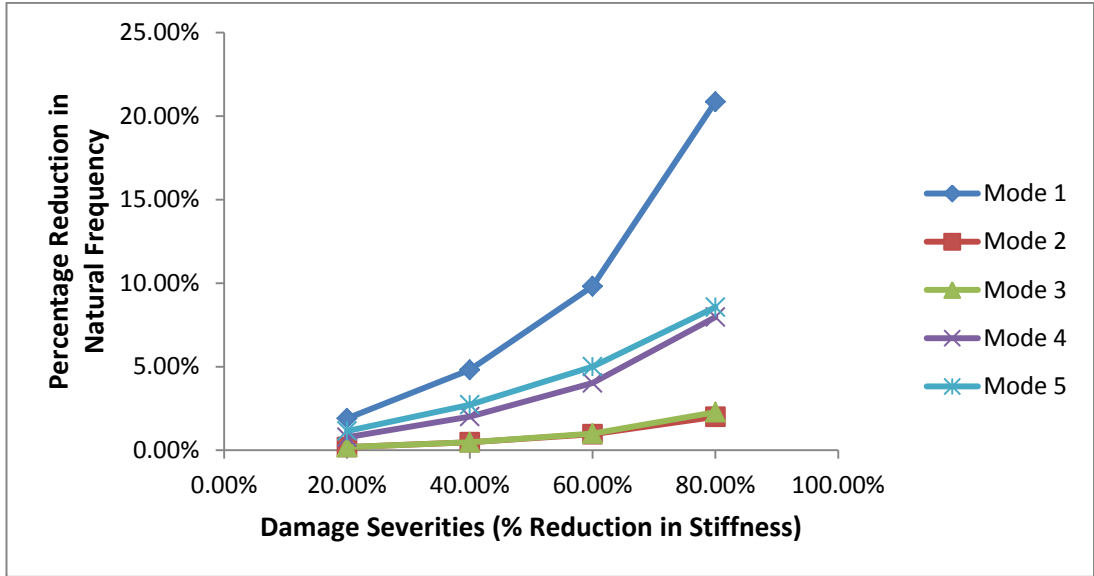


Figure 3.26. Damage at 20% location from the root with changing severities, 2-D Modelling, Model-I case

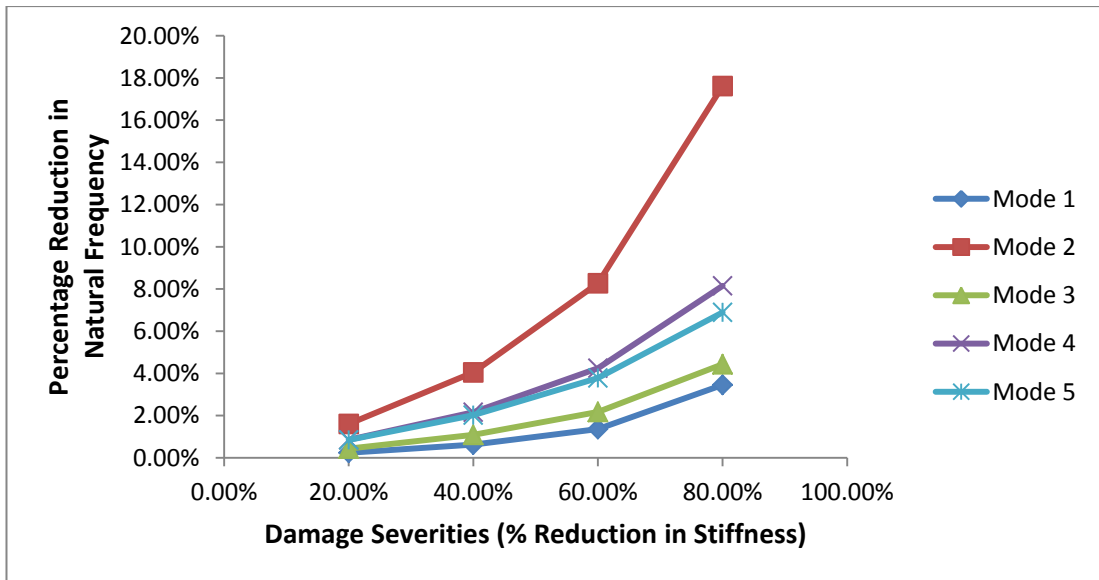


Figure 3.27. Damage at 60% location from the root with changing severities, 2-D Modelling, Model-I case

To exemplify the damage scenarios on Model-II, two examples are provided in this section. The first example given below is the one with damage created on the 13th element with 20% severity. After performing the modal analysis on this damaged case, the following results are obtained and tabulated in Table 3.18.

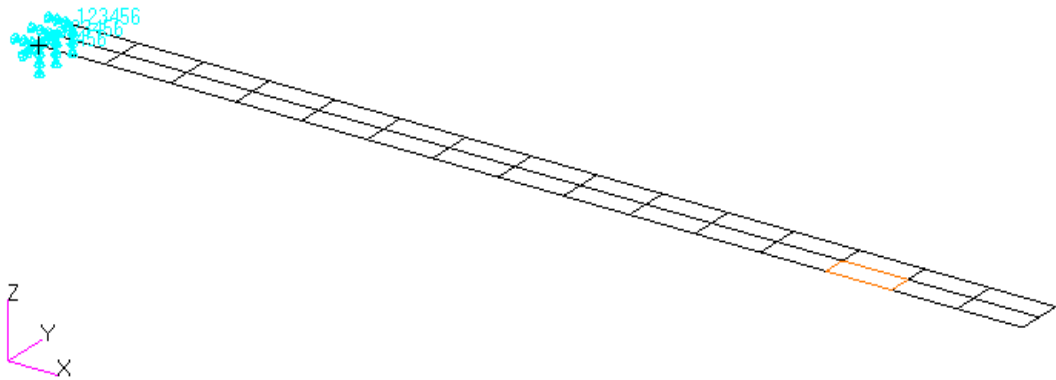


Figure 3.28. Damage located on the 13th element, 2-D Modelling, Model-II case

Table 3.18. First five natural frequencies of single impact damaged cantilever beam; Damaged on the 13th element with 20% severity

Intact Beam	Damaged Beam	% Difference
ω_{n_h} [Hz]	ω_{n_d} [Hz]	
20.77	20.76	0.00
129.26	129.14	0.09
359.45	358.02	0.40
698.78	693.74	0.72
1144.54	1136.20	0.73

[Difference is calculated with Eqn. 3.3]

If an analogy is necessary to be made between single damage cases on Model-II and Model-I, Model-II is the semi section damaged version of Model-I. From this point of view, single damage cases with same severity on Model-II (Table 3.18) having minor effect on the natural frequencies from Model-I (Table 3.9) is acceptable. Below is another example of single impact type damage created by Model-II (Figure 3.29) where the damage is on the 20th element with 40% severity. After performing the modal analysis on this damaged case, the following results are obtained and tabulated in Table 3.19.

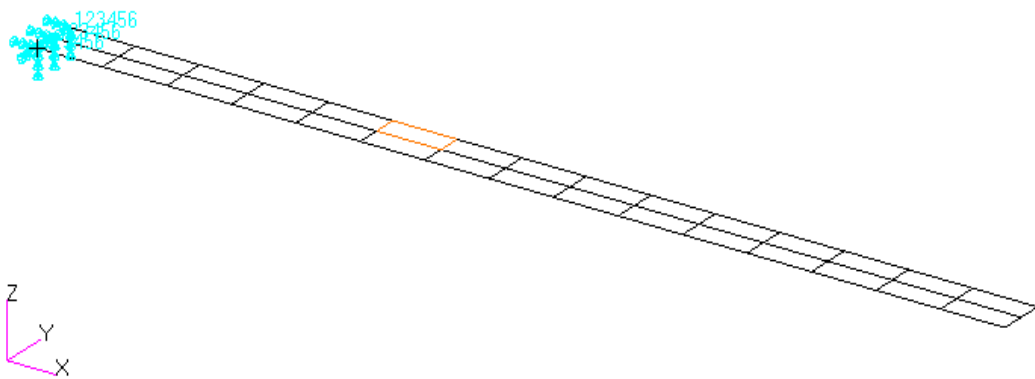


Figure 3.29. Damage located on the 20th element

Table 3.19. First five natural frequencies of single impact damaged cantilever beam; Damaged on the 20th element with 40% severity

Intact Beam	Damaged Beam	% Difference
$\omega_{n_h} [Hz]$	$\omega_{n_d} [Hz]$	
20.77	20.51	1.22
129.26	128.82	0.34
359.45	354.53	1.37
698.78	694.70	0.58
1144.54	1141.05	0.31

[Difference is calculated with Eqn. 3.3]

3.2.2.1.2. Multi Impact Type Damage

In this section, impact type damages on different locations with changing of severities are exemplified on both Model-I and Model-II. A multi impact damage types (Figure 3.30) with same severities are created on the 1st and the 14th elements with 50% severity. After performing the modal analysis on this particular multi damaged case, the results are tabulated in Table 3.20.

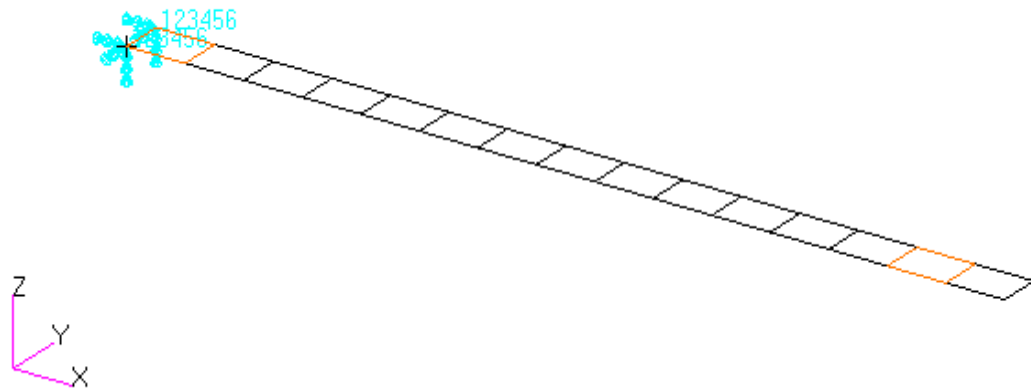


Figure 3.30. Damage located on the 1st and the 14th elements

Table 3.20. First five natural frequencies of multi impact damaged cantilever beam; Damaged on the 1st element with 40% severity and the 14th element with 50% severity

Intact Beam	Damaged Beam	% Difference
ω_{n_h} [Hz]	ω_{n_d} [Hz]	
20.75	19.33	6.85
129.19	122.70	5.02
359.23	342.96	4.53
698.23	661.54	5.20
1143.41	1069.71	6.45

[Difference is calculated with Eqn. 3.3]

As it can be seen from Table 3.20 that the damage cases located near the root and the tip of the cantilever beam affect all the modes in a similar manner. Figure 3.31, on the other hand, shows two damages which are created closer to the mid-span of the beam. Table 3.21 summarises the results comprising the percentage reduction in natural frequencies which are obtained after performing the modal analysis on this particular damaged case.

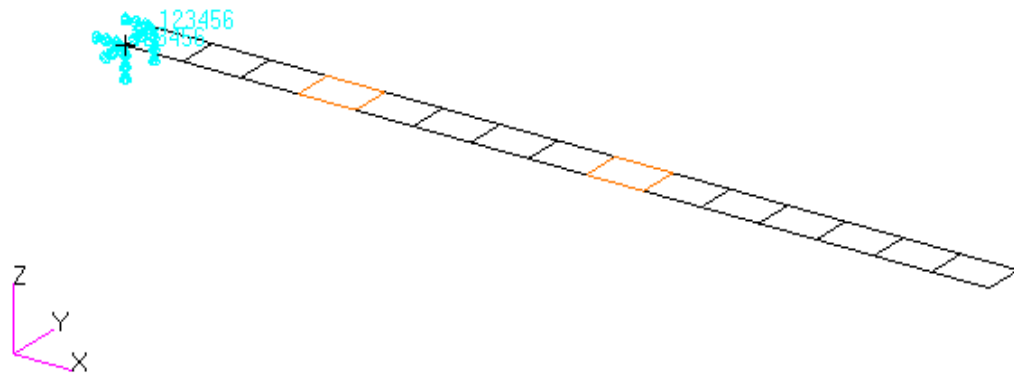


Figure 3.31. Damage located on the 4th and the 9th elements

Table 3.21. First five natural frequencies of multi impact damaged cantilever beam; Damaged on the 4th element with 40% severity and the 9th element with 10% severity

Intact Beam	Damaged Beam	% Difference
$\omega_{n_h} [Hz]$	$\omega_{n_d} [Hz]$	
20.75	19.94	3.93
129.19	128.13	0.83
359.23	350.85	2.33
698.23	675.41	3.22
1143.41	1123.71	1.72

[Difference is calculated with Eqn. 3.3]

In multi impact damage cases regarding the Model-II related parts, the damage locations are not only changing with x but also in y direction. Figure 3.32 presents an example of different damage locations on 2-D FEM (Model-II) which shows a variation both in x and y direction. Damages are created on the 11th and the 22nd elements of the model with 70% and 20% severity respectively. After performing the modal analysis on this particular multi damaged case, the results are tabulated in Table 3.22.

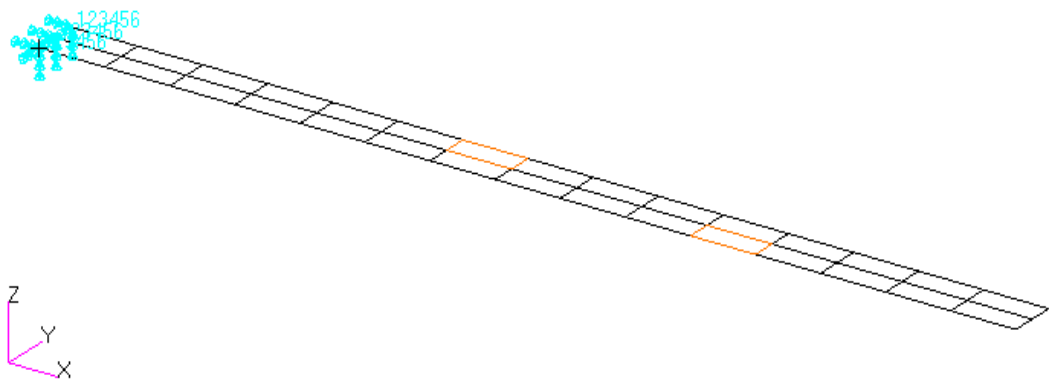


Figure 3.32. Damage located on the 11th and the 22nd elements

Table 3.22. First five natural frequencies of multi impact damaged cantilever beam; Damaged on the 11th element with 70% severity and the 22nd element with 20% severity

Intact Beam	Damaged Beam	% Difference
$\omega_{n_h} [Hz]$	$\omega_{n_d} [Hz]$	
20.77	20.68	0.43
129.26	125.64	2.80
359.45	344.21	4.24
698.78	687.31	2.92
1144.54	1127.72	1.47

[Difference is calculated with Eqn. 3.3]

Figure 3.33 is an example of damage location changing only in x direction and the corresponding modal analysis results are tabulated in Table 3.23.

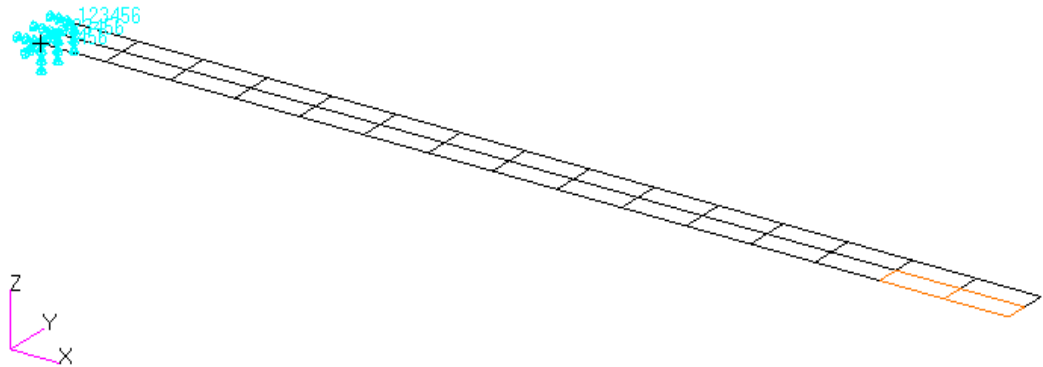


Figure 3.33. Damage located on the 14th and the 15th elements

Table 3.23. First five natural frequencies of multi impact damaged cantilever beam; Damaged on the 14th element with 50% severity and the 15th element with 60% severity

Intact Beam	Damaged Beam	% Difference
$\omega_{n_h} [Hz]$	$\omega_{n_d} [Hz]$	
20.77	20.76	0.00
129.26	129.17	0.07
359.45	358.02	0.40
698.78	691.07	1.10
1144.54	1121.78	1.99

[Difference is calculated with Eqn. 3.3]

3.2.2.2 Saw-cut Type Damage Modelling

In this section single and multi damage cases of saw-cut type damage is given by using 2-D model approaches on Model-I and Model-II.

3.2.2.2.1. Single Saw-cut Type Damage

In this section, for the single saw-cut type damages, some of the scenarios are exemplified first on the Model-I and then on the Model-II. The first example for the Model-I is the same as the one presented for single impact type damage presented in Section 3.2.2.1.1 in Figure 3.23. If the damage is created at same place as a saw-cut type with the same severity in the Model-I, the following results are then obtained and tabulated in Table 3.24.

Table 3.24. First five natural frequencies of single saw-cut damaged cantilever beam; Damage on the 6th element with 40% severity

Intact Beam	Damaged	% Difference
ω_{n_h} [Hz]	Beam	
20.75	18.71	9.87
129.19	121.46	5.98
359.23	335.17	6.70
698.23	693.14	0.68
1143.41	1061.27	7.18

[Difference is calculated with Eqn. 3.3]

As it can be seen and expected from the Table 3.24 that the saw-cut type damage modelled as thickness reduction causes more percentage reduction effect on the natural frequencies than that of the elastic modulus reduction (i.e. impact type damage) when the same severity is applied for both damage models. If the damage is applied on the 7th element with 20% severity, the following results presented in Table 3.25 are then obtained. Further damage scenarios are also investigated regarding the damage located on the 12th element with 80% severity (Figure 3.34) with the corresponding modal analysis results given in Table 3.26.

Table 3.25. First five natural frequencies of single saw-cut damaged cantilever beam; Damage on the 7th element with 20% severity

Intact Beam	Damaged Beam	% Difference
ω_{n_h} [Hz]	ω_{n_d} [Hz]	
20.75	20.35	1.97
129.19	125.08	3.18
359.23	356.21	0.84
698.23	684.89	1.86
1143.41	1117.23	2.29

[Difference is calculated with Eqn. 3.3]

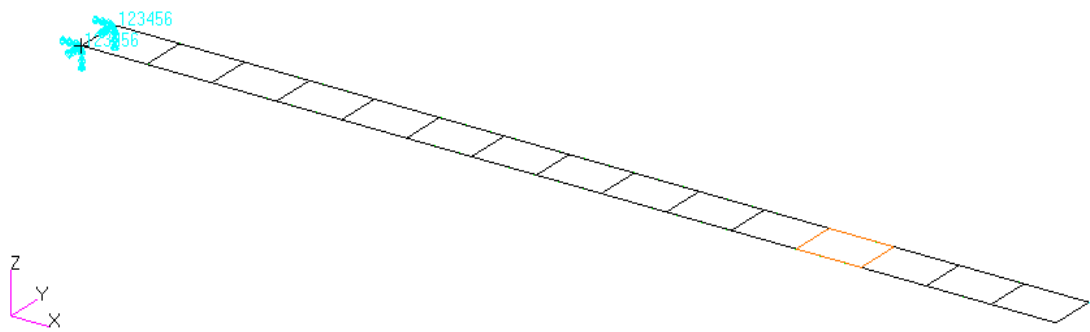


Figure 3.34. Damage located on the 12th element

Table 3.26. First five natural frequencies of single saw-cut damaged cantilever beam; Damage on the 12th element with 60% severity

Intact Beam	Damaged Beam	% Difference
ω_{n_h} [Hz]	ω_{n_d} [Hz]	
20.75	21.23	-2.30
129.19	102.08	20.98
359.23	256.28	28.66
698.23	593.87	14.90
1143.41	1064.38	10.53

[Difference is calculated with Eqn. 3.3]

As it can be seen from Table 3.26 that the changes on natural frequencies with 80% saw-cut type damage is extremely high when it is compared to the impact type damage and this is due to the fact that 60% saw-cut type damage leads almost the loss of that particular element. If the same element is exposed to 32% saw-cut type damage then the following results are obtained and tabulated in Table 3.27.

Table 3.27. First five natural frequencies of single saw-cut damaged cantilever beam; Damage on the 12th element with 32% severity

Intact Beam	Damaged Beam	% Difference
ω_{n_h} [Hz]	ω_{n_d} [Hz]	
20.75	21.13	-1.80
129.19	124.08	3.96
359.23	325.59	9.36
698.23	650.26	6.82
1143.41	1119.93	5.86

[Difference is calculated with Eqn. 3.3]

If the natural frequency changes are then examined by fixing the damage severity, as performed in both 1-D and 2-D modelling Model-I approaches, the effects of changing damage location on the first five out of plane bending modes are obtained again and presented in Figure 3.35 representing the case of 60% saw-cut type damage. If the damage severity is fixed and the effect of changing damage location is examined on 20% and %60 from the root of the structure, Figures 3.36 and 3.37 are obtained respectively. These two figures are actually restating the fact that, different vibration modes are highly sensitive to different damage locations up to different extents.

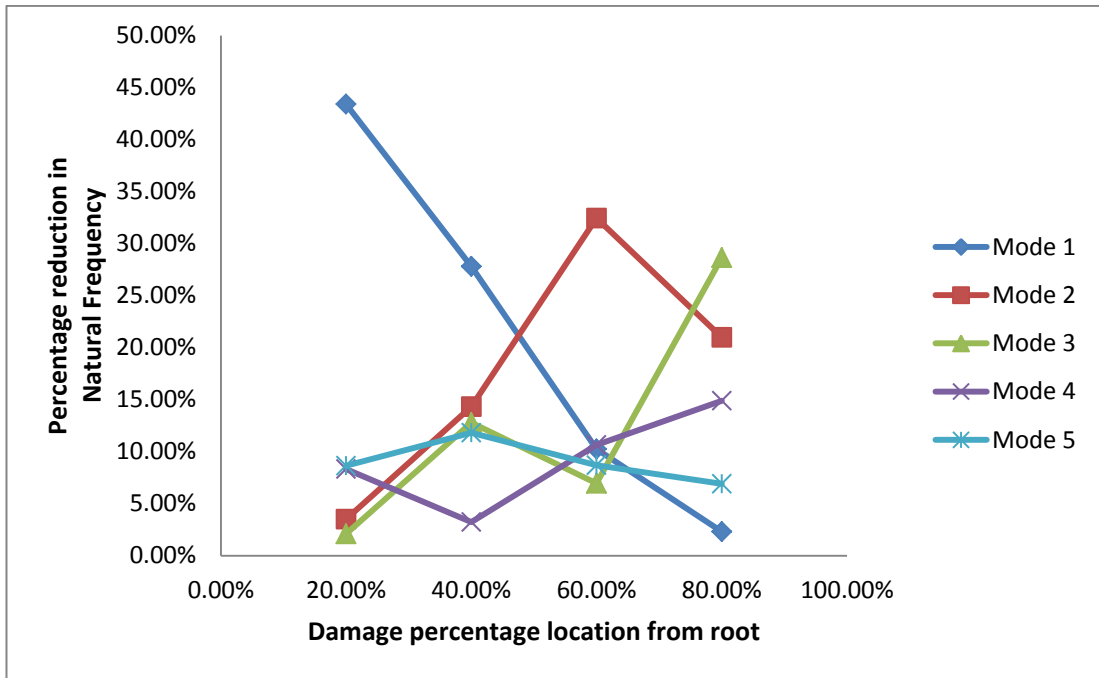


Figure 3.35. Effects of changing damage location on natural frequency (sample case for 60% damage), 2-D Modelling, Model-I case

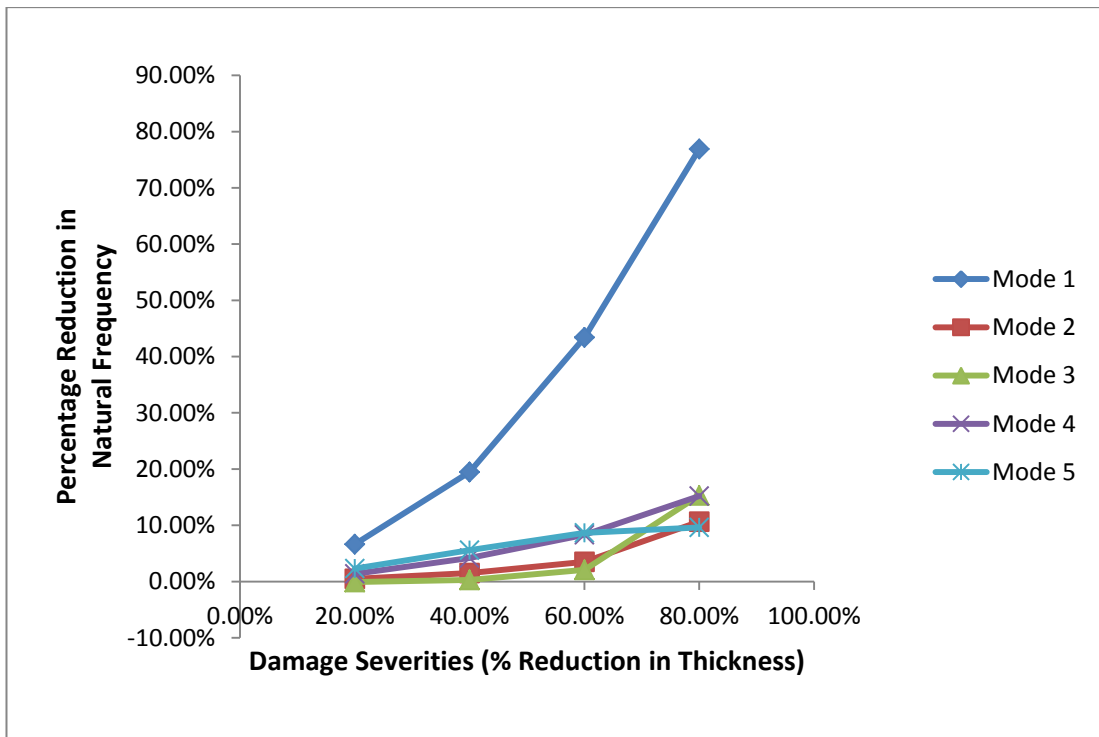


Figure 3.36. Damage at 20% location from the root with changing severities, 2-D Modelling, Model-I case

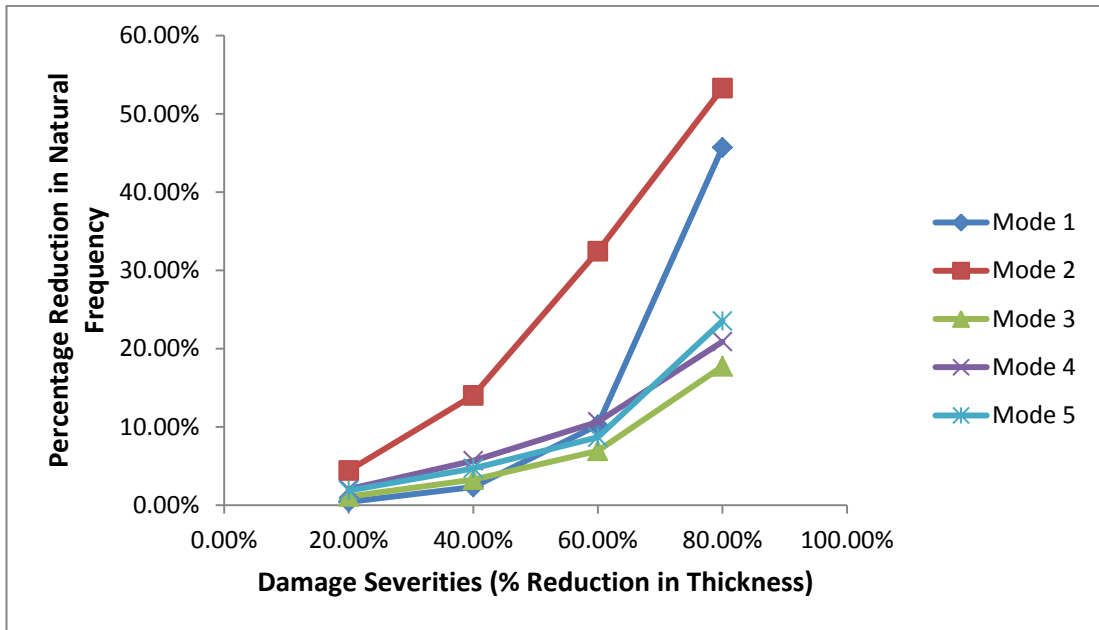


Figure 3.37. Damage at 60% location from the root with changing severities, 2-D Modelling, Model-I case

If saw-cut type damage in Model-II is examined with 10% severity damage on the 5th element (Figure 3.38), the results in Table 3.28 are obtained.

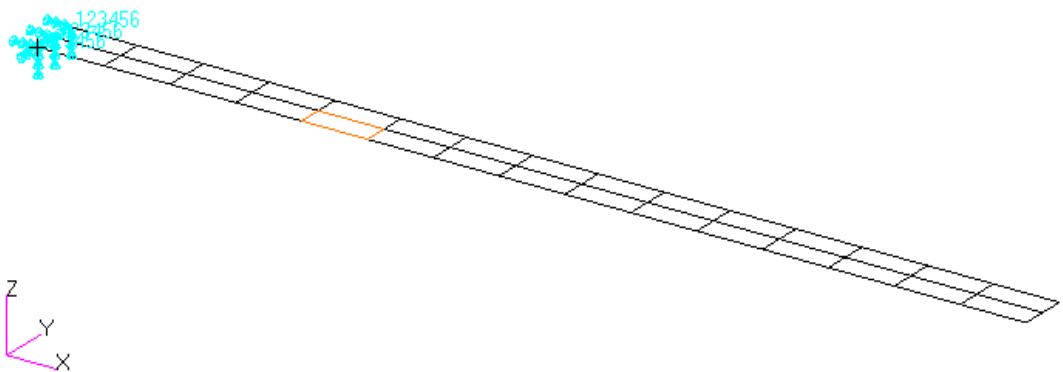


Figure 3.38. Damage located on the 5th element

Table 3.28. First five natural frequencies of single saw-cut damaged cantilever beam; Damaged on the 5th element with 10% severity

Intact Beam	Damaged Beam	% Difference
$\omega_{n_h} [Hz]$	$\omega_{n_d} [Hz]$	
20.77	20.61	0.74
129.26	129.23	0.03
359.45	357.68	0.49
698.78	697.32	0.21
1144.54	1143.65	0.08

[Difference is calculated with Eqn. 3.3]

Single damages on Model-II can be approached as semi sectioned damage on Model-I and as can be seen from natural frequency differences from Table 3.28, semi sectioned damage on beam has less effect on modal characteristics of the structure, as expected. The sample damage scenarios can be extended by a single damage case created on the 25th element of the FEM with the severity of 30% in Model-II (Figure 3.39). The analysis results of this particular damage case are presented in Table 3.29.

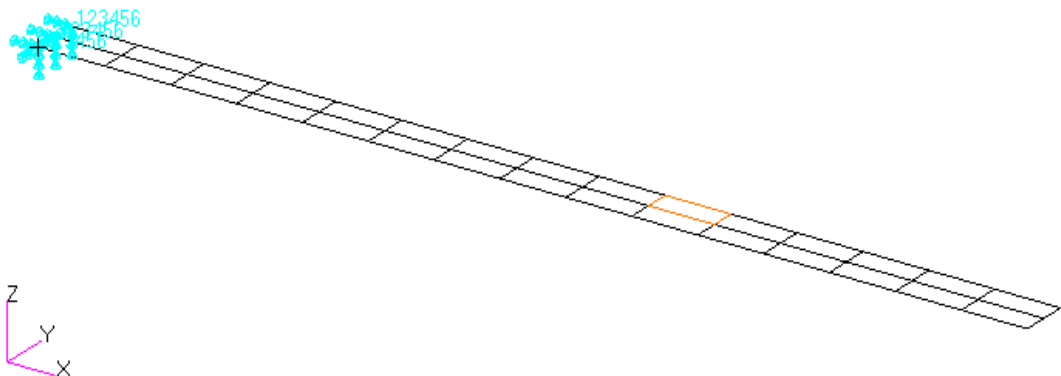


Figure 3.39. Damage located on 25th element

Table 3.29. First five natural frequencies of single saw-cut damaged cantilever beam; Damaged on the 25th element with 30% severity

Intact Beam	Damaged Beam	% Difference
$\omega_{n_h} [Hz]$	$\omega_{n_d} [Hz]$	
20.77	20.81	-0.21
129.26	126.26	2.32
359.45	352.53	1.93
698.78	697.82	0.14
1144.54	1123.96	1.80

[Difference is calculated with Eqn. 3.3]

3.2.2.2.2. Multi Saw-cut Type Damage

For multi damage cases generated on both Model-I and Model-II, the same damage scenarios of the multi impact damages created on 2-D models are used. In this section, various damage cases having multi saw-cut type damage modelling both on Model-I and Model-II cases are presented. The damages created on the 5th and the 13th elements with the same 50% severity and damages created on the 8th element with 20% severity and the 9th element with 40% severity are shown in Figure 3.40 and Figure 3.41 respectively. Their corresponding modal analysis results are also tabulated in Table 3.30 and Table 3.31, respectively.

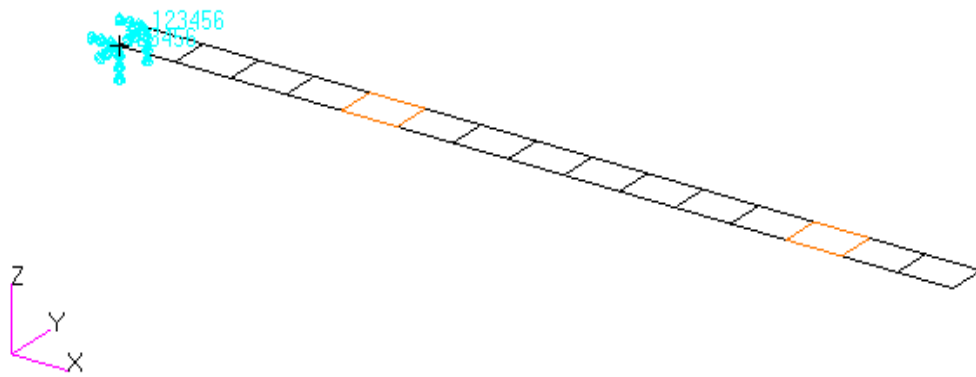


Figure 3.40. Damage located on the 5th and the 13th elements

Table 3.30. First five natural frequencies of multi impact damaged cantilever beam; Damaged on the 5th element with 50% severity and the 13th element with 50% severity

Intact Beam	Damaged Beam	% Difference
ω_{n_h} [Hz]	ω_{n_d} [Hz]	
20.75	17.05	17.84
129.19	120.50	6.73
359.23	268.82	25.17
698.23	536.77	23.08
1143.41	993.09	13.15

[Difference is calculated with Eqn. 3.3]

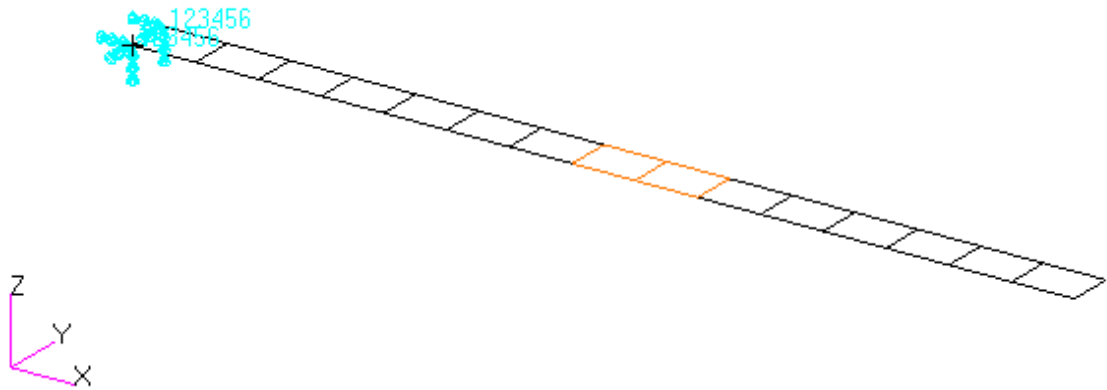


Figure 3.41. Damage located on the 8th and the 9th elements

Table 3.31. First five natural frequencies of multi impact damaged cantilever beam; Damaged on the 8th element with 20% severity and the 9th element with 40% severity

Intact Beam	Damaged Beam	% Difference
ω_{n_h} [Hz]	ω_{n_d} [Hz]	
20.75	20.02	3.54
129.19	108.77	15.81
359.23	346.87	3.44
698.23	651.29	6.67
1143.41	1081.37	9.10

[Difference is calculated with Eqn. 3.3]

As it can be seen and expected from Table 3.30 that saw-cut type damages have greater effect on percentage reduction in natural frequencies than that of in the impact type damage even if the impact type damage is closer to the root of the beam structure (Figure 3.31). More examples for the multi saw-cut type damage on Model-II are given as the damages created on the 10th element with 10% severity and the 17th element with 40% severity and created on the 4th element with 20%

severity and the 28th element with 40% severity. The corresponding modal analysis results are also given in a tabulated form in Table 3.32 and Table 3.33 respectively.

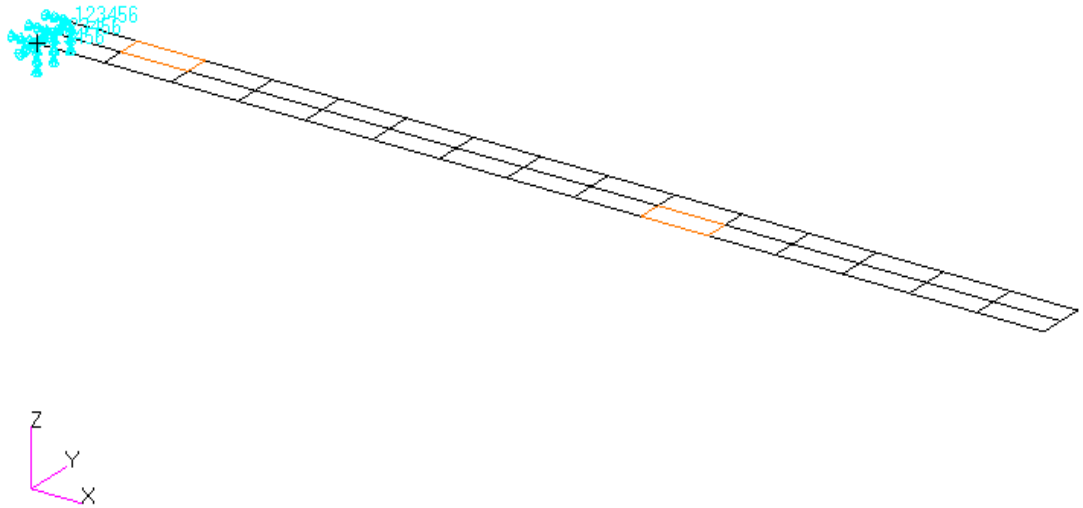


Figure 3.42. Damage located on the 10th and the 17th elements

Table 3.32. First five natural frequencies of multi saw-cut damaged cantilever beam; Damage on the 10th element with 10% severity and the 17th element with 40% severity

Intact Beam ω_{n_h} [Hz]	Damaged Beam ω_{n_d} [Hz]	% Difference
20.77	19.39	6.63
129.26	125.17	3.16
359.45	354.90	1.27
698.78	698.32	0.06
1144.54	1135.12	0.82

[Difference is calculated with Eqn. 3.3]

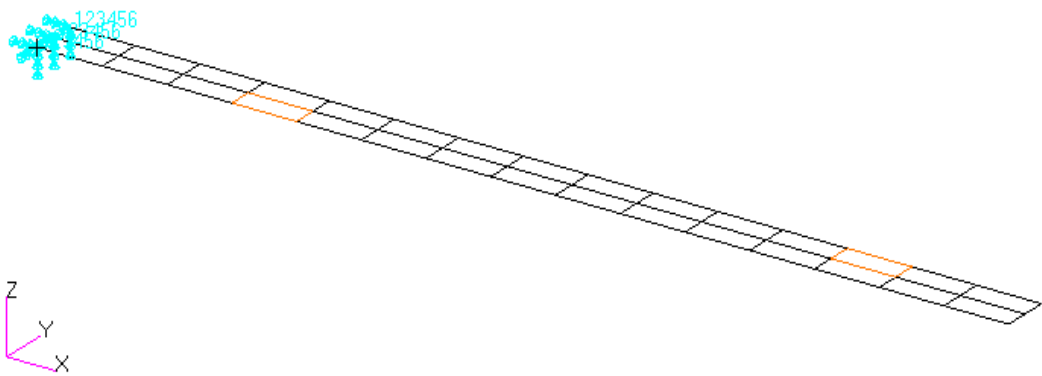


Figure 3.43. Damage located on the 4th and the 28th elements

Table 3.33. First five natural frequencies of multi saw-cut damaged cantilever beam; Damage on the 4th element with 20% severity and the 28th element with 40% severity

Intact Beam ω_{n_h} [Hz]	Damaged Beam ω_{n_d} [Hz]	% Difference
20.77	20.66	0.51
129.26	128.90	0.28
359.45	349.39	2.80
698.78	667.43	4.49
1144.54	1103.53	3.58

[Difference is calculated with Eqn. 3.3]

CHAPTER 4

DAMAGE IDENTIFICATION ALGORITHM

In this section, hybrid-GA optimisation is used to minimise the Residual Force Vector (RFV) in order to identify damage on isotropic beam-like structures modelled via both via 1-D and 2-D approaches in terms of damage location, severity and type. Damage detection system introduced in this study can identify two different damage types. One of which is impact type damage, defined as elastic modulus degradation without loss of mass. The other is saw-cut type damage which also includes mass reduction in addition to elastic modulus changes.

4.1 Damage Sensitive Features

The presence of damage changes structural properties of the structure. These changes can be directly observed on natural frequencies and mode shapes, or can be analysed post processed versions of them such as, curvature mode shape, modal strain energy, etc. As long as it is stated in literature where using more than one feature is beneficial to identify damage which is a non-unique and inverse problem, both natural frequency and mode shape information are used with RFV technique for the damage identification in this study.

Distinct from the literature where damages are simulated analytically, a commercial program Msc. Patran/Nastran[®] is used for both modelling (Chapter 3) and extracting the necessary information for RFV method. The necessary information, which are namely the damaged eigenvalues, corresponding eigenvectors and the intact structure's elemental mass and stiffness matrices, are obtained by means of a special coding so-called Direct Matrix Abstraction Programming (DMAP) of Msc. Nastran[®]. DMAP enables extracting structural

properties of a model in a file(s) and gives opportunity to analyse it/them elsewhere, such as Matlab, which is used in this particular research study. Following this, the effects of the damaged models comprising impact type damage (i.e. percentage reduction in elastic modulus) and/or saw-cut type damage (i.e. percentage reduction in thickness) on the obtained mass and stiffness matrices are represented in the form of sensitivity matrices. Then, these damage sensitivity matrices are embedded into RFV equation (Eqn. 2.9) and it becomes;

$$R_j = \sum_{i=1}^m S_s(\beta_i, i) \cdot [k]_i \cdot \{\phi_{jd}\} - \lambda_{jd} \cdot \sum_{i=1}^m S_m(\beta_i, i) \cdot [m]_i \cdot \{\phi_{jd}\} \quad (4.1)$$

where S_m and S_s stand for mass and stiffness sensitivity matrices, respectively. If impact type damage is in question then S_s is a measure of elastic moduli change, however, if saw-cut type damage is the one in question then both S_m and S_s are measure of thickness change simultaneously. That means that the sensitivity analyses are done for impact type damage with the assumption of having is no change in the mass of the structure by means of an impact and therefore, S_m matrix is not taken into account. Sensitivity analyses are conducted by 10% deviations of the property of interest starting from 10% to 100% of the individual element. In Equation 4.1, variable β_i provides results between 0 and 1, which are representing complete loss of an element of a structure and undamaged structure, respectively.

After performing these analyses, some checks on the constructed system are then performed, such as (if all elements are assumed as intact):

- $[K_h] = \sum_{i=1}^m S_s(1, i) \cdot [k]_i$
- $[M_h] = \sum_{i=1}^m S_m(1, i) \cdot [m]_i$
- $[\phi]^T [K_h] [\phi] = \text{diag}(\lambda)$
- $[\phi]^T [M_h] [\phi] = [I]$

where $[I]$ is the identity matrix, $[\phi]$ is the normalised eigenvector matrix and T stands for the transpose of a matrix. The above four equations are not only for the verification of both sensitivity matrices and application of BC's but also for the correctness of the extracted features. After obtaining, analysing and synthesizing

these matrices given in Eqn. 4.1, the solution of the problem turns out to be simple minimisation issue. Additionally, both its ability to explore whole solution space and being non-gradient while searching makes Genetic Algorithm (GA) to be a candidate for this optimisation problem.

4.2 Optimisation Problem

The schematic of the detection procedure given in Figure 4.1 actually sums up how the optimisation routine works. As it is seen from the figure, the 1st part is for the preparation of the damage detection system. For this purpose, Matlab [55] and Msc. Nastran work simultaneously on intact FEM model as mentioned in Section 4.1. The 2nd part, on the other hand, is responsible from getting information of the damaged structure which is in fact the external input to the system. This can also be done either by providing experimental analysis results of the damaged structure or by creating hypothetical damage scenarios via FE modelling and analysis results. Damaged models generated on FEMs are preferred in this research study in order to check damage detection system performance and to avoid costly experimental tests and analyses. The modelling of damage and creation of various scenarios in FEM are explained in Chapter 3, Sections 3.2.1 and 3.2.2. The 3rd part is the optimization part of the system which is handled by means of both Genetic Algorithm and non-linear optimization hybrid system which belong to the optimization toolbox of the Matlab [56]. In the optimisation algorithms, in order to reach a solution, boundary conditions are set to values between 0.3 and 1.0 by providing a correlation with the severities simulating various damage scenarios.

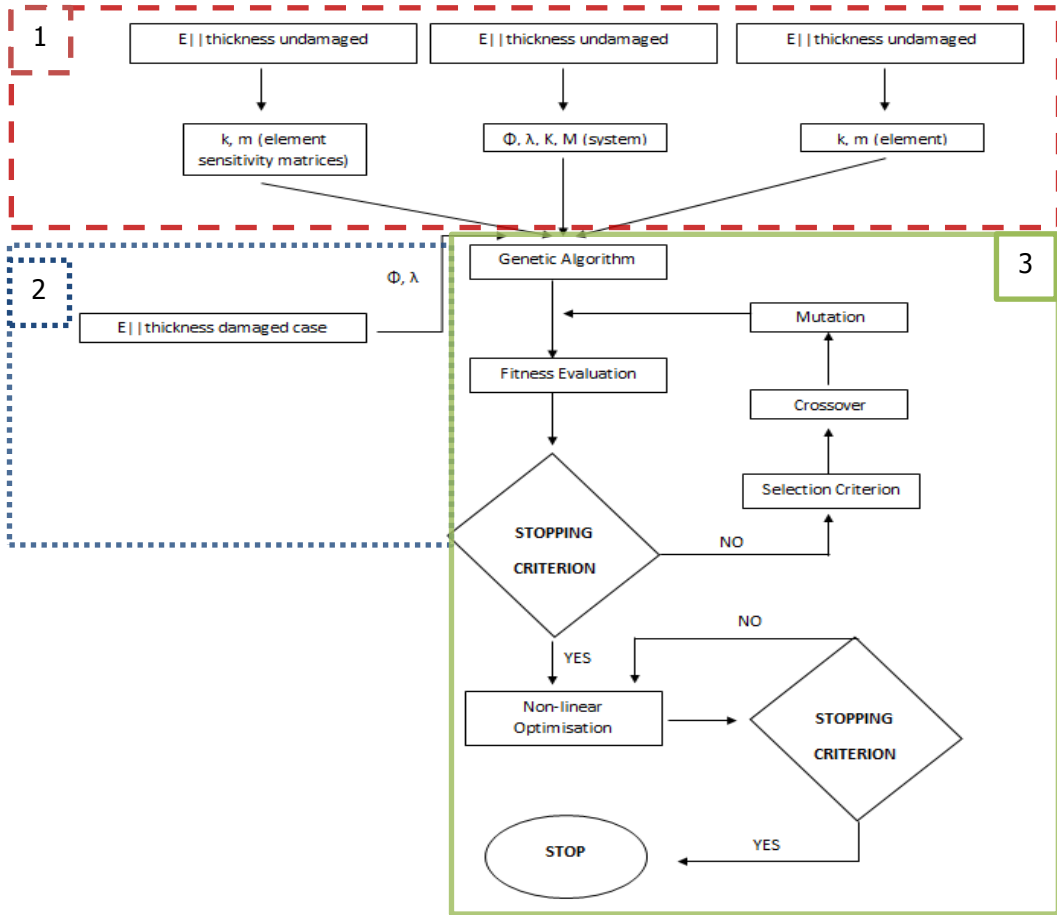


Figure 4.1. Schematic of the Damage Detection Procedure

4.2.2 Genetic Algorithm

In this thesis, GA, which is a solver of Matlab optimisation toolbox, is applied on structural damage identification in order to minimise the objective function which is given in the following equation;

$$F_j = \sum_{j=1}^n \text{norm} \left\{ \sum_{i=1}^m S_s(\beta_i, i) \cdot [k]_i \cdot \{\phi_{jd}\} - \lambda_{jd} \cdot \sum_{i=1}^m S_m(\beta_i, i) \cdot [m]_i \cdot \{\phi_{jd}\} \right\} \quad (4.2)$$

where $\{\phi_{jd}\} = j^{\text{th}}$ mode shape of the damaged structure and "n" is the number of mode shapes that are used to be optimised. The optimisation is performed over Equation 4.2 by making it approach to zero after certain number of iterations and/or generations.

Norm of a vector, which corresponds to any j^{th} value of Eqn. 4.2, is calculated via Matlab as in Equation 4.3 represented below.

$$F_j = \sqrt{\sum_{k=1}^l f_k^2} \quad (4.3)$$

where l is the total number of elements of the vector and f_k is the k^{th} element of the vector. This equation enables to minimise the total distance to 0 of the objective function. In order to decide the amount of information used (i.e. the number of eigenvalues and the corresponding eigenvectors, namely the mode shapes) while this minimisation is performed; the following analysis on number of eigenvalues and eigenvectors is conducted.

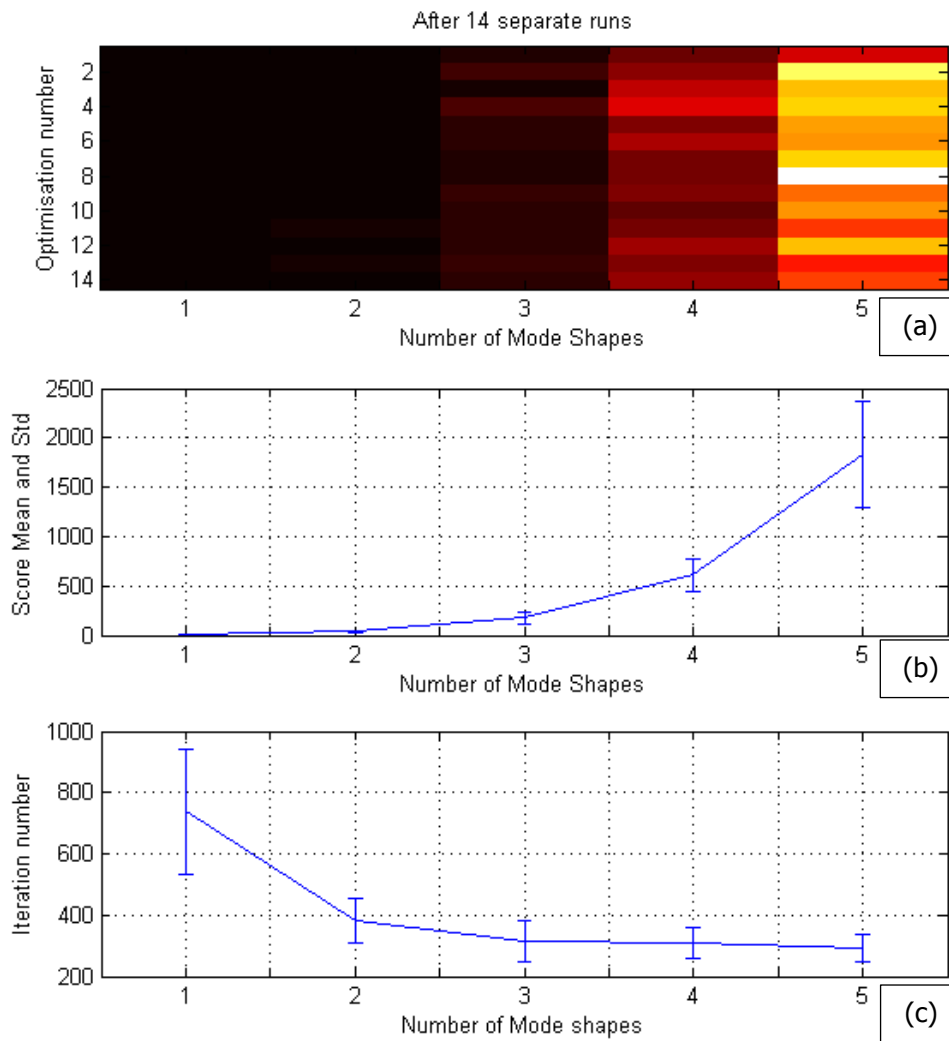


Figure 4.2. Effect of number of mode shapes in objective function on the optimisation procedure (a) Color-coded display of the best fitness values in each run (b) Means and standard deviations of the best fitness values (c) Number of iterations and its standard deviations

The above analysis is conducted by means of applying GA on a randomly selected damage scenario (i.e. in this case it is 50% impact type damaged on the 5th element of the 1-D model (Figure 3.2)). In order to reduce the uncertainty on results due to random data generation in GA and to investigate the effects of the number of mode shapes used in the objective function, various numbers of re-runs (14 times in this particular case) are performed. Figure 4.2(a) represents the colour-

coded display of the best fitness values of each run. Increasing darkness in colour code symbolises the closeness to the intended objective function value. Figure 4.2(b) shows the means and standard deviations of the best fitness values over the 14 different runs. The solid lines in the figure represent the mean of the final objective function values and vertical bars represent the standard deviations of the final objective function value. Figure 4.2(c) shows the number of iterations depending on the number of mode shapes. It can also be seen from the figure that the increasing number of mode shapes somehow confuses optimisation procedure since the mean and standard deviation of the best fitness values are increased. Therefore, by considering both the number of iterations and the objective function results, the first two modes are chosen for further analysis and used in the objective function. While minimising Eqn. 4.3, GA requires some characteristic parameters, such as selection, crossover and mutation that affect the performance (i.e. convergence level and optimisation time) of the algorithm. The characteristic parameters and the corresponding variable pairs are chosen as; crossover functions "heuristic", crossover fraction data "1", crossover operators "two point", mutation function "uniform" and population "100" [57].

Regarding the damage prediction results for 1-D damage scenarios, GA alone does not provide satisfactory results in some damage cases when the pre-determined GA characteristic settings are used. For example, Figure 4.3 is the representation of the results for detection of saw-cut type damage with 30% severity on the 6th element. The solution for this case is taken as the best one obtained from five different simulations (i.e. five individual GA runs) for the same damage scenario (Appendix A.1).

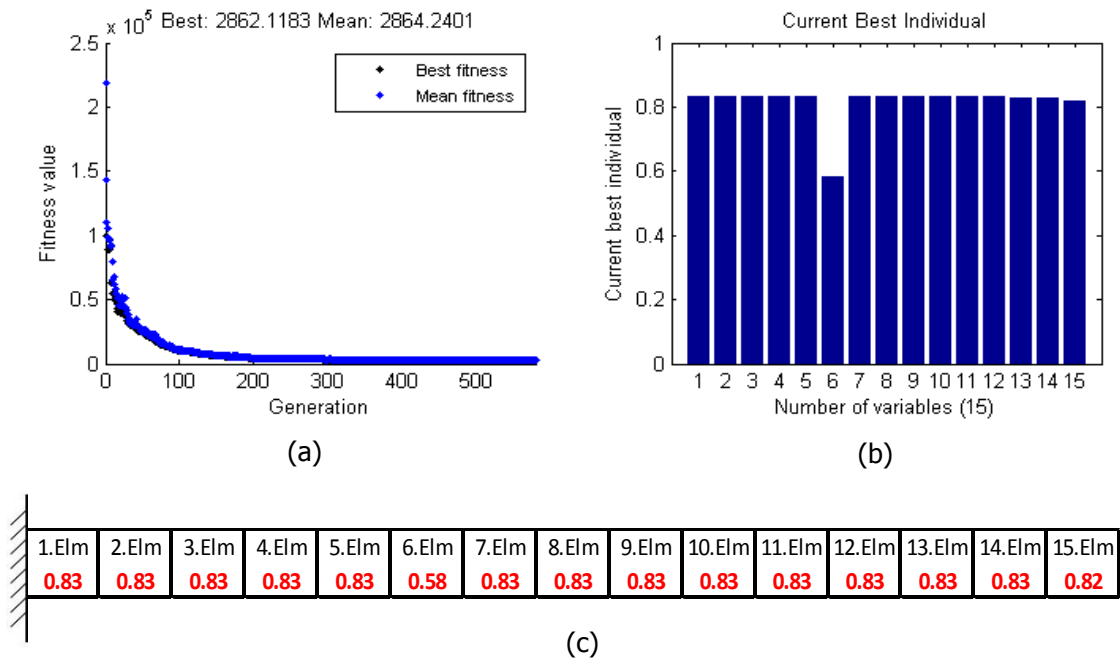


Figure 4.3. GA results for 30% damage on the 6th element
 (a) History of convergence (b) Identified damage location and severity
 (c) Numerical result of identified state

Red font and bold style written numbers in this thesis, as in Figure 4.3 (c), indicates damage locations and corresponding intactness levels of the elements. As it can be seen from Figure 4.3(b) that these settings have some convergence problem in the solution as they provide values lower than 1 for “current best individual”, which is referred as the “intactness level” throughout the thesis, by indicating a False-Positive damages. In the above analysis, four stopping criteria in GA are set by the characteristic parameters and the corresponding variable pairs as; generations (i.e. number of iteration) “Infinity”, Time “Infinity”, fitness limit (i.e. function value aimed) “0” and function tolerance (i.e. cumulative change in fitness function) “ 10^{-9} ”. As a result, the algorithm finds the damage on the 3rd element with low accuracy in terms of severity. Additionally, the intactness level of the all other elements does not converge to 1 as if they are not intact. To overcome this problem, a tuning on GA characteristic parameters is required and first, crossover function is changed from “two point” to “scattered” in order to homogenise the information passing towards parents. This change is performed based on the assumption that, the increasing dispersed information may lead the algorithm to

check more space easily. Then, the crossover fraction is taken into account and all the other set of parameters are fixed.

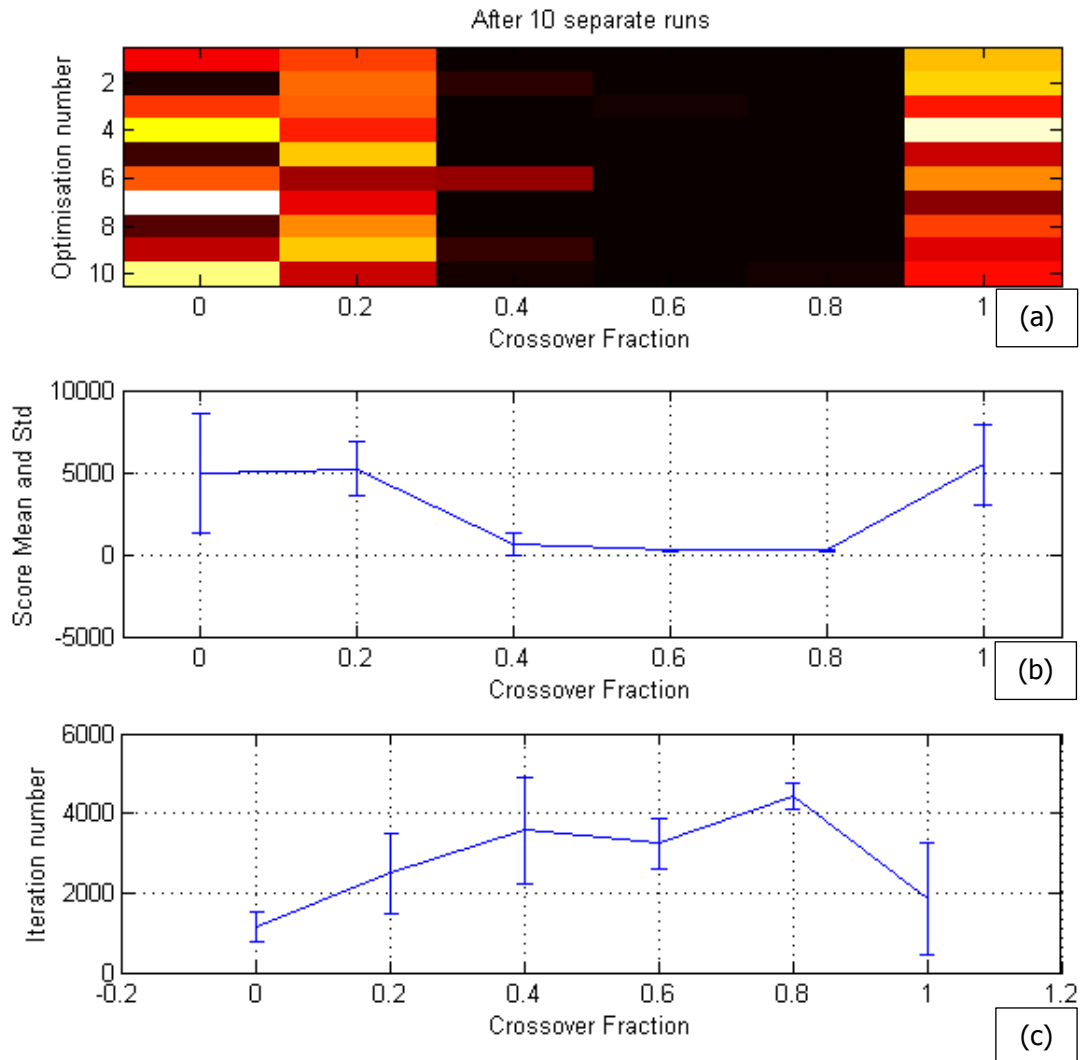


Figure 4.4. Crossover Fraction Selection (a) Color-coded display of the best fitness values in each run (b) Means and standard deviations of the best fitness values (c) Number of iterations and its standard deviations

Figure 4.4(b) represents the means and standard deviations of the best fitness values over 10 detections for each of the values of the crossover fraction. Detected damage scenario in this particular case is 30% impact type damage on the 1st element and it is modelled by the 2-D Model-I (Figure 3.4). Figure 4.4(a), on the

other hand, shows a colour-coded display of the best fitness values in each generation. Increasing darkness in colour code symbolises the closeness to the intended objective function value as also shown in Figure 4.2. Figure 4.4(c) represents the corresponding iteration numbers and the crossover fraction of 1 means that all children other than elite ones are crossover children, whereas, crossover fraction of 0 indicates that all children are mutation children. It can be seen from Figure 4.4(c) that crossover fraction of 0 (i.e. all mutation children) and 1 (i.e. without any mutation) provide the worst results in between other options. Having both minimum objective function values and standard deviations between those results, the crossover fraction value is selected as 0.8. Second parameter change is performed on mutation function by changing it from "uniform" to "adaptive feasible". While "uniform" mutation function makes changes on genes in a random manner, "adaptive feasible" function's changes stands by selecting generation directions adaptively with respect to last successful and unsuccessful generations. Following those setting arrangements, initial population specifying the first population creation interval is set as [0.5; 1.0] in order to help the algorithm by narrowing down solution space for the first population. Selection function is assigned as "roulette" which traces the solution areas by simulating the roulette wheel in casinos. The algorithm uses a randomly assigned number to select one of the sections of the wheel with a probability which is equal to its area. In this selection scheme, probability of selection is proportional to the fitness of the chromosome. Although it is claimed that roulette wheel selection is inherently slow [47], in order to have a possible global optimum convergence in the solution, it is used throughout the study. Population size specifies how many individuals there are in each generation. Increasing population size increases search of detail in the solution space and this reduces the probability to get stuck into a local minimum rather than finding a global optimum. However, increasing population size decreases the algorithm speed. After several trial runs, population size is decreased from 100 from 50 to increase the algorithm speed. As a summary, the parameters assigned to GA algorithm in this thesis are as follows; Selection option is chosen as "Roulette", crossover function is selected as "scattered", crossover fraction is assigned as "0.8", mutation function is chosen as 'adaptive feasible' with a population size of "50". In addition to those, elite count, which is the number of

individuals with the best fitness values in the current generation guaranteeing to survive to the next generation, is taken as "2". According to these settings, GA calculates next generation which comprises "2 elite children", " $0.8 \times 50 = 40$ crossover children" and "8 individual mutation children".

Figure 4.5 is an example for impact type damage detection case on 2-D Model-I and the iterations stops at 947 with a final objective function value of approximately 3806 which is expected as zero (or closer) in order to reach fully identified intactness levels of the elements on a structure. The below simulation finds damage and its location with a superb accuracy; besides, it somehow indicates false-positive damages on various elements (i.e. elements from 13 to 15). Therefore it is decided to combine GA power of finding promising regions for the solution space with a speed of "local optimiser". Therefore, constrained nonlinear multivariable function of Matlab (so-called FMINCON) is chosen as the hybrid optimiser.

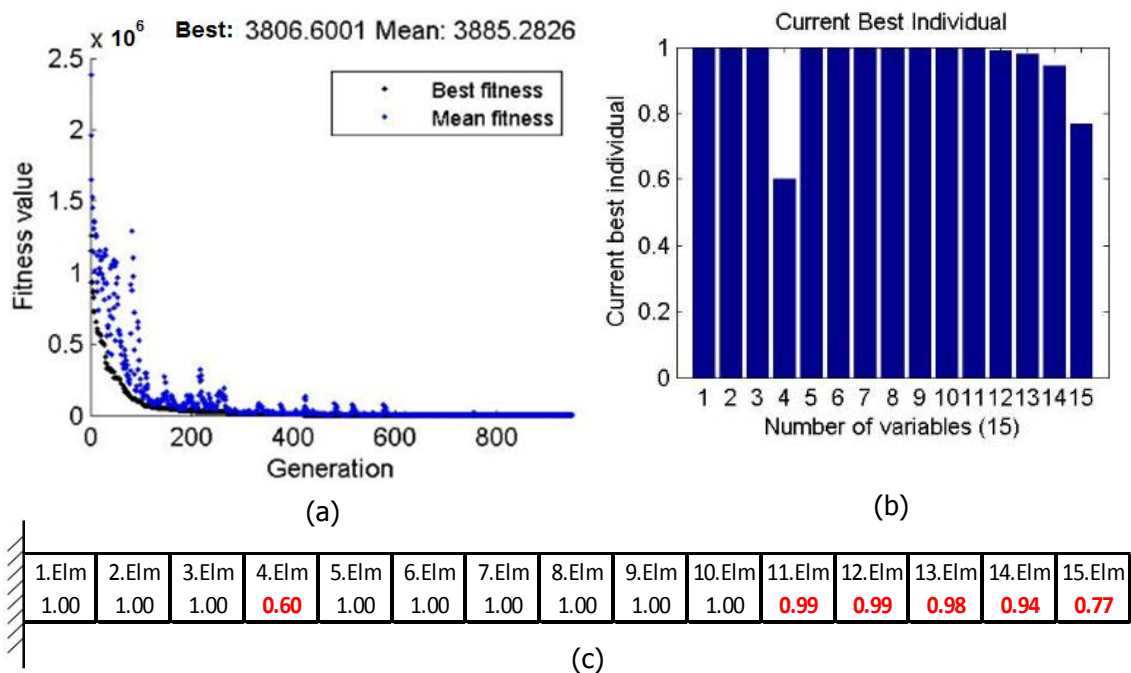


Figure 4.5. GA results for 40% damaged on the 4th element
 (a) History of convergence (b) Identified damage location and severity
 (c) Numerical result of identified state

4.2.3 Constrained Non-Linear Optimisation

Non-linear optimisation function working with GA is "FMINCON" which is the acronym of "Find MINimum of CONstraint nonlinear multivariable function". Constrained minimisation is the problem of finding a local minimum in predefined constrained solution space of a scalar function. "FMINCON" has four different algorithm options for non-linear minimisation, which are; thrust-region-reflective algorithm [58], active-set algorithm [59], interior-point algorithm [60] and sequential quadratic programming (SQP) [61] algorithm. "FMINCON" uses a Hessian [62], the second derivatives of Lagrangian [63], to minimise any function. The above listed algorithms only change how Hessian is handled by the "FMINCON". FMINCON uses thrust region reflective as a standard algorithm, however, it requires gradient equation of the objective function. Due to not supplying a gradient equation to MATLAB, the algorithm changes option automatically to active-set and this set is used as a default one for all FMINCON optimisation runs. In addition to that, various FMINCON parameters affecting stopping criteria are set to let optimisation routine continue as much as it can. For this purpose, termination tolerance on the function value (TolFun) and termination tolerance on variable value (TolX) decreased from 10^{-6} (i.e. a default value) to 10^{-9} . Maximum number of iterations allowed (MaxIter) and maximum number of function evaluations allowed (MaxFunEvals) are also increased to 10000 (i.e. an arbitrarily large value) to avoid algorithm to stop before one of the TolX or TolFun criterion is satisfied. So as to see whether the "FMINCON" works alone on damage detection or not, it is used over few damage scenarios. These test runs show some convergence problems and go no further than showing the power of GA in finding the solution space. Figure 4.6 is an example for this situation where initial guess is taken as 0.3 for all elements.

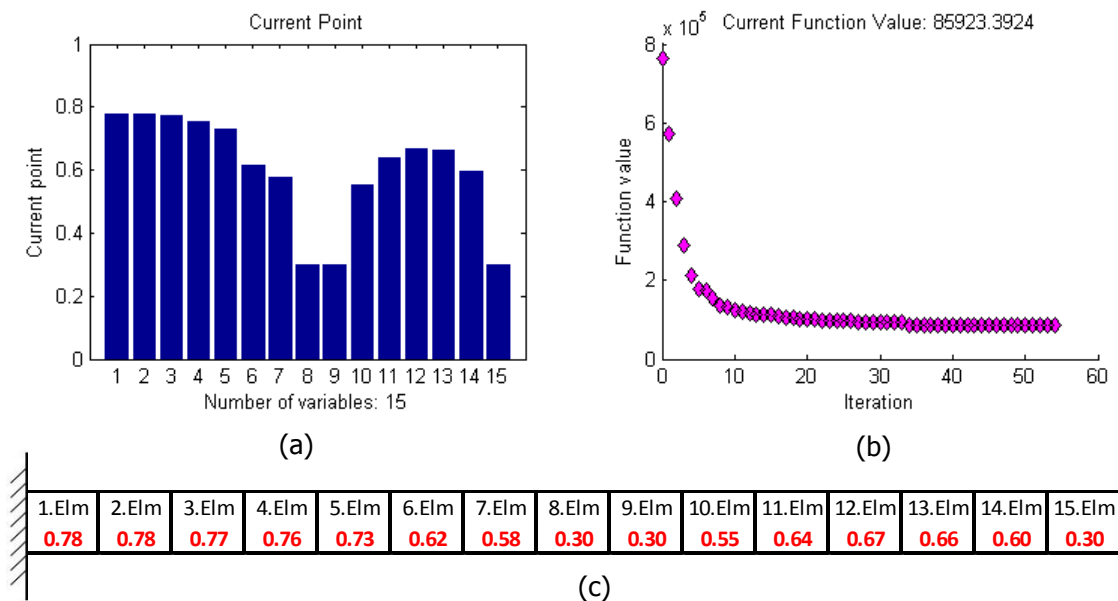
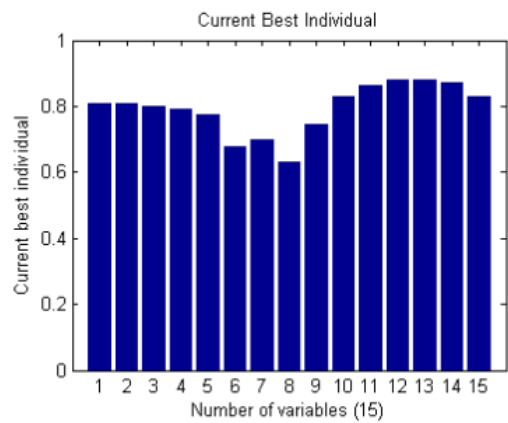
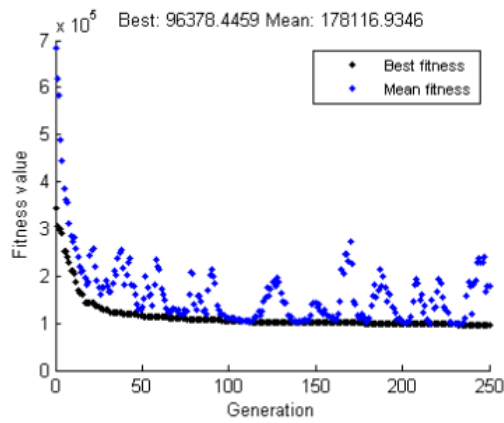


Figure 4.6. FMINCON results for 10% damage on the 6th element
 (a) Identified damage location and severity (b) History of convergence
 (c) Numerical result of identified state

Figure 4.6 corresponds to 10% saw-cut type damage on the 6th element of the 1-D beam model, however, FMINCON provides as if all the elements are damaged with changing severities (Figure 4.6 (c)). Although the performance of FMINCON is not very satisfying for this particular case (Figure 4.6 (c)), it is known that the performance of FMINCON in the optimisation depends highly on initial guesses. Therefore, several runs having various initial guesses (i.e. guesses both in a particular interval with incremental changes or generated in random manner) are presented in the Appendix A.2. If the guidance of GA for finding promising regions in solution space and the speed of the "FMINCON" is combined by limiting the iteration number of GA with 250 and enabling "FMINCON" to continue from where the GA left the variables, the case in Figure 4.6 is re-run with the hybrid system, the following results (Figure 4.7(c)) are then obtained.

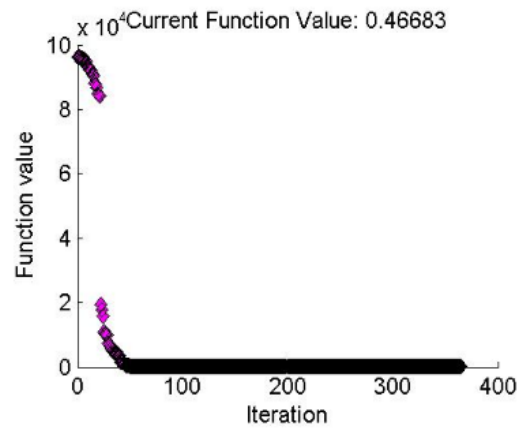
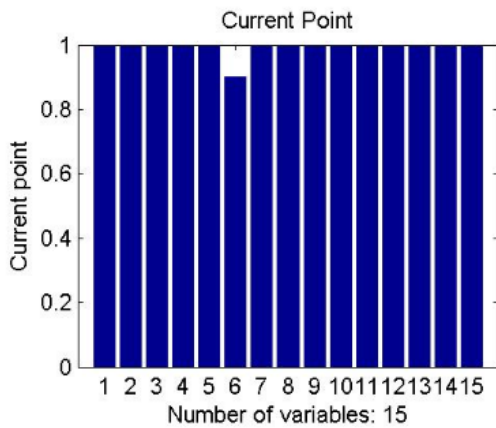


(a) (b)

1.Elm	2.Elm	3.Elm	4.Elm	5.Elm	6.Elm	7.Elm	8.Elm	9.Elm	10.Elm	11.Elm	12.Elm	13.Elm	14.Elm	15.Elm
0.81	0.81	0.80	0.79	0.78	0.68	0.70	0.63	0.74	0.83	0.86	0.88	0.88	0.87	0.83

(c)

Figure 4.7. GA results for 10% damage on the 6th element
 (a) History of convergence (b) Identified damage location and severity
 (c) Numerical result of identified state



(a) (b)

1.Elm	2.Elm	3.Elm	4.Elm	5.Elm	6.Elm	7.Elm	8.Elm	9.Elm	10.Elm	11.Elm	12.Elm	13.Elm	14.Elm	15.Elm
1.00	1.00	1.00	1.00	1.00	0.90	1.00	1.00	1.00	1.00	1.00	1.00	1.00	1.00	1.00

(c)

Figure 4.8. FMINCON results as a part of the hybrid system for 10% damage on the 6th element (a) Identified damage location and severity
 (b) History of Convergence (c) Numerical result of identified state

As the GA-only-system stops after 8086.08 seconds with some convergence problems (Figure 4.5), the above hybrid-GA-system stops after 4005.79 seconds with fully convergence. This shows nothing but the performance and the effectiveness of the hybrid detection system used in the analysis. The more analyses results regarding the designed hybrid system on damage scenarios are included in detail in Chapter 5.

CHAPTER 5

DAMAGE IDENTIFICATION RESULTS

5.1 1-D Damage Detection

In this section, 1-D damage detection results obtained by applying hybrid-GA optimisation algorithm on damage scenarios are presented. Firstly, impact type damage results are given with single and multi-damage sub-categories and then saw-cut type damage detection results are provided with same sub-categories. Finally, damage type decision mechanism is explained under the investigation of damage type section.

5.1.1 Impact Type Damage

For impact damage identification on 1-D model, detection algorithm is tested on pre-defined (see Section 3.2.1.1) damage scenarios. In all parts, only one sample damage detection result is presented along 105 different single damage scenarios and twice the number of elements for multi damage scenarios.

5.1.1.1 Single Damage Scenarios

As a sample damage case, the below results correspond to the impact type damage on the 3rd element with 40% severity (Figure 3.8). As explained before, GA narrows down the solution space of the optimisation problem within 250 iterations, which is shown in Figure 5.1 and then pass the problem to non-linear optimisation for further iterations. Non-linear optimisation (i.e. FMINCON) works as a part of the hybrid optimisation routine and the starting point for the optimisation problem (i.e. investigation for the damage) is given on Figure 5.1(c). While GA needs

approximately 400 generations to reach a solution in the detection (Figure 4.2 - 2 mode shapes part), only 250 of them used in this particular application. Then, FMINCON takes the problem and concludes rapidly compared to the GA for the final decision of damage detection.

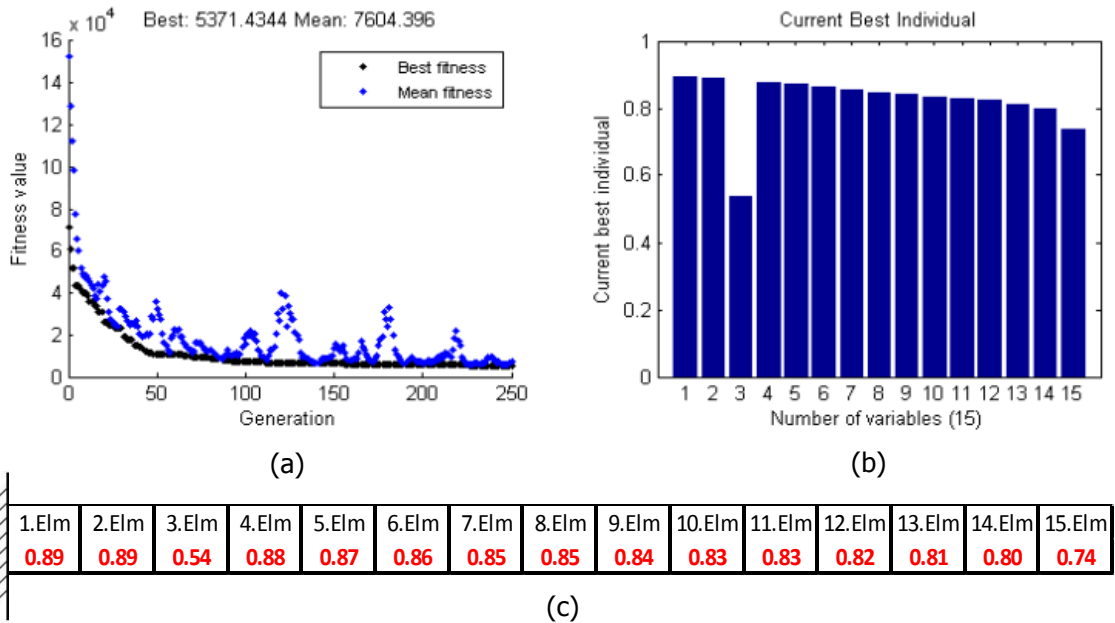


Figure 5.1. GA results for 40% damage on the 3rd element
 (a) History of Convergence (b) Identified damage location and severity (c)
 Numerical result of identified state

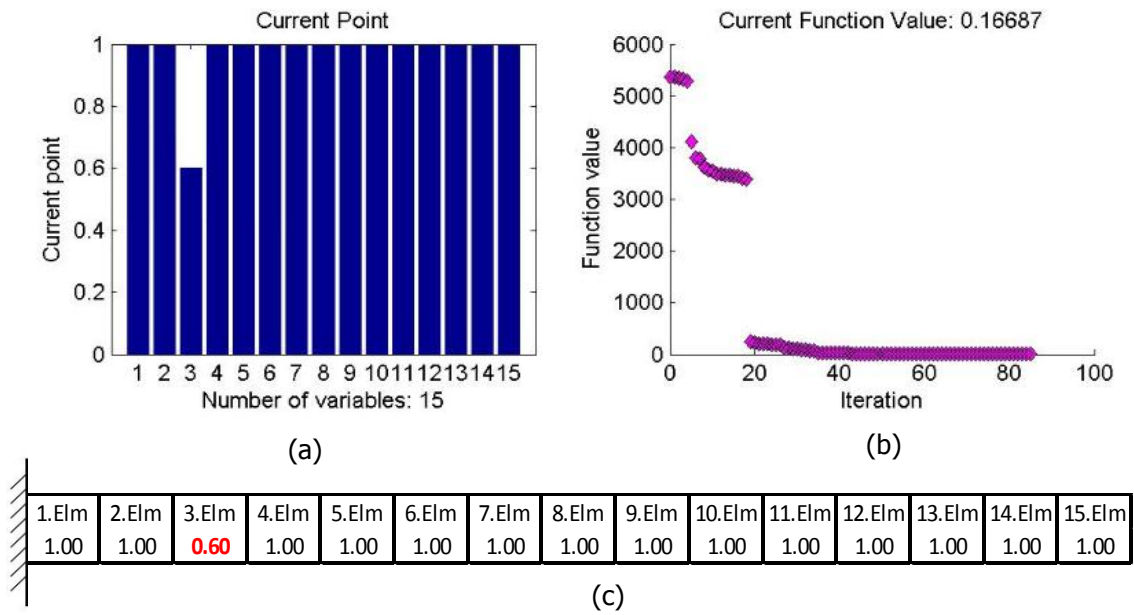


Figure 5.2. FMINCON results as a part of the hybrid system for 40% damage on the 3rd element (a) Identified damage location and severity (b) History of Convergence (c) Numerical result of identified state

As it can be seen from the Figure 5.2(c) that, the damage locations and corresponding intactness levels of the elements (i.e. red font and bold style written numbers) do not belong to the final solution of the optimisation (i.e. 250 generations of the GA) but they are just rough estimated for the locations of the damage(s).

5.1.1.2 Multi Damage Scenarios

In order to investigate whether the algorithm works on multi damage cases or not, damage detection procedure is tested on damage scenarios which are twice the number of elements and are created by random damage scenario generator as mentioned in Section 3.2.1.1. Damage generator creates damage(s) in a way that, damages are at two different locations for each individual case and each single element experiences two different severities at the end of the overall damage scenarios.

Figure 5.3 is an example for multi impact damage case. In addition to single 40% damage on the 3rd element case represented in Section 5.1.1.1, there is also

20% damage on the 12th element in this example (Figure 3.14). GA results for 250 iterations before passing the problem to FMINCON routine is shown in Figure 5.3(c).

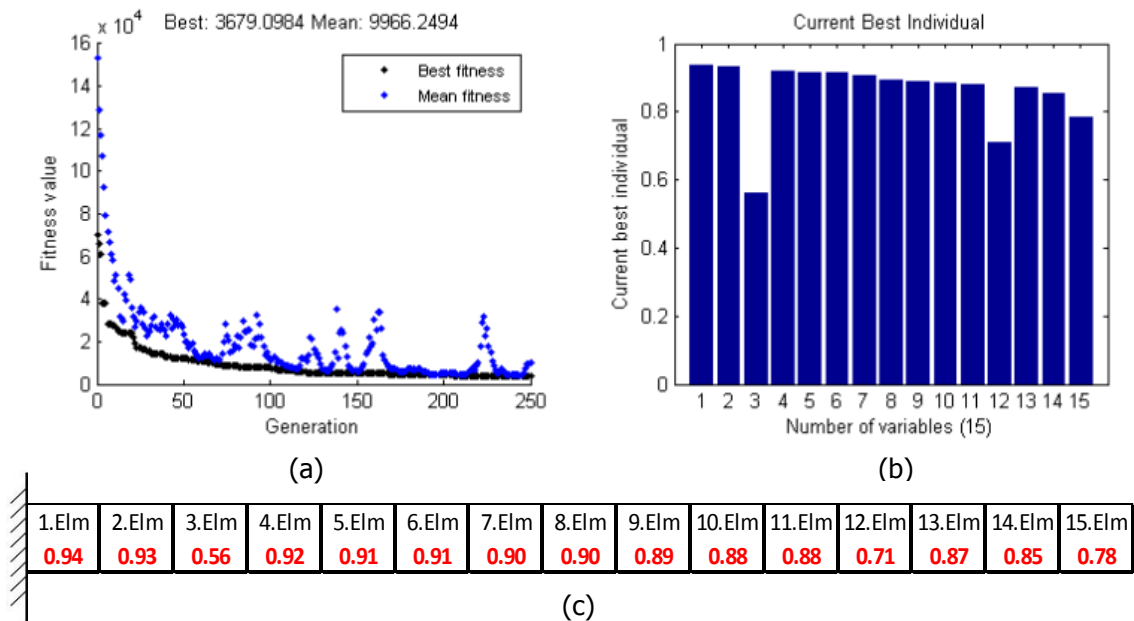


Figure 5.3. GA results for 40% damage on the 3rd element and 20% damage on the 12th element (a) History of Convergence (b) Identified damage location and severity (c) Numerical result of identified state

After FMINCON deals with the optimisation problem, it stops with objective function value of 0.20 (Figure 5.4 (b)), which is so close the intended one (i.e. zero) by finding the exact damage locations and severities (Figure 5.4(c)). Damage locations are indicated with red bold font at FMINCON part as well.

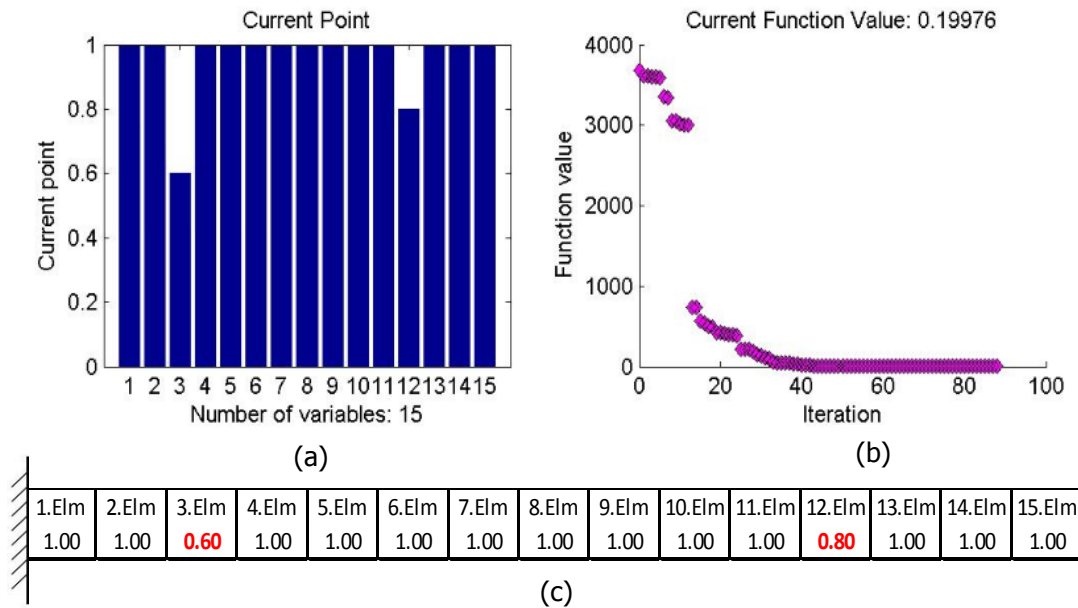


Figure 5.4. FMINCON results as a part of the hybrid system for 40% damage on the 3rd element and 20% damage on the 12th element

(a) Identified damage location and severity (b) History of Convergence

(c) Numerical result of identified state

5.1.2 Saw-cut Type Damage

In this section, one of the sample cases for the damage scenarios (Figure 3.16) is presented here for the saw-cut type damage.

5.1.2.1 Single Damage Scenarios

Damage detection algorithm is applied to saw-cut type damage model presented in Figure 3.16 where the damage is on the 4th element with 20% severity and the Figures 5.5 and Figure 5.6 are obtained. Figure 5.5 is the GA results after 250 generations. Figure 5.5(a) is the convergence history of the GA, Figure 5.5(b) is the identified state of the structure for 250 generations and Figure 5.5(c) is the numerical representation of Figure 5.5 (b) on corresponding cantilever beam which is already given in Figure 3.2 (b).

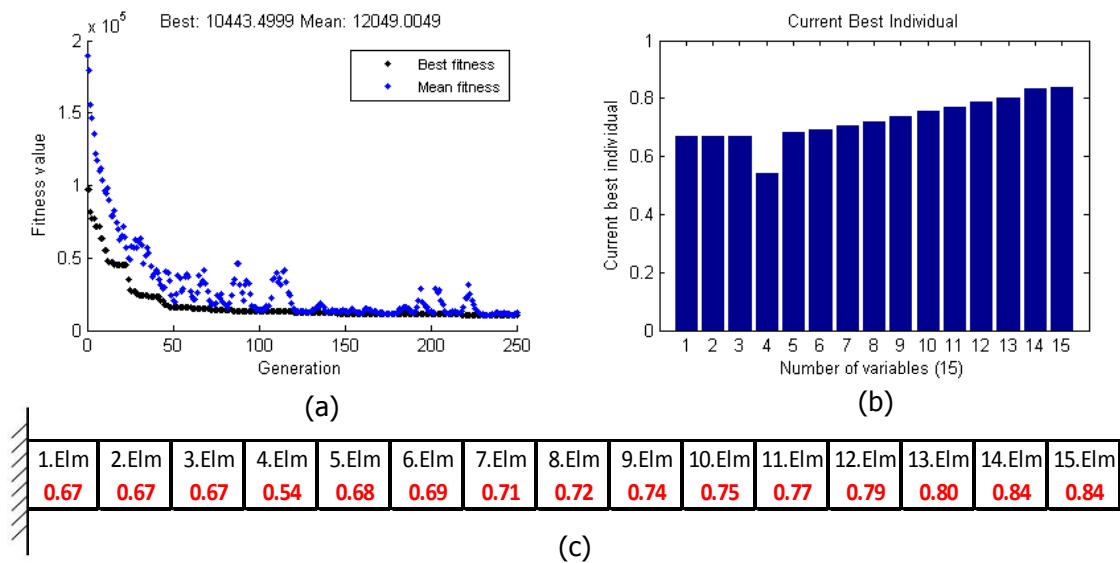


Figure 5.5. GA results for 20% damage on the 4th element
 (a) History of convergence (b) Identified damage location and severity
 (c) Numerical result of identified state

Following GA part, FMINCON starts to optimise the problem from the points presented in Figure 5.5(c) and concludes the optimisation with a very close value of 0.45 to the desired objected value of 0.

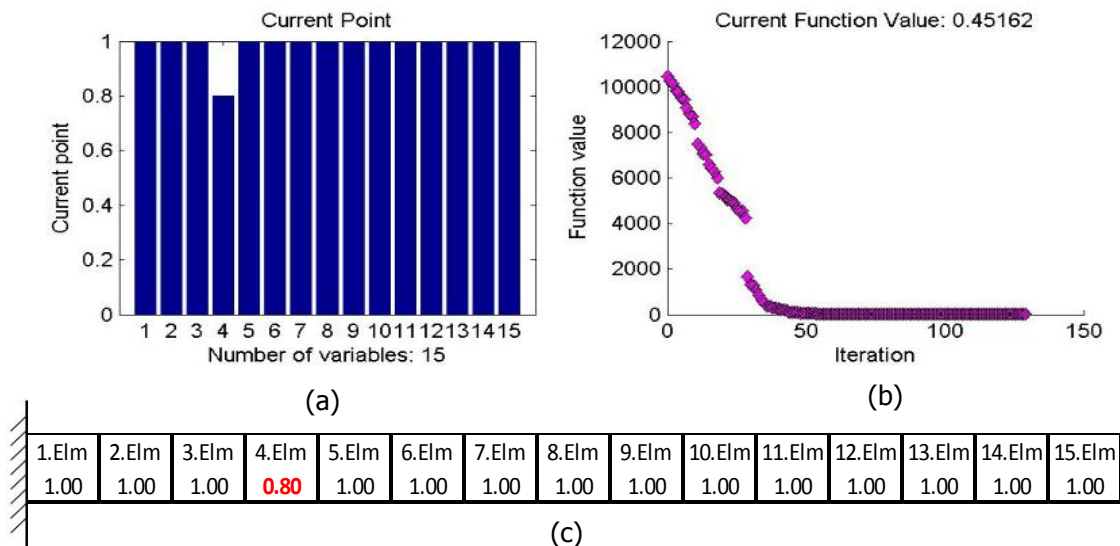


Figure 5.6. FMINCON results as a part of the hybrid system for 20% damage on the 4th element (a) Identified damage location and severity
 (b) History of Convergence (c) Numerical result of identified state

5.1.2.2 Multi Damage Scenarios

For multi saw-cut damage detection, the case given in Figure 3.21 is selected. In this sample case, damages are on the 2nd and 14th element with 10% severities. GA starts optimisation with its specified parameters to create 250 generations and then leaves the optimisation problem with the results shown in Figure 5.7(c).

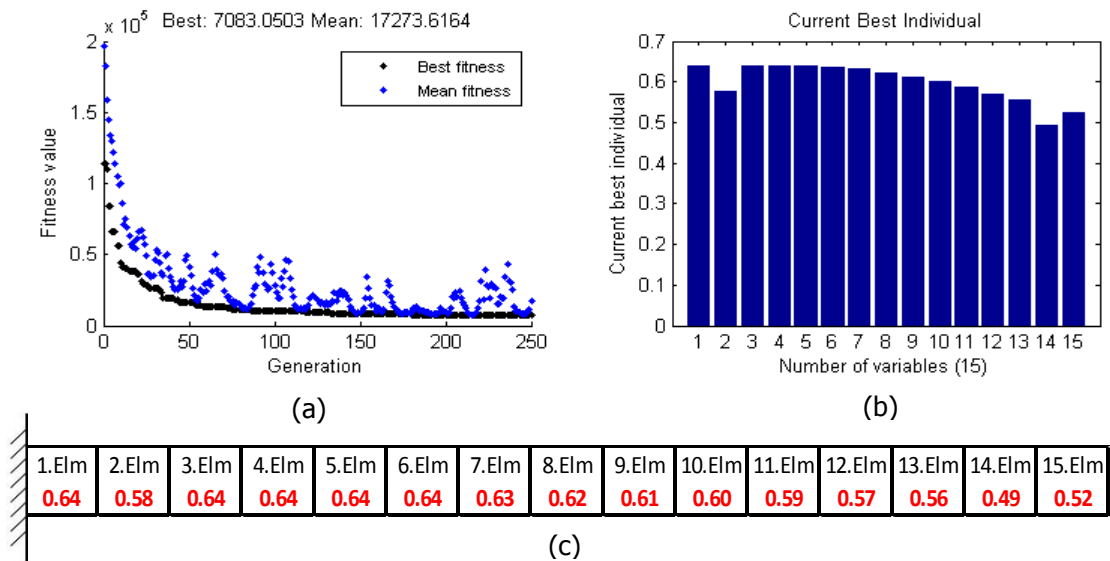


Figure 5.7. GA results for 10% damage on the 2nd element and 10% damage on the 14th element (a) History of Convergence (b) Identified damage location and severity (c) Numerical result of identified state

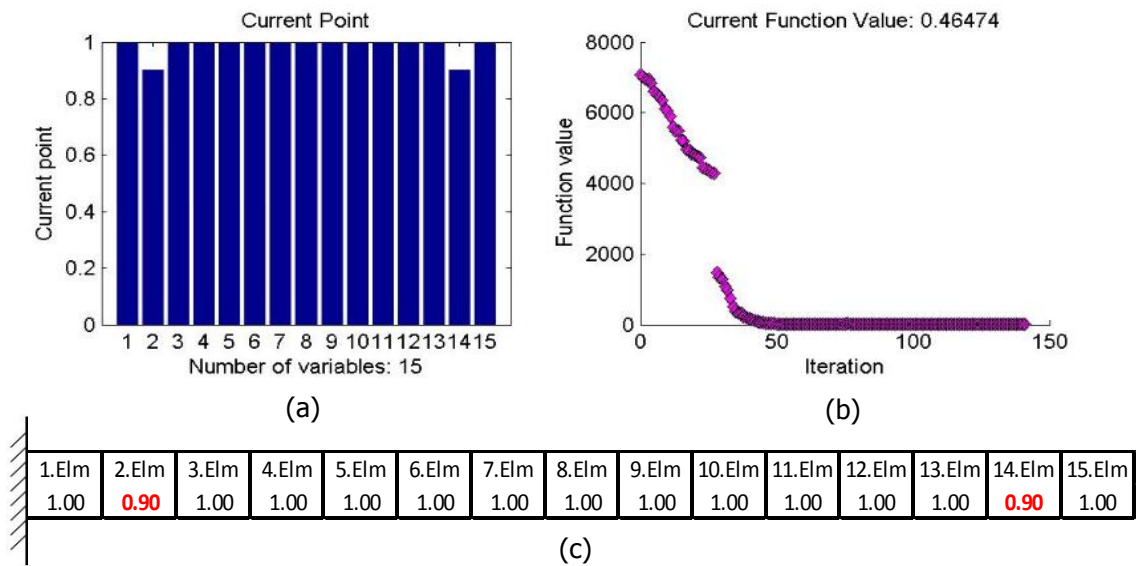


Figure 5.8. FMINCON results as a part of the hybrid system for 10% damage on the 2nd element and 10% damage on the 14th element

- (a) Identified damage location and severity
- (b) History of Convergence
- (c) Numerical result of identified state

Having obtained the results from GA part, FMINCON handle the rest of the optimisation as a part of hybrid system and ends the optimisation problem with given intactness levels presented in Figure 5.8(c). It can be seen from Figure 5.8(c) that the damages are on the 2nd and the 14th elements with same 10% severities are predicted perfectly.

5.1.3 Investigation of Damage Type in 1-D Approach

RFV method is not used as a damage type detector in the literature; however using different sensitivity matrices for the stiffness matrices gives an opportunity to detect the damage type. Damage detection mechanism shown in Figure 4.1 Part 2 is repeated twice in order to select which damage type fits more on the given state of the damaged structure. Fittest one is decided by comparing their convergence levels (i.e. the lowest objective function value is being the fittest). For instance, if damaged structure's two eigenvalues and corresponding eigenvectors are given and the damage detection algorithm is asked to find the damage type, severity and location, then the detection system follows the following procedure and first, it pretends as if the damage is impact type and tries to simulate the following (Figure 5.9) and then it finds the optimum simulation for the impact type damaged structure (Figure 5.10).

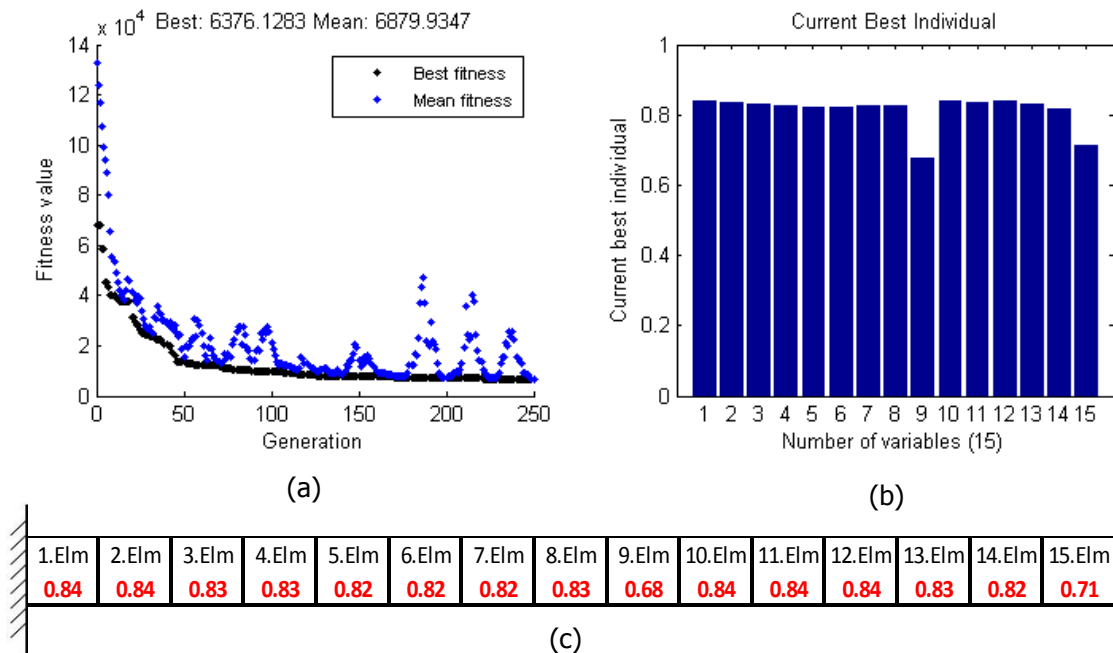


Figure 5.9. GA results for 20% damage on the 9th element – Impact type damage simulation (a) History of Convergence (b) Identified damage location and severity (c) Numerical result of identified state

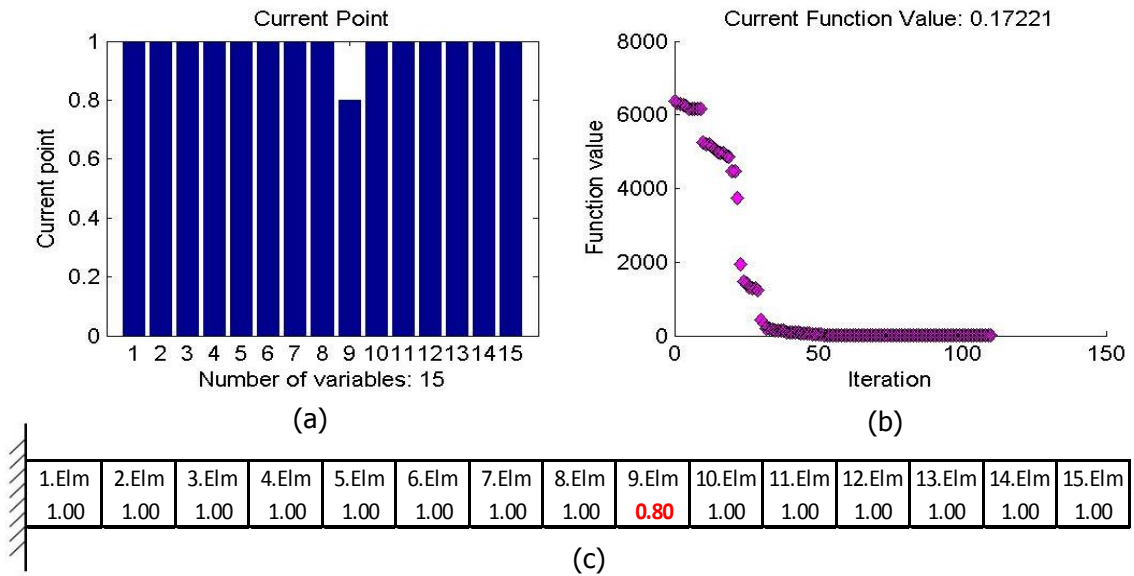


Figure 5.10. FMINCON results as a part of the hybrid system for 20% damage on the 9th element – Impact type damage simulation (a) Identified damage location and severity (b) History of Convergence (c) Numerical result of identified state

Then it pretends as if the damage is saw-cut and tries to simulate the following (Figure 5.11) and finds the optimum simulation for the saw-cut damage as well (Figure 5.12).

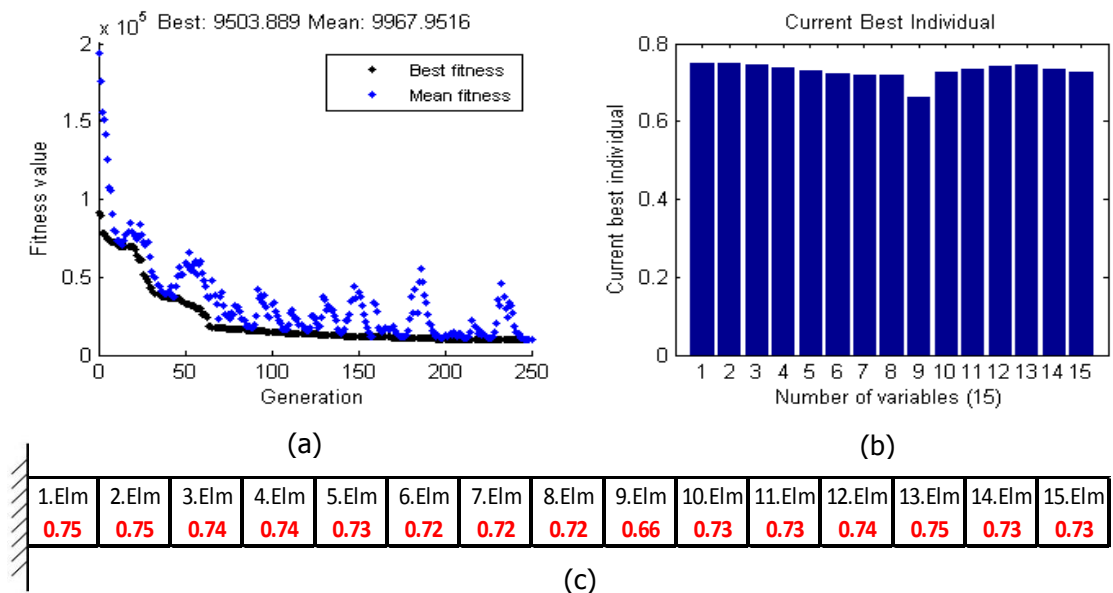


Figure 5.11. GA Result for 20% damage on the 9th element – Saw-cut type damage simulation (a) History of Convergence (b) Identified damage location and severity (c) Numerical result of identified state

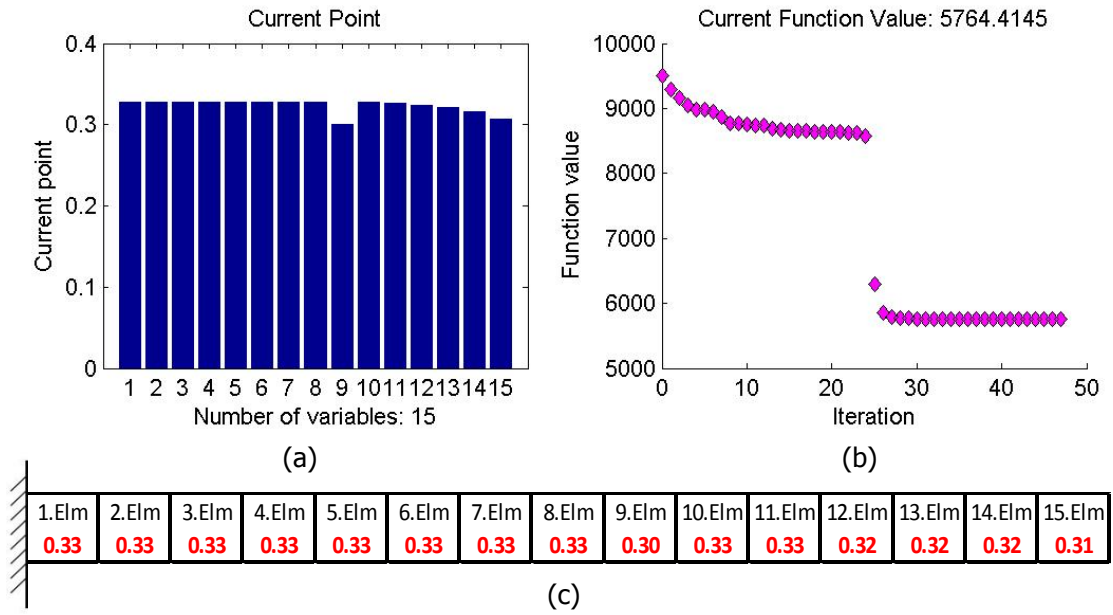


Figure 5.12. FMINCON results as a part of the hybrid system for 20% damage on the 9th element – Saw-cut type damage simulation (a) Identified damage location and severity (b) History of Convergence (c) Numerical result of identified state

Finally, it compares the simulations fitness levels by looking their final objective function values, which are 0.17 and 5764.41 for impact type and saw-cut type damage respectively. Lowest objective function value points out the damage type and the structure’s damaged state. Therefore, in this case, damage type is an impact type and on the 9th element with 20% severity.

The below case a 20% saw-cut damage on the 9th element is taken as an example. If the damage on above analysis are created as a saw-cut then the decision mechanism works in the following manner; first it pretends as if the damage is impact one and tries to simulate the following (Figure 5.13) and then it finds the optimum simulation for the impact structure (Figure 5.14). Then, the algorithm pretends as if the damage is saw-cut and it tries to simulate (Figure 5.15) and finally it finds the optimum simulation for the saw-cut type damaged structure (Figure 5.16). By looking their final objective function values which are 17103.51 and 0.42 for impact type and saw-cut type damage respectively, the algorithm decides the damage type as a saw-cut one on the 9th element with 20% severity.

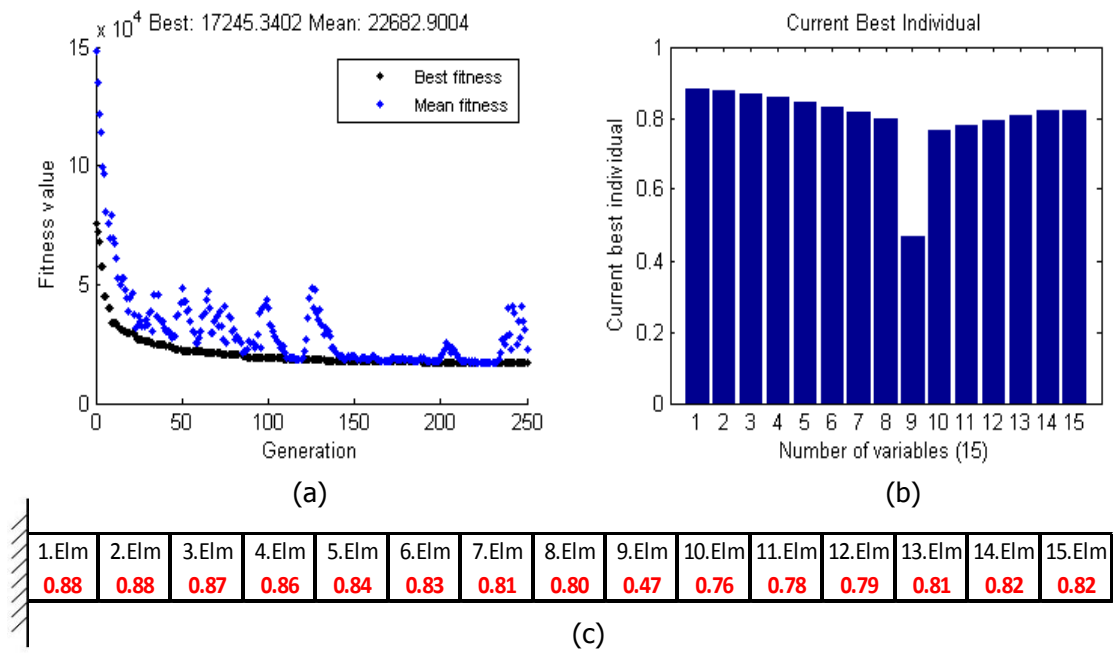


Figure 5.13. GA results for 20% damage on the 9th element – Impact type damage simulation (a) History of Convergence (b) Identified damage location and severity (c) Numerical result of identified state

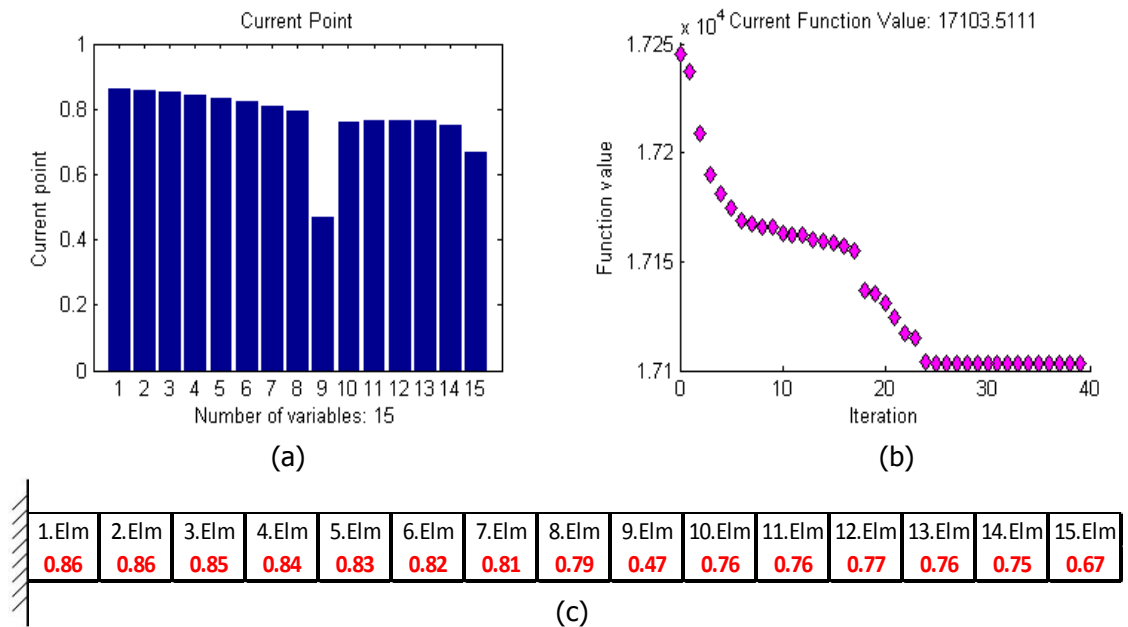


Figure 5.14. FMINCON results as a part of the hybrid system for 20% damage on 9th element – Impact type damage simulation (a) Identified damage location and severity (b) History of Convergence (c) Numerical result of identified state

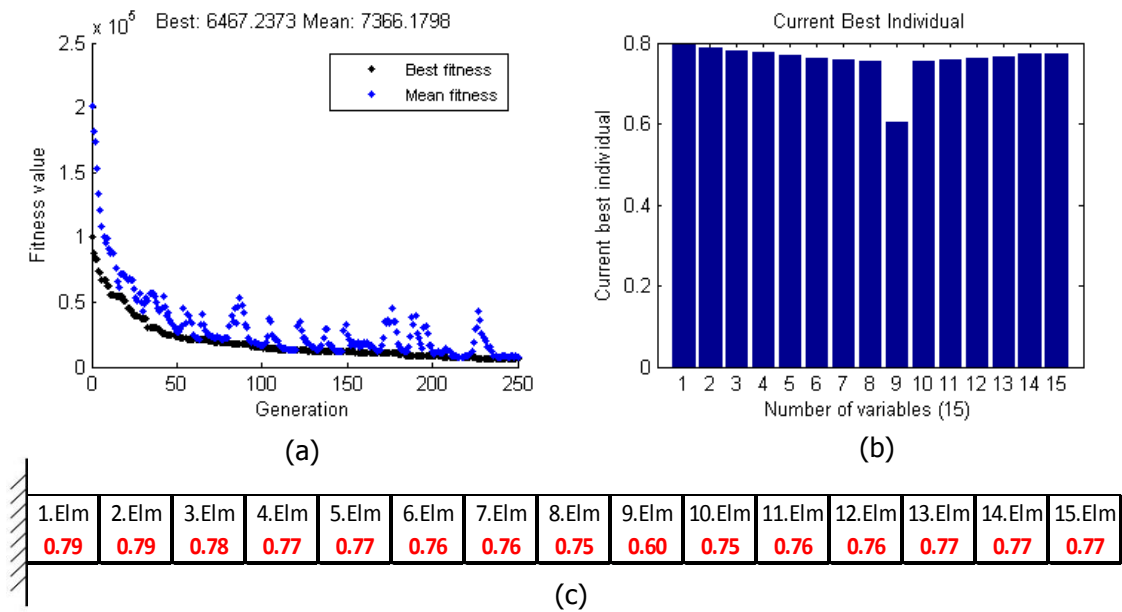


Figure 5.15. GA results for 20% damage on the 9th element – Saw-cut type damage simulation (a) History of Convergence (b) Identified damage location and severity (c) Numerical result of identified state

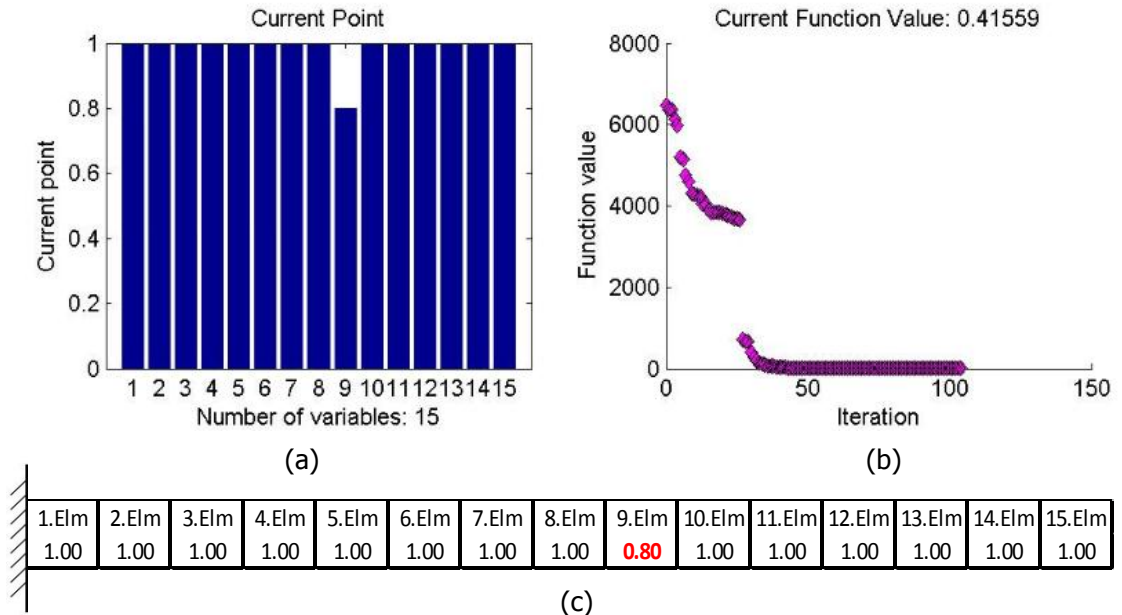


Figure 5.16. FMINCON results as a part of the hybrid system for 20% damage on the 9th element Saw-cut type damage simulation (a) Identified damage location and severity (b) History of Convergence (c) Numerical result of identified state

5.2 2-D Damage Detection

In this section, exemplification of damage detection algorithm results on the 2-D models (i.e. both Model-I and Model-II introduced in Section 3.2.2) are presented. In all parts, only one sample damage detection result is presented along 105 different single damage scenarios and twice the number of elements for multi damage scenarios.

5.2.1 Impact Type Damage

Impact type damage is categorised as both single and multi-impact as in 1-D damage detection case presented in Section 5.1. Moreover, damage detection sample cases are chosen and the results are given regarding both Model-I and Model-II in this section.

5.2.1.1 Single Damage Scenarios

For Model-I, the damage scenario presented in Figure 3.24 is selected for the analysis. In this particular case damage is on the 15th element with 20% severity. The results for GA optimisation part are given in Figure 5.17 where part (c) is the final state of the GA results after 250 generations.

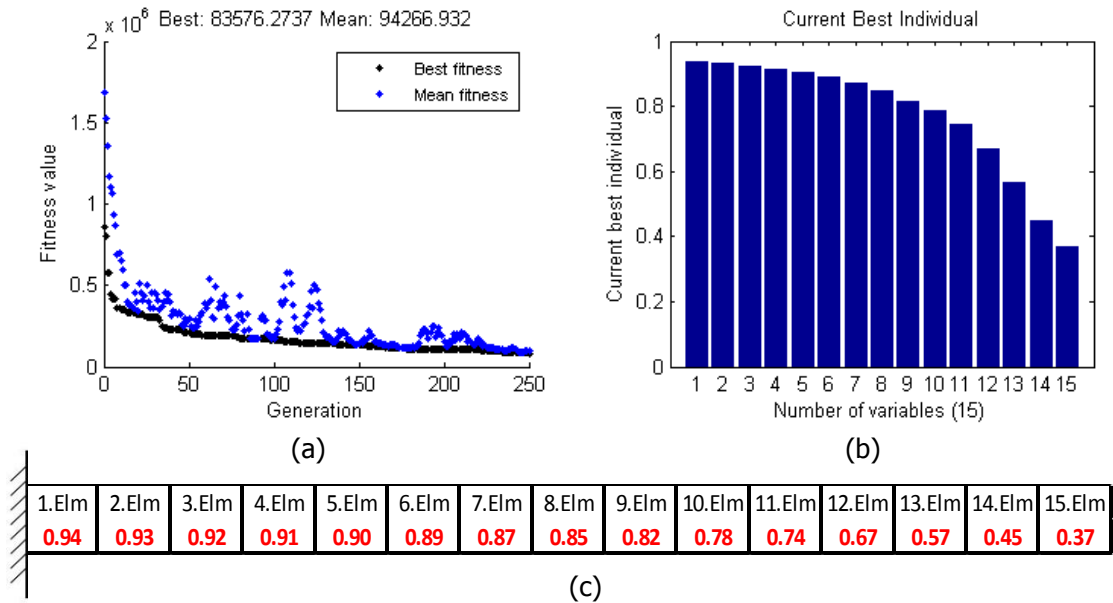


Figure 5.17. GA Result for 20% damage on the 15th element
 (a) History of Convergence (b) Identified damage location and severity
 (c) Numerical result of identified state

As it can be seen from the Figure 5.18(c) that FMINCON finds the exact damage location and the corresponding damage severity with an approximate objective function (Figure 5.18 (b)).

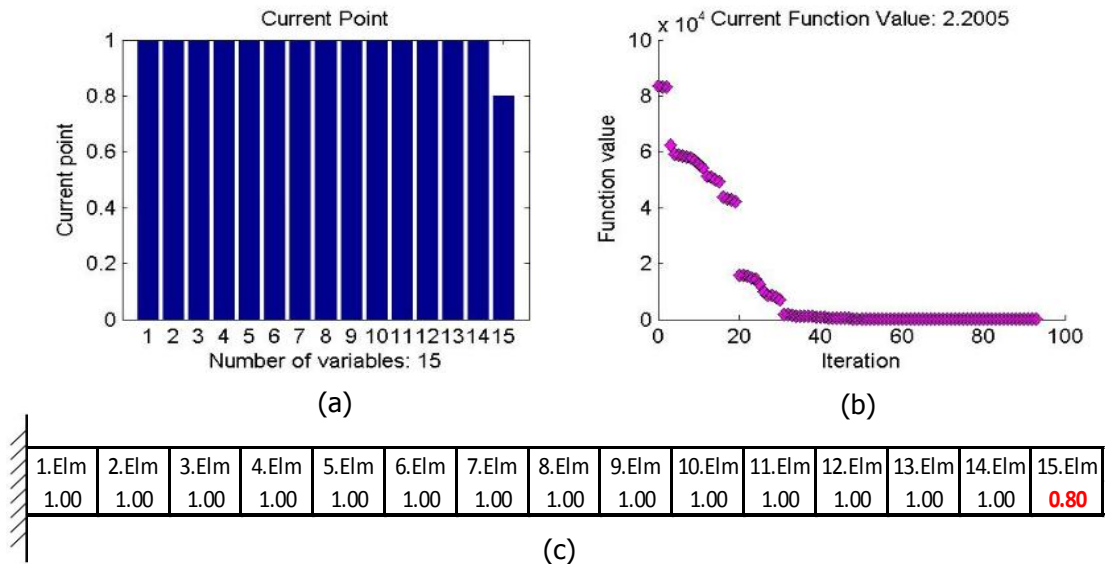


Figure 5.18. FMINCON results as a part of the hybrid system for 20% damage on the 15th element case (a) Identified damage location and severity
 (b) History of Convergence (c) Numerical result of identified state

Performing damage detection algorithm for 40% damage on the 20th element of the Model-II (Figure 3.29), Figure 5.19 can be obtained in terms of GA results. As can be seen from Figure 5.19, GA almost identifies the damage location and severity for this particular case. However, purely identified damage state of the structure is found by FMINCON as given in Figure 5.20(c).

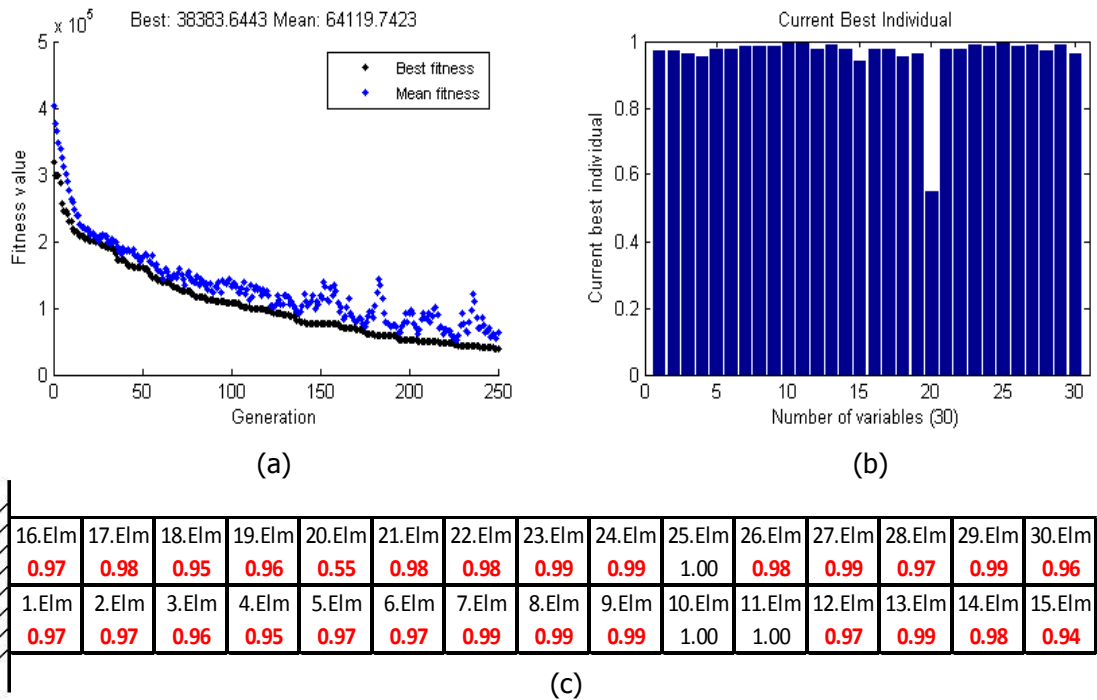


Figure 5.19. GA Result for 40% damage on the 20th element

- (a) History of Convergence (b) Identified damage location and severity
(c) Numerical result of identified state

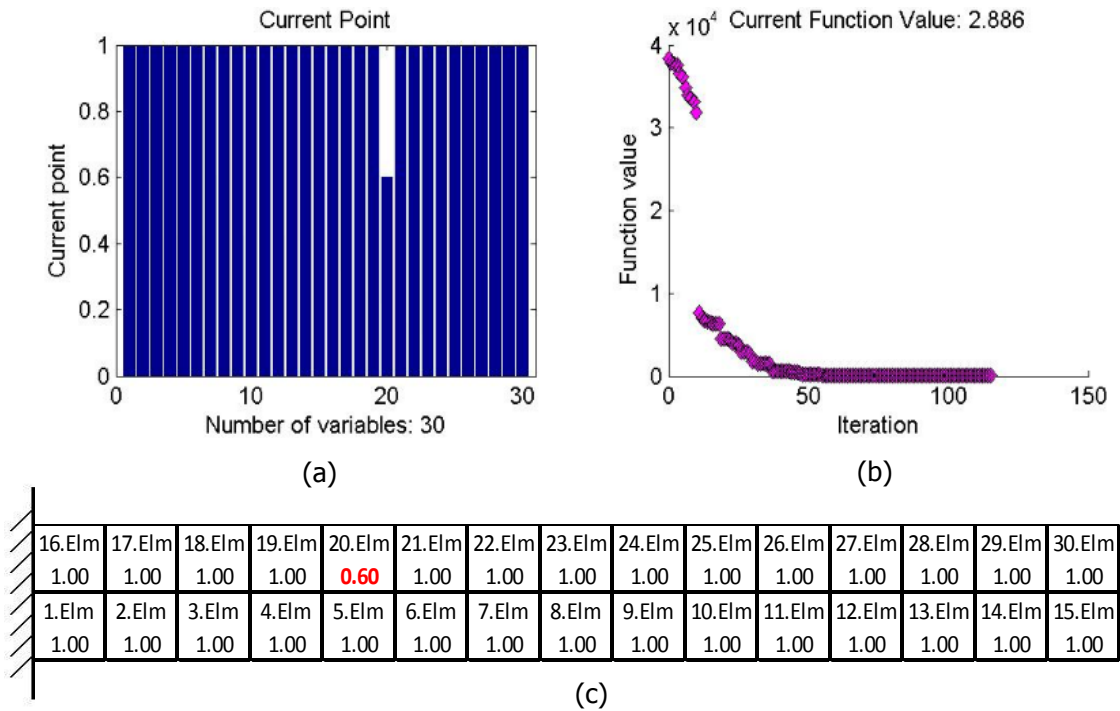


Figure 5.20. FMINCON results as a part of the hybrid system for 40% damage on the 20th element (a) Identified damage location and severity (b) History of Convergence (c) Numerical result of identified state

5.2.1.2 Multi Damage Scenarios

To exemplify damage detection result for multi damage on Model-I, the damage scenario represented on Figure 3.30 is used. After performing the damage detection algorithm on the damage case, Figure 5.21 is obtained for GA part result; Figure 5.21 (b) shows approximately that the damage locations are on 1st and 14th elements of the structure, by having lower intactness levels from the neighbour elements intactness levels. Using this information, FMINCON ends the optimisation problem with the result represented on Figure 5.22.

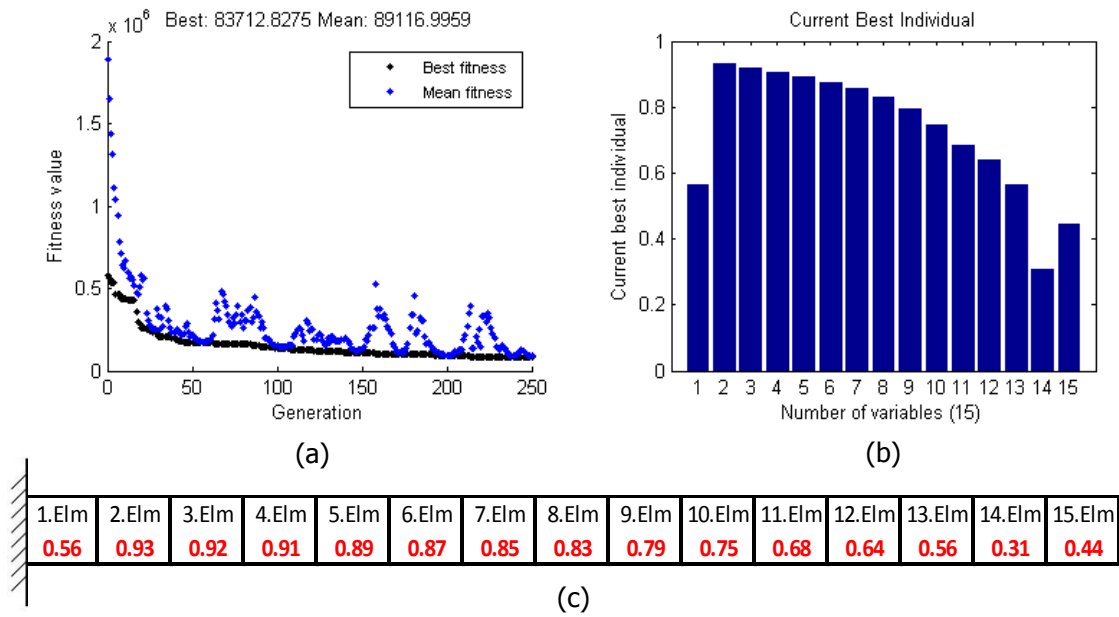


Figure 5.21. GA results for 40% damage on the 1st element and 50% damage on the 14th element (a) History of Convergence (b) Identified damage location and severity (c) Numerical result of identified state

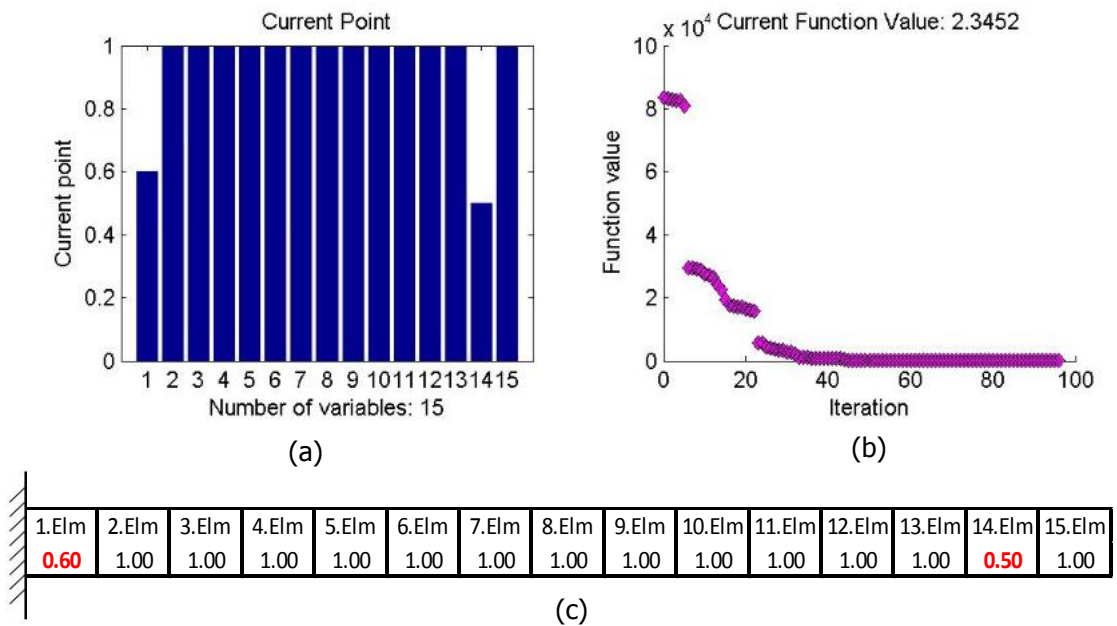


Figure 5.22. FMINCON results as a part of the hybrid system for 40% damage on the 1st element and 50% damage on the 14th element (a) Identified damage location and severity (b) History of Convergence (c) Numerical result of identified state

For multi damage cases on Model-II; damage detection algorithm is not only checked for the lateral sided two damages, but also one sided two damages in scenarios. One of the examples of this condition is shown on Figure 3.33. For that case damages are on the 14th and on the 15th elements with 50% severity and 40% severity, respectively. Performing the optimisation algorithm on the problem gives the following results; for the GA part of the optimisation, Figure 5.23 is obtained. Following GA, the FMINCON results are given in Figure 5.24 and it can be seen from this figure that the optimisation algorithm finds the damage locations and severities with superb accuracy with a very satisfactory objective function value of 2.61.

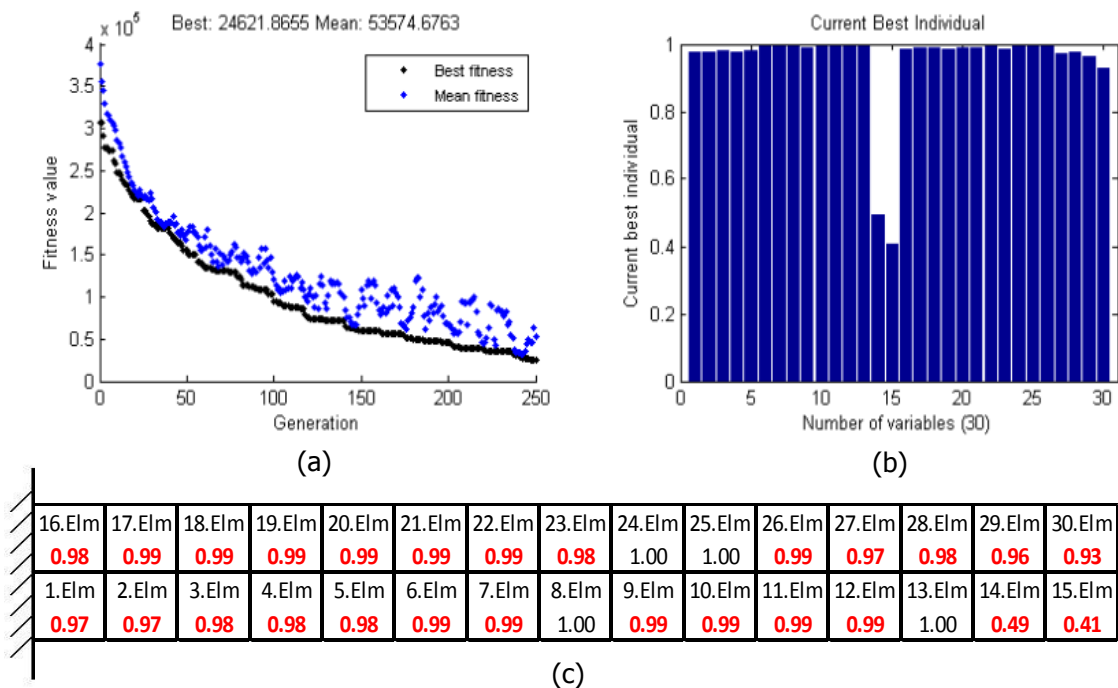


Figure 5.23. GA results for 50% damage on the 14th element and 60% damage on the 15th element (a) History of convergence (b) Identified damage location and severity (c) Numerical result of identified state

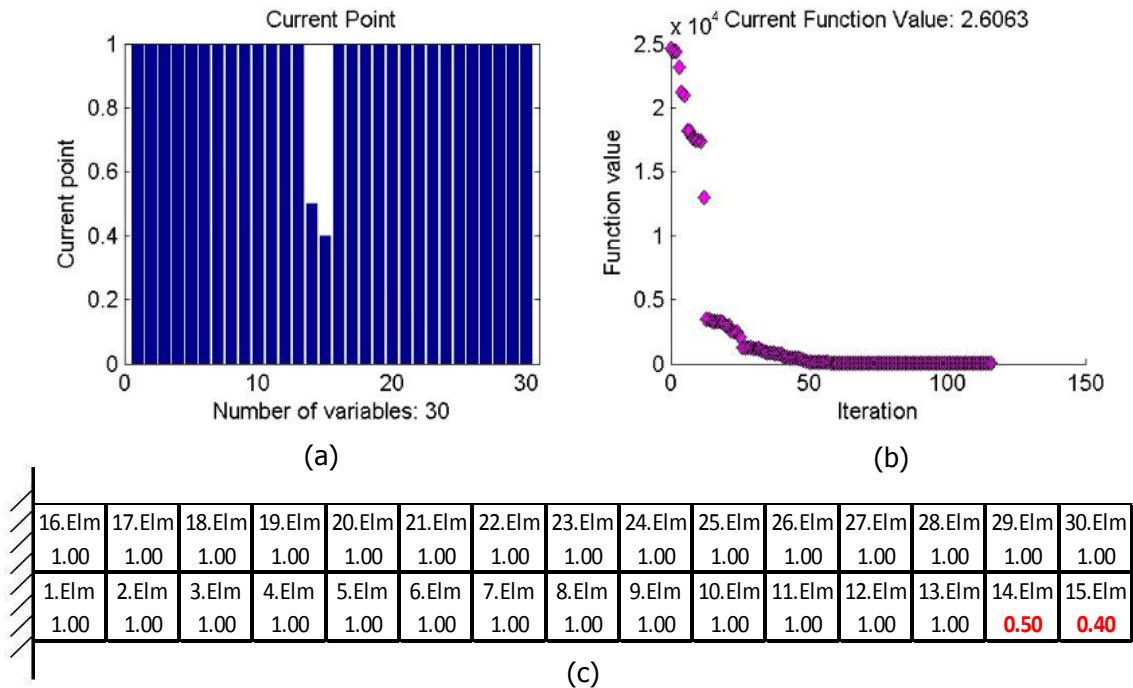


Figure 5.24. FMINCON results as a part of the hybrid system for 50% damage on 14th element and 60% damage on the 15th element (a) Identified damage location and severity (b) History of convergence (c) Numerical result of identified state

5.2.2 Saw-cut Type Damage

Saw-cut type damage is also categorised as both single and multi-impact cases. Additionally, damage detection sample cases are chosen and the results are given regarding both Model-I and Model-II for this particular damage type.

5.2.2.1 Single Damage Scenarios

Single impact damage modelling given with Figure 3.23 in Section 3.2.2.1.1 is also used here for single saw-cut damage as a reference and the sample case to test the damage detection algorithm is given in Figure 5.25 representing the GA results only.

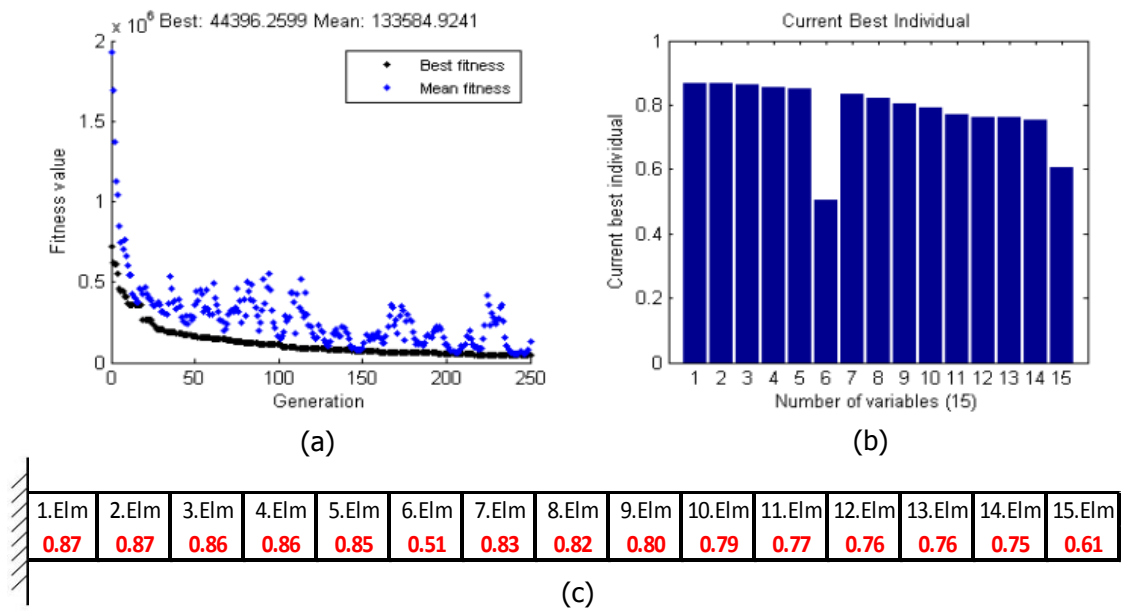


Figure 5.25. GA results for 40% damage on the 6th element (a) History of convergence (b) Identified damage location and severity (c) Numerical result of identified state

After taking optimisation problem from where the GA left (Figure 5.25(c)) and handing over to FMINCON, the hybrid algorithm concludes the results shown in Figure 5.26.

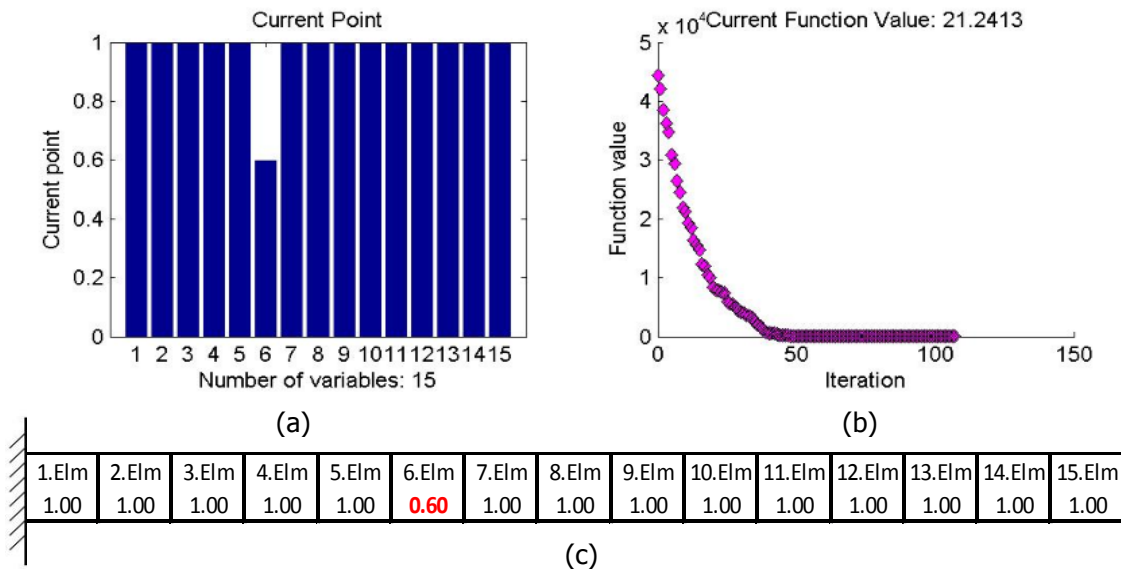


Figure 5.26. FMINCON results as a part of the hybrid system for 40% damage on the 6th element (a) Identified damage location and severity (b) History of Convergence (c) Numerical result of identified state

It can also be seen from Figure 5.26(c) that the damage is found on the 6th element with 40% severity.

For Model-II, the case shown in Figure 3.38 is selected to be identified by damage detection algorithm. On this model, damage is assigned on the 5th element of the structure with 10% severity. After performing the optimisation algorithm on the damage case, Figure 5.27 is obtained as GA part results and Figure 5.28 provides the FMINCON result as a part of the hybrid system. GA results for the saw-cut type damage detection (Figure 5.27(b)) is not as clear as impact type damages (Figure 5.19) to resemble the damage locations. However, narrowing down the solution space with FMINCON is vital for the optimisation system. Figure 5.28(c) shows the identified intactness levels of the elements of the structure and as it can be seen from that particular figure that the damage is found on the 5th element with 10% severity as expected.

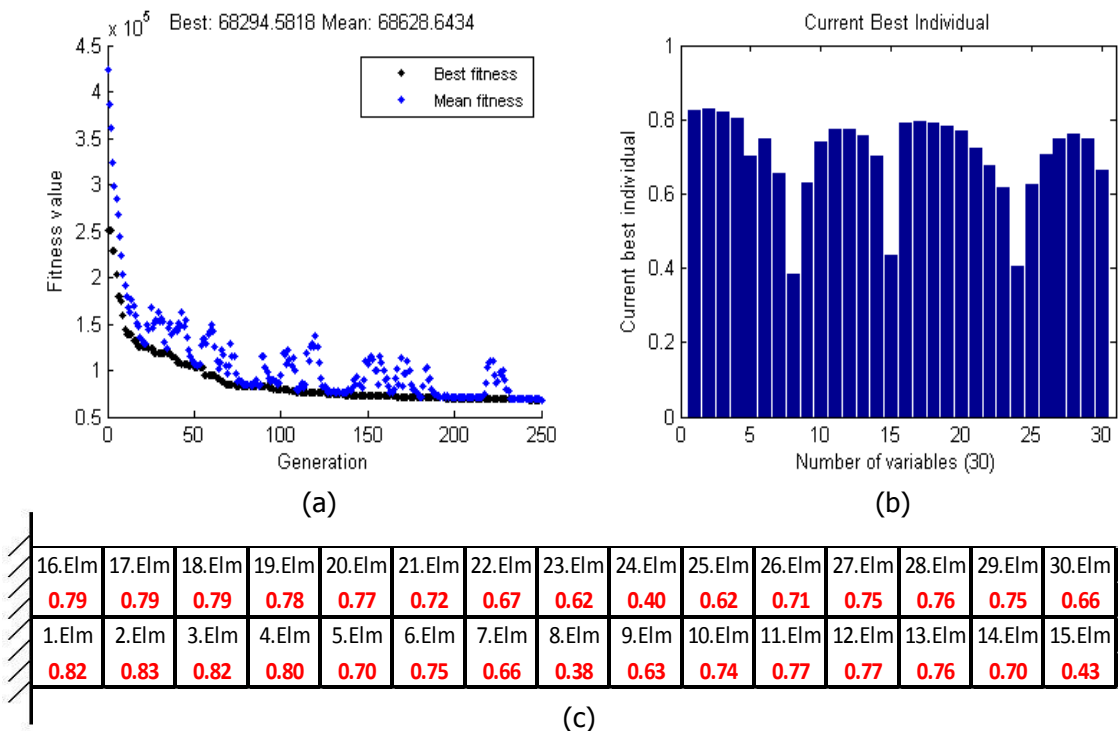


Figure 5.27. GA results for 10% damage on the 5th element
 (a) History of Convergence (b) Identified damage location and severity
 (c) Numerical result of identified state

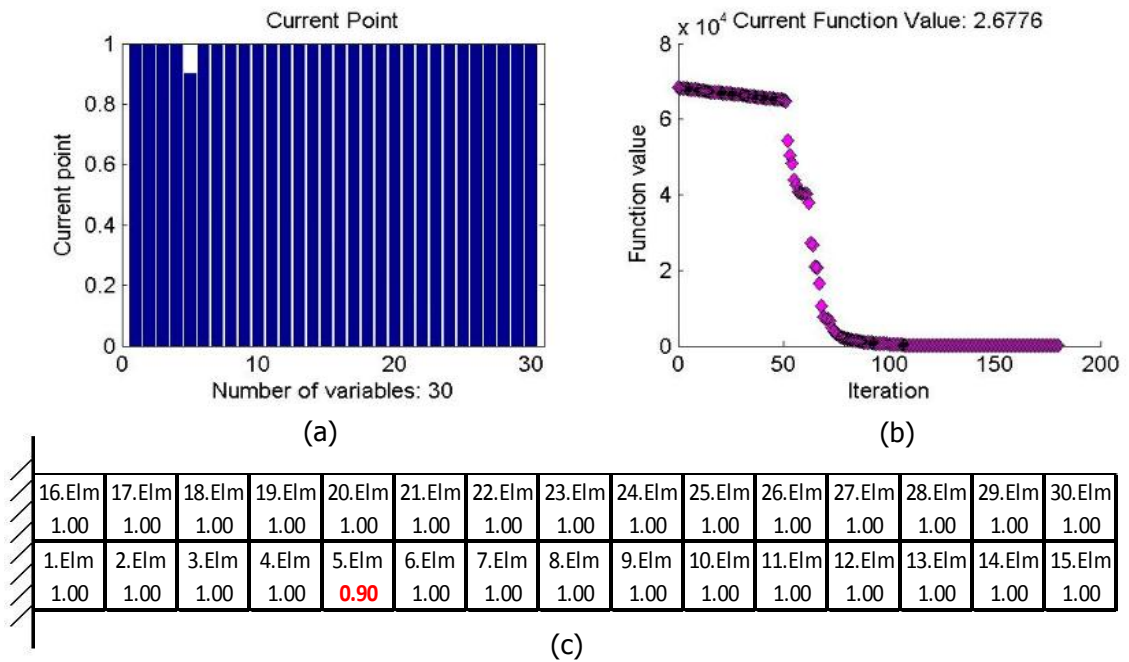


Figure 5.28. FMINCON results as a part of the hybrid system for 10% damage on the 5th element (a) Identified damage location and severity (b) History of Convergence (c) Numerical result of identified state

5.2.2.2 Multi Damage Scenarios

The damage case shown in Figure 3.40 is selected and tried to be detected by the optimisation algorithm. In this particular case, damages are modelled on the 5th element and on the 13th element with same severities of 50%.

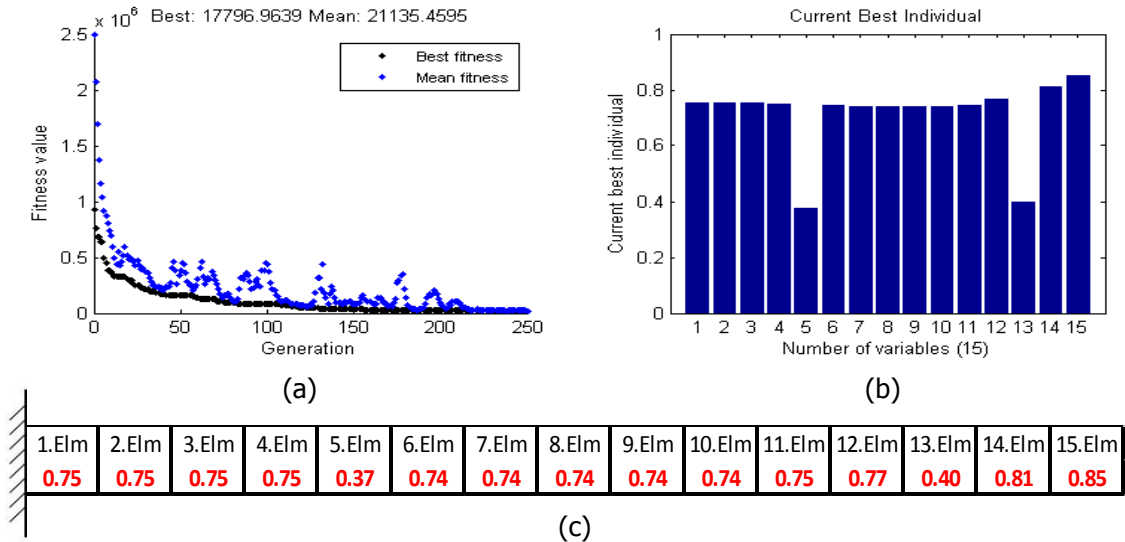


Figure 5.29. GA results for 50% damage on the 5th element and 50% damage on the 13th element (a) History of Convergence (b) Identified damage location and severity (c) Numerical result of identified state

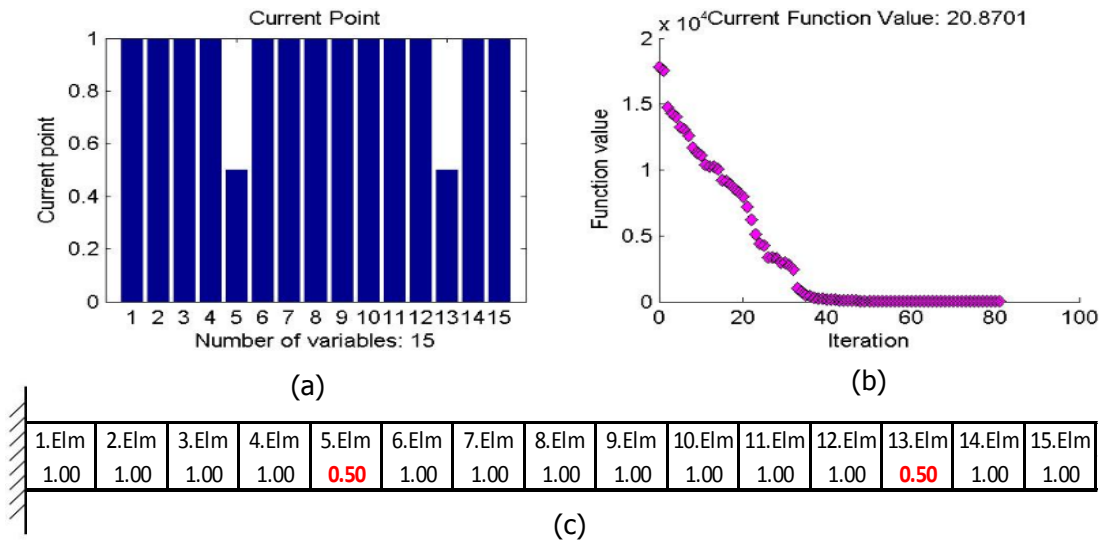


Figure 5.30. FMINCON results as a part of the hybrid system for 50% damage on the 5th element and 50% damage on the 13th element

(a) Identified damage location and severity (b) History of Convergence
(c) Numerical result of identified state

In this damage detection analysis, GA results after 250 generations are given in Figure 5.29(c). Then, FMINCON takes over the optimisation and the final result of the algorithm for the identified state of the structure is given in Figure 5.30(c) from which the damage locations can be found both on the 5th element and the 13th elements with the same severities of 50% as expected.

FEM representation given in Figure 3.42 is chosen as a multi damage detection example for the Model-II where the damages on both the 10th and the 17th elements with 10% and 40% severities respectively. By performing the damage detection algorithm on the specified problem, the Figure 5.31 and Figure 5.32 are obtained as the GA and FMINCON part respectively. The final optimisation results provided by the Figure 5.32(c) show the exact locations and the severities of the damages.

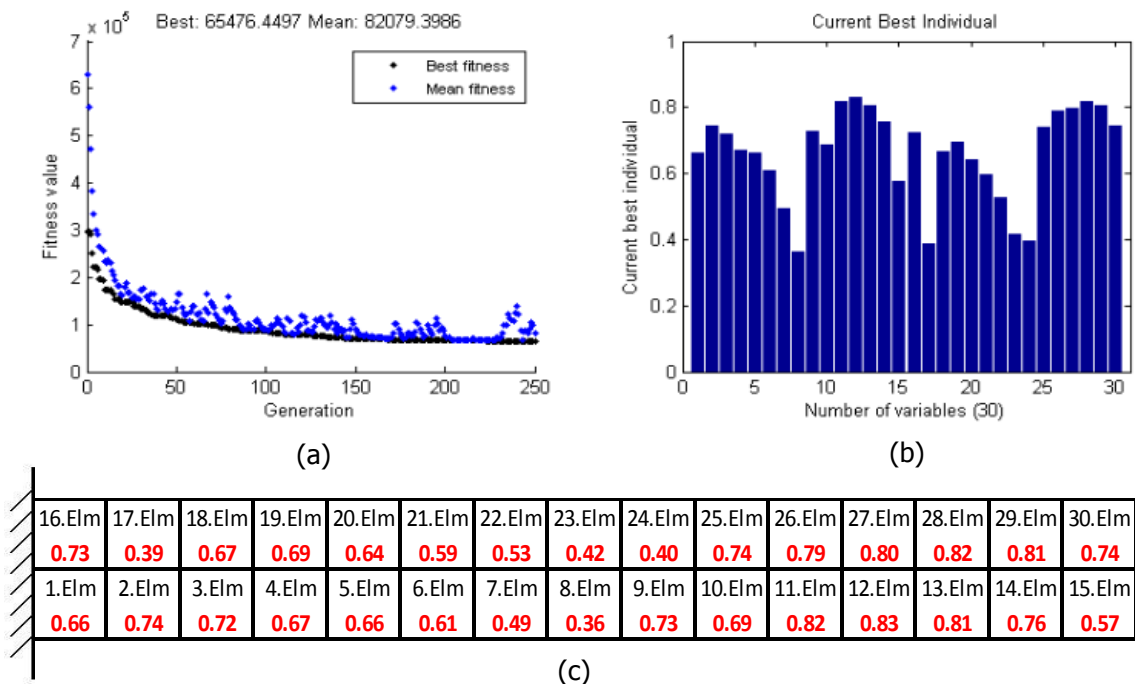
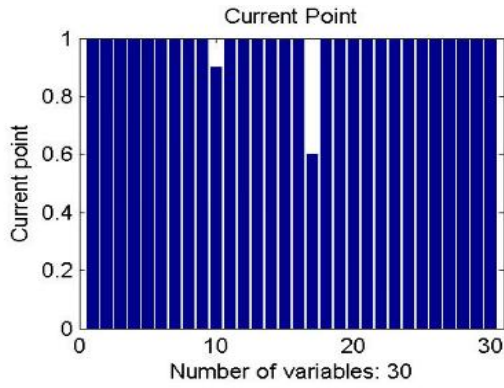
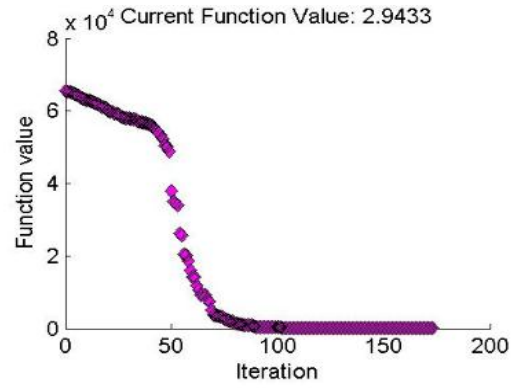


Figure 5.31. GA results for 10% damage on the 10th element and 40% damage on the 17th element (a) History of Convergence (b) Identified damage location and severity (c) Numerical result of identified state



(a)



(b)

16.Elm	17.Elm	18.Elm	19.Elm	20.Elm	21.Elm	22.Elm	23.Elm	24.Elm	25.Elm	26.Elm	27.Elm	28.Elm	29.Elm	30.Elm
1.00	0.60	1.00	1.00	1.00	1.00	1.00	1.00	1.00	1.00	1.00	1.00	1.00	1.00	1.00
1.Elm	2.Elm	3.Elm	4.Elm	5.Elm	6.Elm	7.Elm	8.Elm	9.Elm	10.Elm	11.Elm	12.Elm	13.Elm	14.Elm	15.Elm
1.00	1.00	1.00	1.00	1.00	1.00	1.00	1.00	1.00	0.90	1.00	1.00	1.00	1.00	1.00

(c)

Figure 5.32. FMINCON results as a part of the hybrid system for 10% damage on the 10th element and 40% damage on the 17th element

(a) Identified damage location and severity (b) History of Convergence

(c) Numerical result of identified state

5.2.3 Investigation of Damage Type in 2-D Approach

The procedure explained in Section 5.3.1 in detail is also followed here for the investigation of the damage type in 2-D approach. In this section, the results of the damage detection algorithm are presented regarding both Model-I and Model-II approaches. These two models have also various types of damages namely; impact and saw-cut type. The sample damage cases investigated here are chosen according to the previously considered damage cases. The results are presented again in terms of both “the GA solution part only” and “the final decision part” after the application of FMINCON as a part of the hybrid damage detection system.

Impact Type Damage Detection (Model-I)

The first sample case is the impact type damage on the 9th element with 20% severity in Model-I. The algorithm pretends first as if the damage is impact type and tries to simulate the following (Figure 5.33) and then it finds the optimum simulation for the impact type damaged structure (Figure 5.34). Following this algorithm goes for a second pretending as if the damage is this time a saw-cut type and tries to simulate the following (Figure 5.35) and then it finds the optimum simulation for the saw-cut type damaged structure (Figure 5.36).

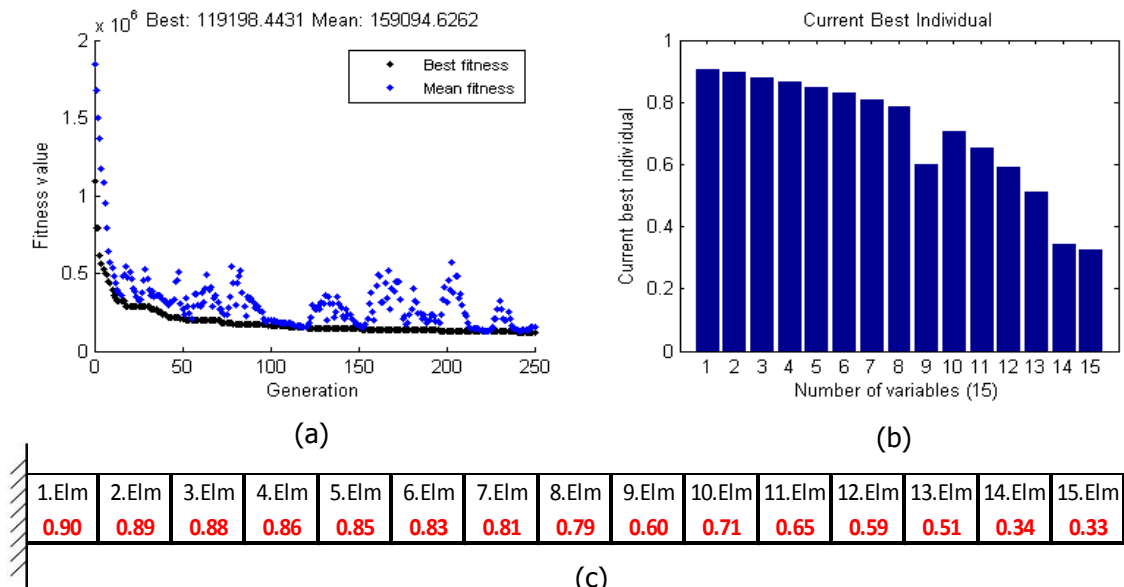


Figure 5.33. GA Result for 20% damage on the 9th element – Impact type damage simulation, Model-I (a) History of Convergence (b) Identified damage location and severity (c) Numerical result of identified state

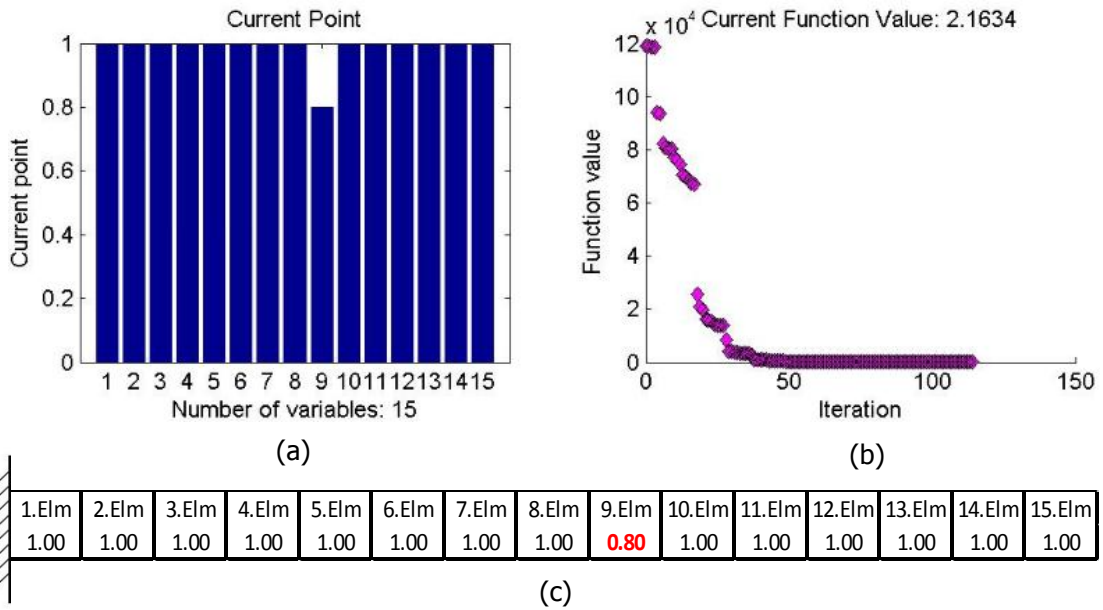


Figure 5.34. FMINCON results as a part of the hybrid system for 20% damage on the 9th element – Impact type damage simulation, Model-I

(a) Identified damage location and severity (b) History of Convergence

(c) Numerical result of identified state

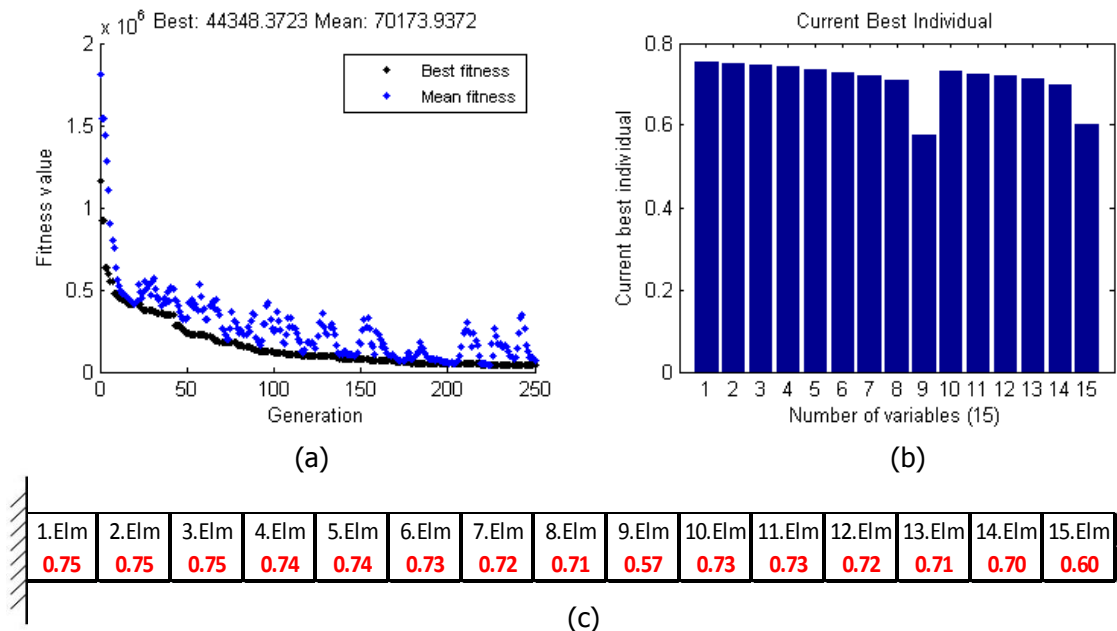


Figure 5.35. GA Result for 20% damage on the 9th element – Saw-cut type damage simulation, Model-I (a) History of Convergence (b) Identified damage location and severity (c) Numerical result of identified state

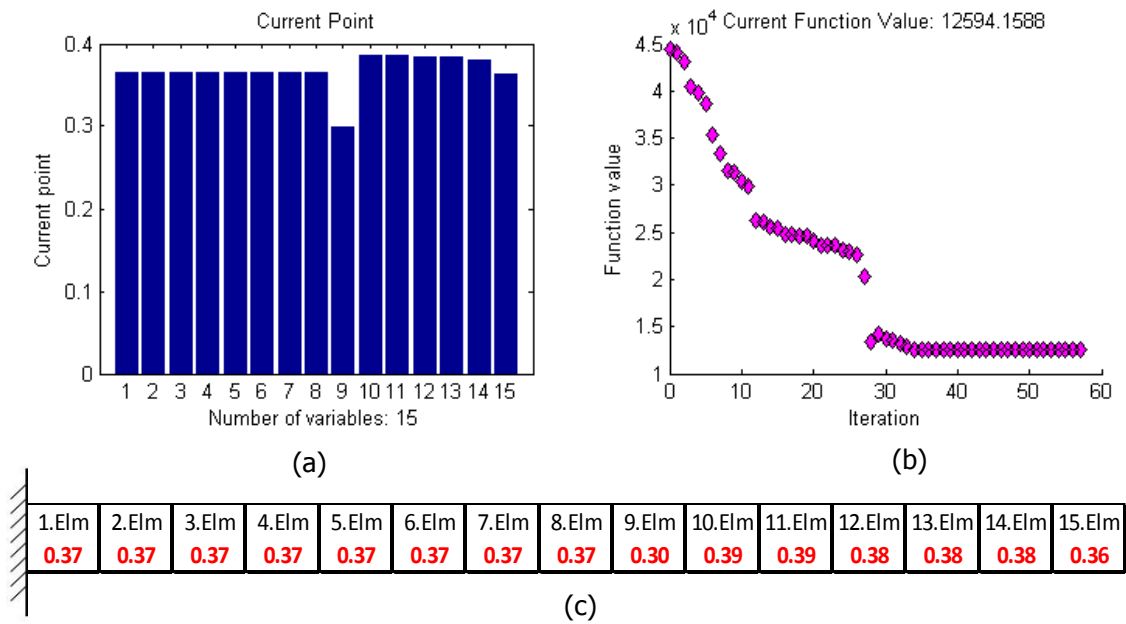


Figure 5.36. FMINCON results as a part of the hybrid system for 20% damage on the 9th element – Saw-cut type damage simulation, Model-I
 (a) Identified damage location and severity (b) History of Convergence
 (c) Numerical result of identified state

Finally, it compares the simulations fitness levels by looking their final objective function values, which are 2.16 and 12594.16 for impact type and saw-cut type damage respectively. Lowest objective function value points out the damage type and the structure’s damaged state. Therefore, in this case, damage type is an impact type and on the 9th element with 20% severity (Figure 5.34).

Saw-cut Type Damage Detection (Model-I)

The predictions which are performed for the Impact Type Damage Detection (Model-I) are also performed for the Saw-cut Type Damage Detection (Model-I) and the results are given from Figures 5.37 to Figures 5.40 as a second example.

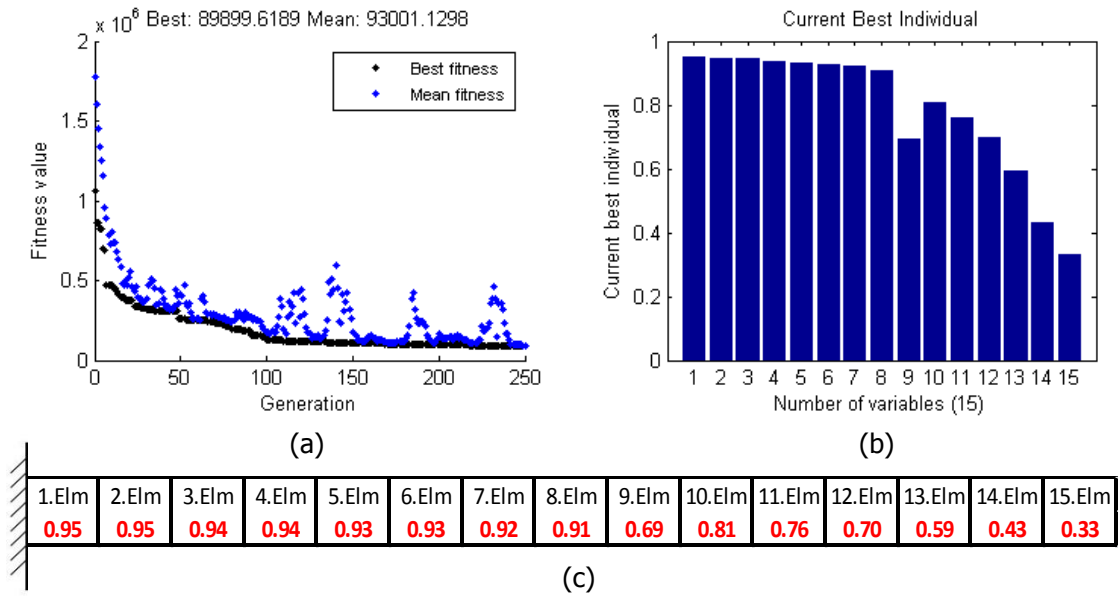


Figure 5.37. GA Result for 20% damage on the 9th element – Impact type damage simulation, Model-I (a) History of Convergence (b) Identified damage location and severity (c) Numerical result of identified state

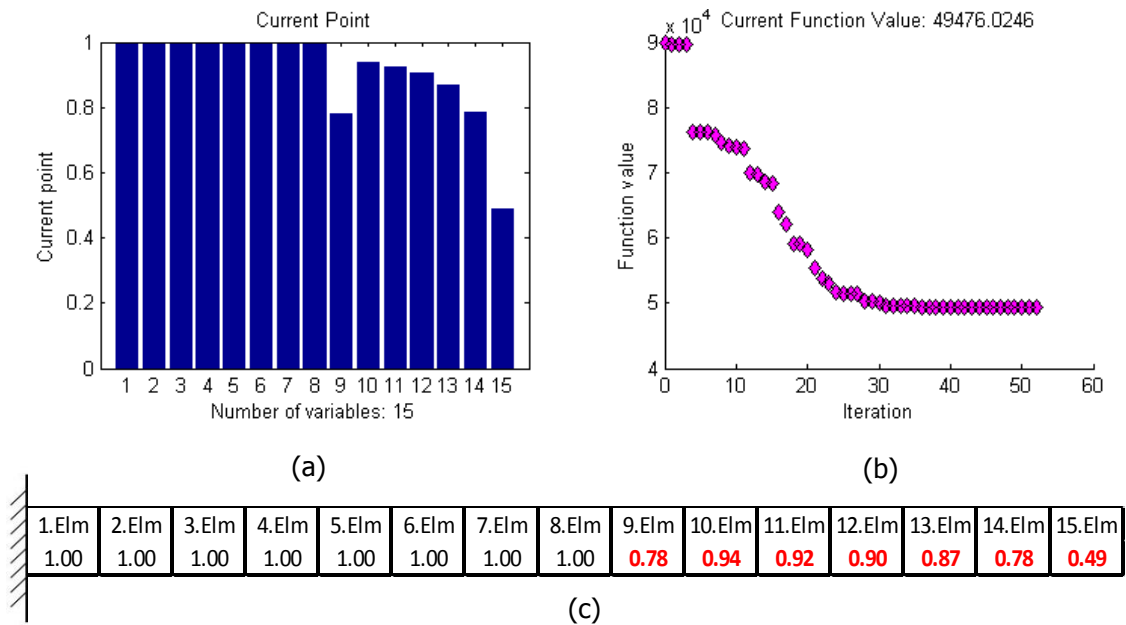


Figure 5.38. FMINCON results as a part of the hybrid system for 20% damage on 9th element – Impact type damage simulation, Model-I (a) Identified damage location and severity (b) History of Convergence (c) Numerical result of identified state

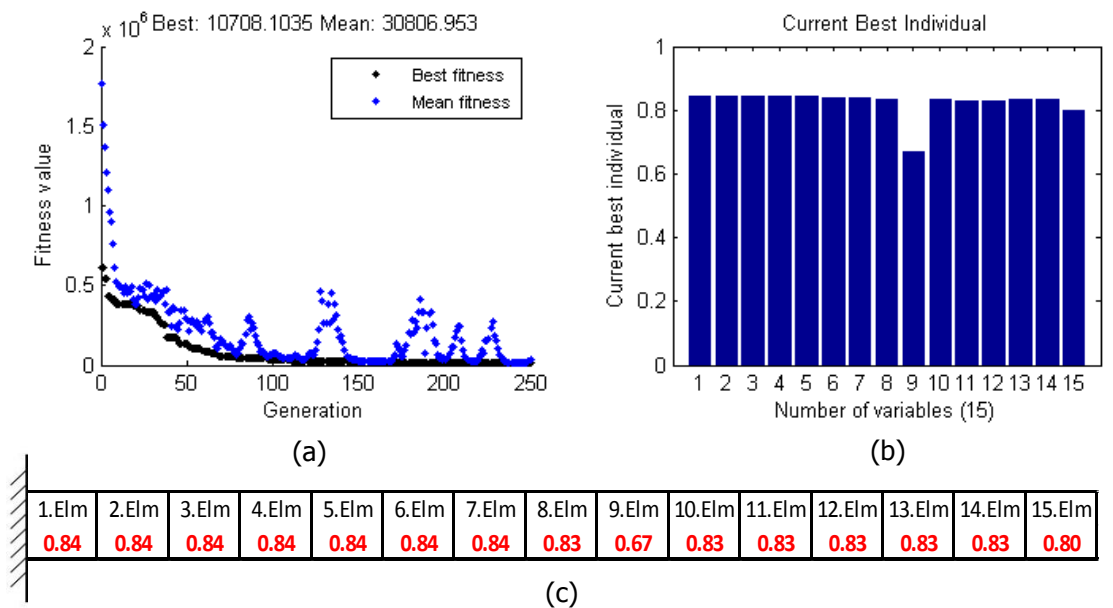


Figure 5.39. GA Result for 20% damage on the 9th element – Saw-cut type damage simulation, Model-I (a) History of Convergence (b) Identified damage location and severity (c) Numerical result of identified state

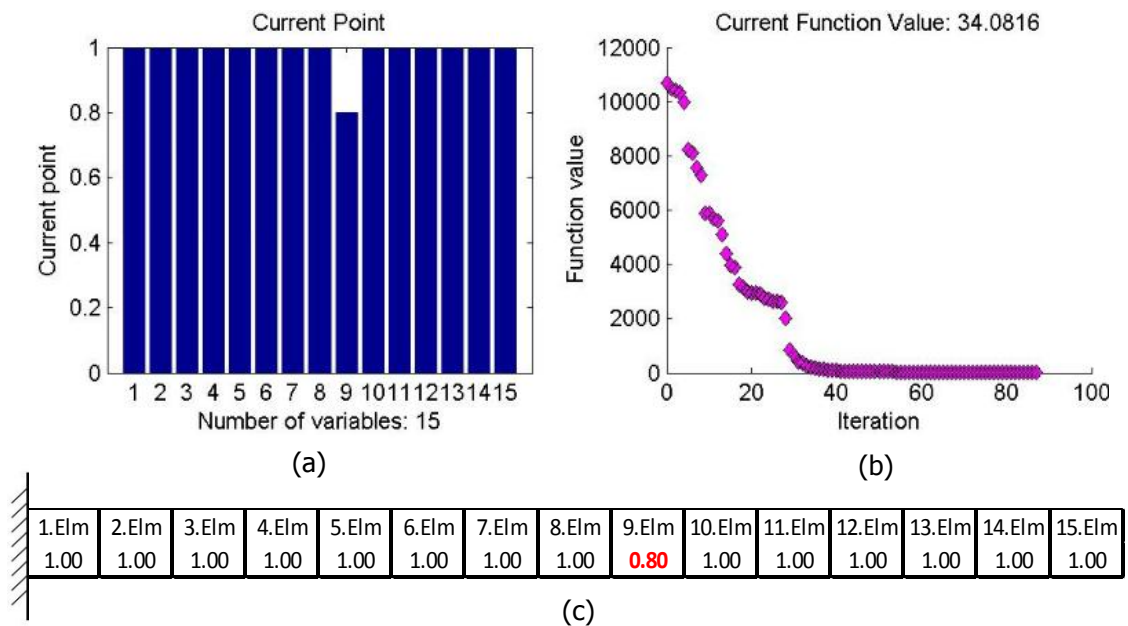


Figure 5.40. FMINCON results as a part of the hybrid system for 20% damage on 9th element – Saw-cut type damage simulation, Model-I (a) Identified damage location and severity (b) History of Convergence (c) Numerical result of identified state

By looking their final objective function values which are 49476.02 and 34.08 for impact type and saw-cut type damage respectively. Lowest objective function value points out the damage type and the structure's damaged state. Therefore, in this case, damage type is a saw-cut type and on the 9th element with 20% severity (Figure 5.40).

Impact Type Damage Detection (Model-II)

The third sample case is the impact type damage on both the 9th element and 24th element with 20% severity in Model-II and the results are given from Figures 5.41 to Figures 5.44.

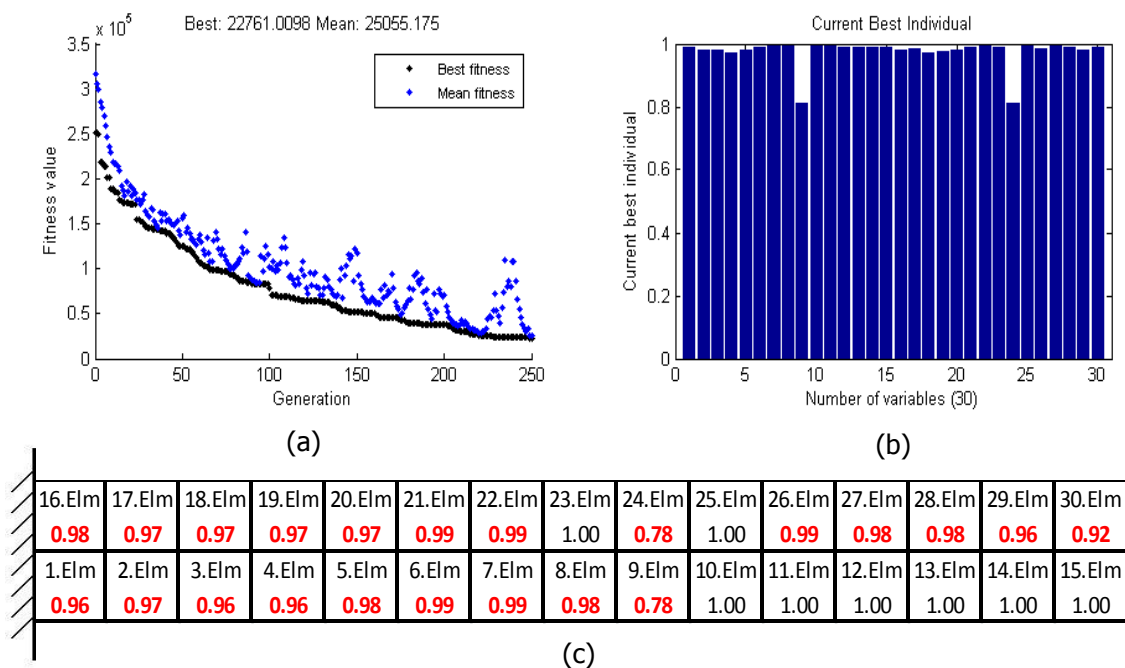


Figure 5.41. GA Result for 20% damage on both the 9th element and 24th element – Impact type damage simulation, Model-II (a) History of Convergence (b) Identified damage location and severity (c) Numerical result of identified state

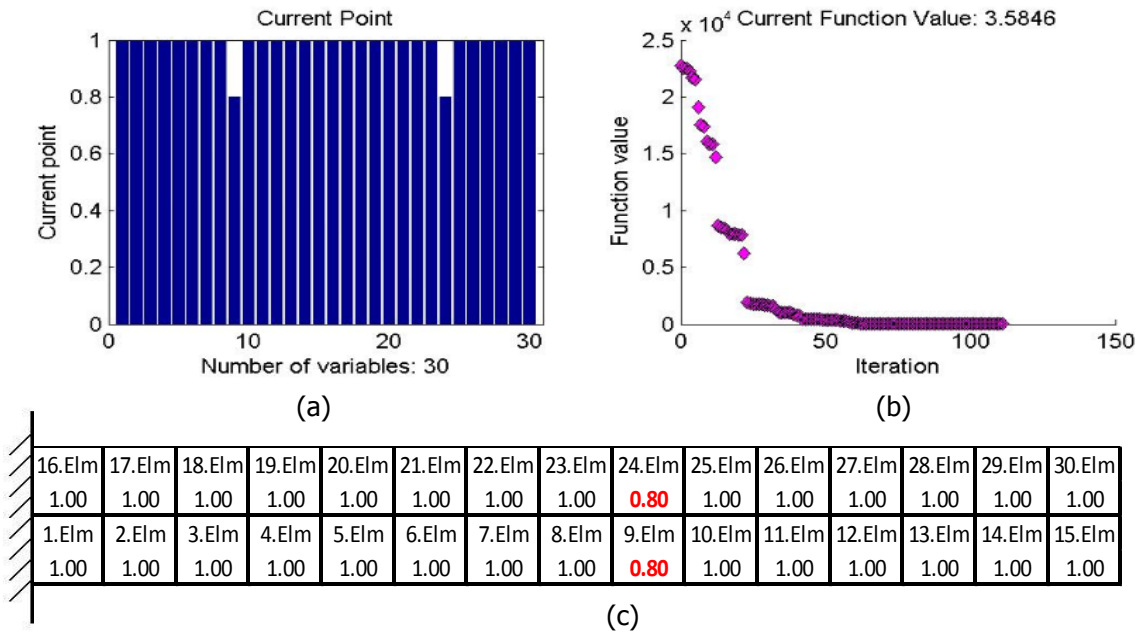


Figure 5.42. FMINCON results as a part of the hybrid system for 20% damage on both the 9th element and 24th element – Impact type damage simulation, Model-II
 (a) Identified damage location and severity (b) History of Convergence
 (c) Numerical result of identified state

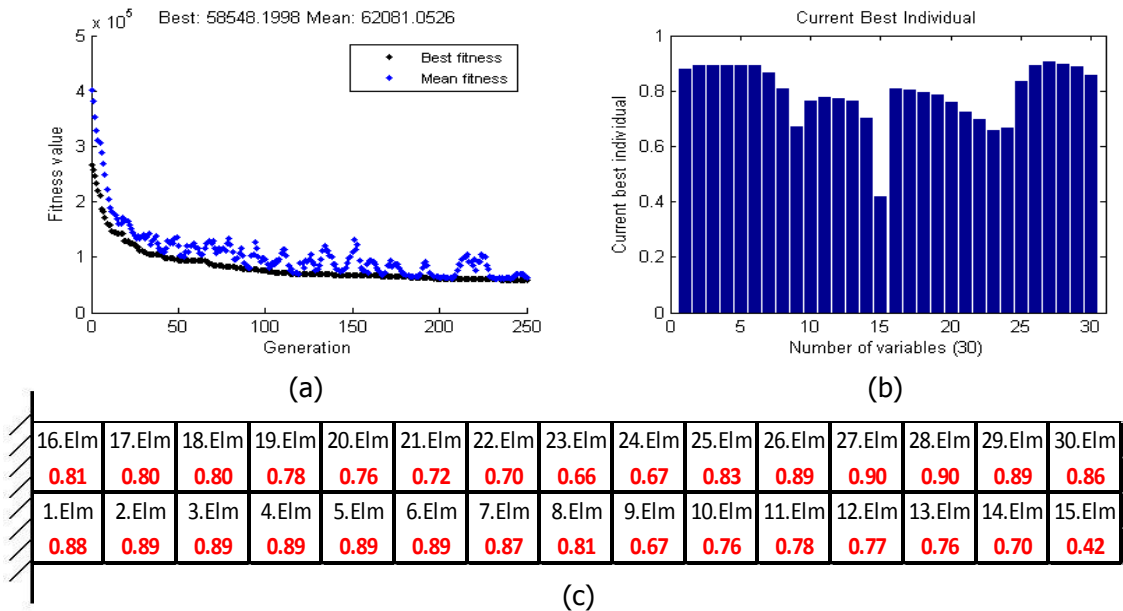


Figure 5.43. GA Result for 20% damage on both the 9th element and 24th element – Saw-cut type damage simulation, Model-II (a) History of Convergence
 (b) Identified damage location and severity (c) Numerical result of identified state

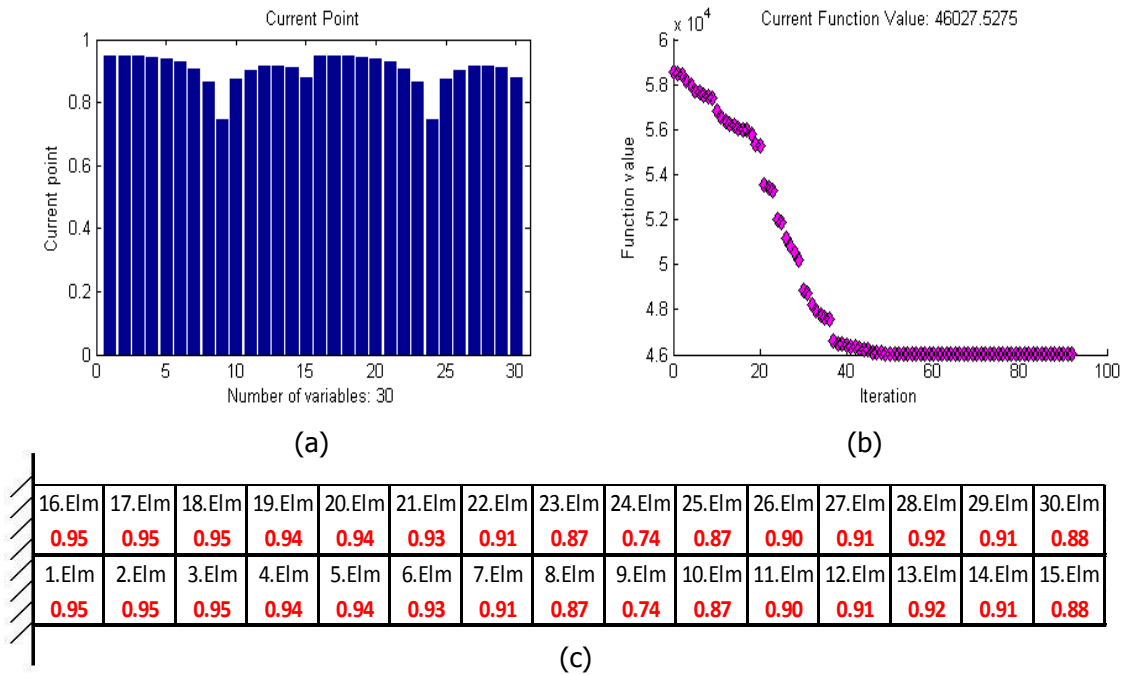


Figure 5.44. FMINCON results as a part of the hybrid system for 20% damage on both the 9th element and 24th element – Saw-cut type damage simulation, Model-II
 (a) Identified damage location and severity (b) History of Convergence (c) Numerical result of identified state

The algorithm compares the simulations fitness levels by looking their final objective function values, which are 3.58 and 46027.53 for impact type and saw-cut type damage respectively and in this case, damage type is an impact type and on both the 9th element and the 24th element with same severities of 20% (Figure 5.42).

Saw-cut Type Damage Detection (Model-II)

The predictions which are performed for the Impact Type Damage Detection (Model-II) are also performed for the Saw-cut Type Damage Detection (Model-II) and the results are given from Figures 5.45 to Figures 5.48 as a forth example.

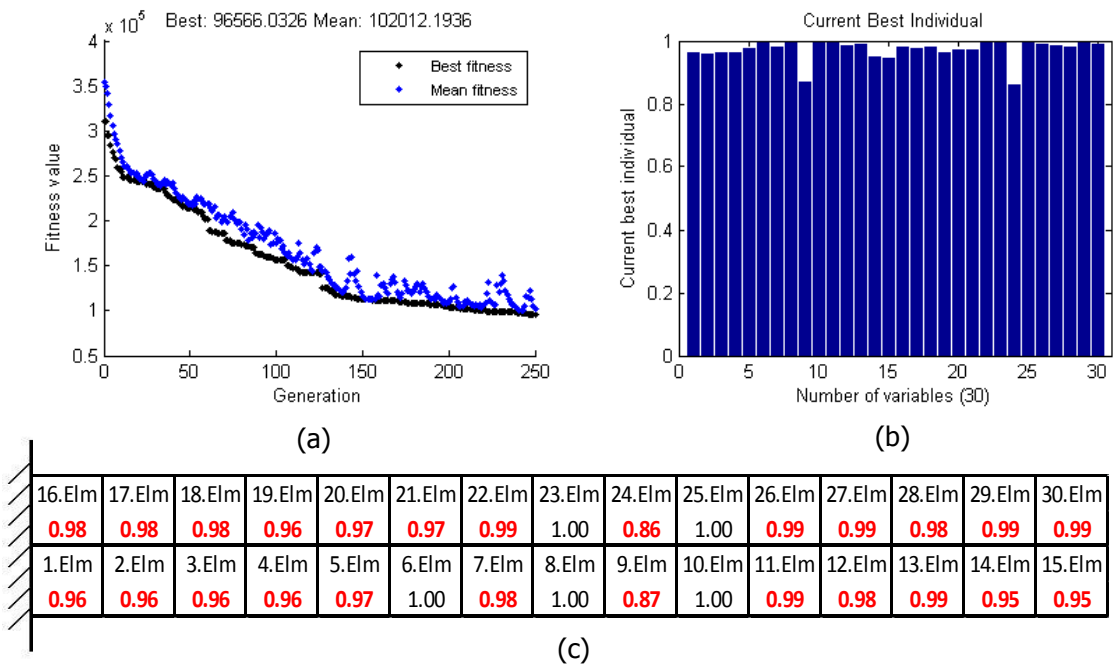


Figure 5.45. GA Result for 20% damage on both the 9th element and 24th element – Impact type damage simulation, Model-II (a) History of Convergence (b) Identified damage location and severity (c) Numerical result of identified state

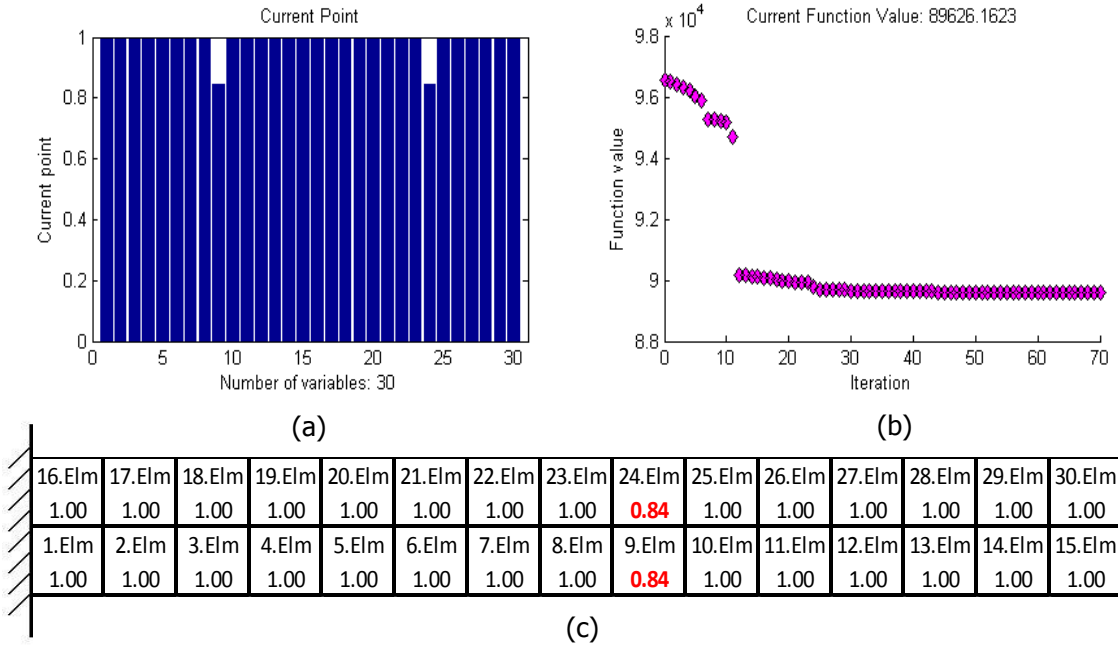


Figure 5.46. FMINCON results as a part of the hybrid system for 20% damage on both the 9th element and 24th element – Impact type damage simulation, Model-II (a) Identified damage location and severity (b) History of Convergence (c) Numerical result of identified state

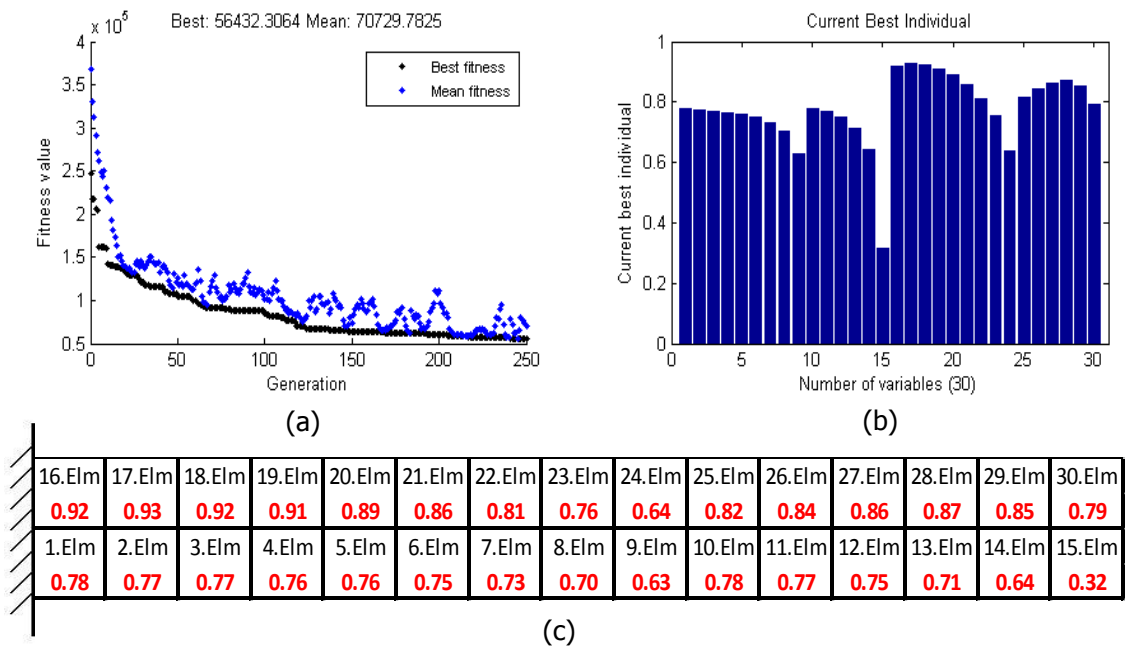


Figure 5.47. GA Result for 20% damage on both the 9th element and 24th element – Saw-cut type damage simulation, Model-II (a) History of Convergence (b) Identified damage location and severity (c) Numerical result of identified state

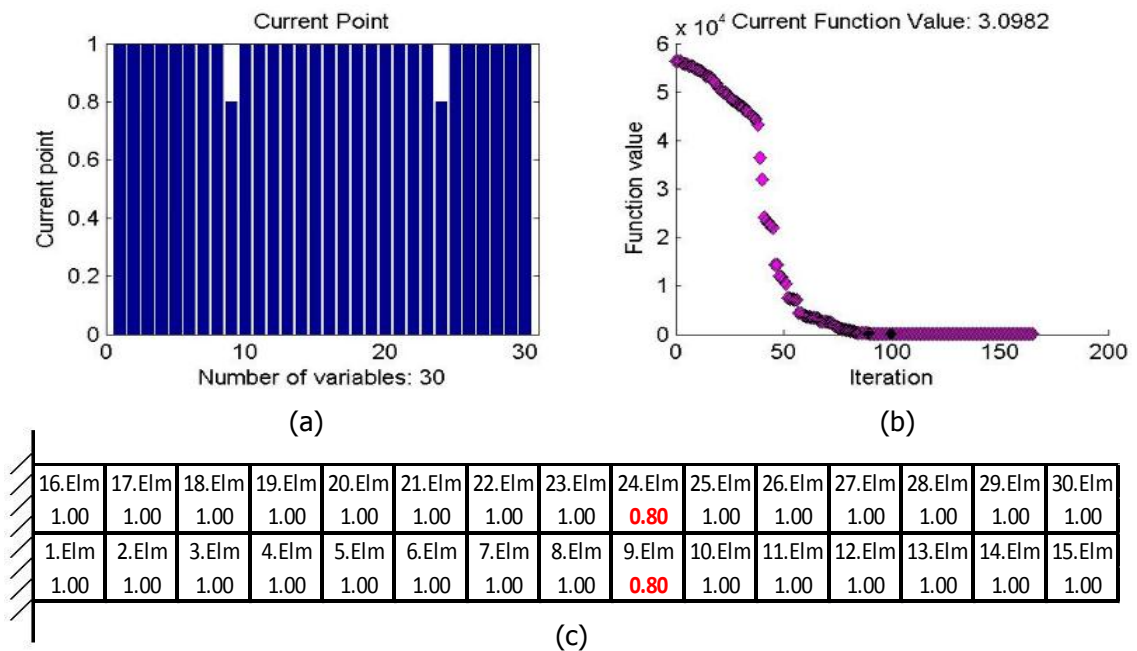


Figure 5.48. FMINCON results as a part of the hybrid system for 20% damage on both the 9th element and 24th element – Saw-cut type damage simulation, Model-II (a) Identified damage location and severity (b) History of Convergence (c) Numerical result of identified state

The algorithm compares the simulations fitness levels by looking their final objective function values, which are 89626.16 and 3.10 for impact type and saw-cut type damage respectively and in this case, damage type is an saw-cut type and on both the 9th element and the 24th element with same severities of 20% (Figure 5.48).

CHAPTER 6

CONCLUSIONS

6.1 General Conclusions

The main objective of this thesis is to design a combined genetic algorithm and non-linear optimisation system for identification of structural damage of a cantilever isotropic beam regarding its location, severity and type. The vibration-based features, both natural frequencies (i.e. eigenvalues) and displacement mode shapes (i.e. eigenvectors) of the structure in the first two out of plane bending modes, are selected as damage features for various types of damage comprising both impact and saw-cut types.

In the first part of the thesis, FEM of the beam is generated via 1-D modelling approach and the validation of the model is performed via normal mode dynamic analysis. Then, the comparisons with both classical beam theory and a benchmark article [10] results are also made. This model is extended to 2-D model by only changing the element type used in FEM and so-called "Model-I" is obtained and then by keeping the number of elements in span-wise direction and doubling the lateral-wise elements in number, the second model, "Model-II", is generated via 2-D modelling approach. Following the results of the normal mode dynamic analysis and the checks for mesh independency, the validations of the intact beam structure models are finally made. Having obtained the verified intact structure models, different types of damages are defined and modelled via FEM. The impact type damage is modelled as an elastic modulus reduction whereas the saw-cut type one is in terms of thickness reduction. Then, various damage scenarios are created and the results obtained from the first two out of plane bending modes are tabulated in

order to show the effects of the damage on those natural frequencies. With these scenarios, the inverse and non-unique problem of the damage identification is investigated and the importance of using of more than one natural frequency information is also stressed.

In the second part of the thesis, the residual force vectors (i.e. damage sensitive features) are obtained and minimised via a combined genetic algorithm and non-linear optimisation. In order to find both optimum numbers of mode shapes to use as damage features and optimum GA characteristic parameters (i.e. crossover fraction) several re-runs of GA is performed and interpretations are made by using the mean of the obtained final objective function values. Efficiency of the optimisation system is also increased by using hybrid GA system and the identification studies are performed for damage location and severity.

In the final part of this study, the performance of the proposed combined genetic algorithm and non-linear optimisation system is tested on various damage scenarios created at different locations with different severities for both single and multi damage cases and the results of the damage identification system regarding these scenarios on a cantilever beam structure are presented. The obtained results indicate that the proposed method used in this study proved itself as an effective one in the determination of type, severity and location of the damage created on beam-like structures.

6.2 Recommendations for Future Work

In this thesis a combined genetic algorithm and non-linear optimisation system which uses RFV as an objective function is designed and used in the identification of structural damage of a cantilever isotropic beam regarding its location, severity and type.

The recommendations for the future works of this study can be listed as follows:

- In FE modelling, only isotropic structures are examined due to ease of interpretation of both elastic modulus and thickness reduction on the stiffness and mass matrices of the structure. Impact and saw-cut type damage characteristics could be approximated on orthotropic structures

as well. Additionally, different type damages which are more specific for composite structures such as fibre breakage, matrix cracking and delamination could also be investigated.

- Throughout the thesis, two different element types (i.e. bar2 and quad4) of Msc. Patran[®] are used for 1-D and 2-D modelling of the structure. Different types of elements such as 3-D or composite elements depending on the shape/type of the structure could also be used and introduced to the algorithm for the investigation of various damage types.
- The method comprising the use of residual force vector (RFV) is designed only for undamped systems and therefore the damping effects are not taken into account. Damping effects could also be included in the analyses of real structures regarding their real boundary conditions as well.
- Damage identification success (i.e. accuracy of the estimation of damage location and severity) of the combined optimisation algorithm (genetic algorithm with FMINCON) used in this thesis somehow comes from the fact that a free noise data is taken from finite element analysis and introduced to the algorithm. The damage detection system could be checked by using experimental data as well.
- The main Matlab code, which is generated in order to deal with both the interface and optimization part of the system, calls various sub functions (e.g. element and/or sensitivity matrices, system variables, etc.) and therefore, increasing mesh density or modelling of complex structures may cause some problems due to hardware limitations regarding the computation time. So, due to having large percentage of zeros, element mass and stiffness matrices could be converted to sparse matrices having tremendously small memory allocation and the system performance could be improved.
- Residual force vector (RFV) method is used for the detection of damage types by comparing their corresponding objective function values obtained from simulations. This technique, therefore, can differentiate -

only- purely impact or purely saw-cut type damages. This means that the multi damages comprising both impact and saw-cut type occurred on the same structure can't be detected and/or differentiated. However, if damage locations are detected on limited number of elements by using more local methods such as mode shape curvature, then the interpretation of these damages could be done via proposed method in this thesis.

REFERENCES

1. **Yang, Q.W. and Liu, J.K.** *Structural Damage Identification Based on Residual Force Vector*. s.l. : Journal of Sound and Vibration 305: 298-307, 2007.
2. **Rao, M.A., Srinivas, J. and Murthy, B.S.N.** *Damage Detection in Vibrating Bodies Using Genetic Algorithms*. s.l. : Comput Struct 2004;82(11-12):963-8, 2004.
3. **Yun, C. B. & Bahng E.Y.** *Substructural Identification Using Neural Networks*. s.l. : Computer and Structures, 77, 41-52, (2000).
4. **Mares, C. and Surace, C.** *An Application of Genetic Algorithms to Identify Damage in Elastic Structure*. s.l. : Journal of Sound and vibration ;195(2):195-215, 1996.
5. **Panigrahi, S.K., Chakraverty, S. and Mishra, B.K.** *Vibration Based Damage Detection in a Uniform Strength Beam Using Genetic Algorithm*. s.l. : Meccanica. , (2009).
6. **Meruane, V. and Heylen, W.** *Damage Detection by a Real-Parameter Hybrid Genetic Algorithm*. Poland : Proceedings of the Fourth European Workshop on Structural Health Monitoring, 1073-1080, July 2008.
7. **Rytter, A.** *Vibration based inspection of civil engineering structures Doctoral Dissertation*. s.l. : Department of Building Technology and Structural Engineering, University of Aalborg, 1993.
8. **Rieger, N. F.** *The Relationship Between Finite Element Analysis and Modal Analysis*. New York : Journal of Sound & Vibration, 1986.
9. **Zak A., Krawczuk and W. Ostachowicz.** *Vibration Analysis of Composite Plate with Closing Delamination*. s.l. : Journal of Intelligent Material Systems and Structures 12: 545 , 2001.
10. **Friswell, M.I., Penny, J.E.T. and Garvey, S.D.** *A Combined Genetic Eigensensitivity Algorithm for the Location of Damage in Structures* . s.l. : Comput. Struct ;69: 547-556., 1998.

11. **Kim , J.T., et al.** *Damage Identification in Beam-Type Structures: Frequency-Based Method vs. Mode-Shape-Based Method.* s.l. : Engineering Structures, 25, 57-67, 2003.
12. **Carden, E.P. and Fanning, P.** *Vibration Based Condition Monitoring: A Review.* s.l. : Structural Health Monitoring , 2004.
13. **Şahin, M.** *Damage Identification in Beam-like Structures by Vibration-based Analysis and Artificial Neural Networks.* s.l. : University of Southampton, March 2004.
14. **Qiao, Jialai Wang and Pizhong.** *Improved Damage Detection for Beam-type Structures using a Uniform Load Surface.* s.l. : Structural Health Monitoring 6:99, 2007.
15. **Hao, Hong, Asce, M. and Xia, Yong.** *Vibration-based Damage Detection of Structures by Genetic Algorithm.* s.l. : J. Comput. Civil Eng. vol. 16, no. 3, pp. 222–229, 2002.
16. **Hu, J.S. ve Hwu, C.** *Free Vibration of Delaminated Composite Sandwich Beams.* s.l. : AIAA J. 33 pp. 1911-1918, 1995.
17. **De Roeck, G., Peeters, B. and Maeck, J.** *Dynamic monitoring of civil engineering structures.* Chania, Crete, Greece : In: Computational Methods for Shell and Spatial Structures, IASS-IACM, 2000.
18. **Wang, Zhichun Yang and Le.** *Structural Damage Detection by Changes in Natural Frequencies.* s.l. : Journal of Intelligent Material Systems and Structures 21:309 , 2010.
19. **Hu, N, et al.** *Damage assessment of structures using modal test data.* s.l. : International Journal of Solids and Structures 38 3111-3126, 2001.
20. **Allemang, R.J.** *The Modal Assurance Critetion (MAC): twenty years of use and abuse.* Los Angeles, CA, U.S.A. : Proceedings of IMAC 20, the International Modal Analysis Conference, 397-405, 2002.
21. **Fox, C.H.J.** *The Location of Defects in Structures: A Comparison of use of Natural Frequency and Mode Shape Data.* s.l. : Proceeding of the International Modal Analysis Conference, 10(1), 522-528, 1992.
22. **Farrar, C.R. and Doebling, S.W.** *An Overview of Modal-Based Damage Identification Methods.* s.l. : Engineering Analysis Group, Los Alamos National Laboratory, Los Alamos, NM.

23. **Messina, A., Contursi, T. and Williams, E.J.** *Structural damage detection by a Sensitivity and Statistical-based method.* s.l. : Journal of Sound and Vibration, 216(5), 791-808, 1998.
24. **Araujo dos Santos, J.V., Soares, C.M.M. and Pina, H.L.G.** *A Damage Identification Numerical Model Based on the Sensitivity of Orthogonality Conditions and Least Squares Techniques.* s.l. : Computers and Structures, 78, 283-291, 2000.
25. **Khan, A.Z., Stanbridge, A.B. and Ewins, D.J.** *Detecting Damage in Vibrating Structures with a Scanning LDV.* s.l. : Optics and Lasers in Engineering, 32, 583-592.
26. **Waldron, K., et al.** *Damage Detection using Finite Element and Laser Operational Deflection Shapes.* s.l. : Finite Elements in Analysis and Design, 38(3), 193-226, 2002.
27. **De Roeck, D. and Wahab, M.M.A.** *Damage Detection in Bridges Using Modal Curvatures: Application to a Real Damage Scenario.* s.l. : Journal of Sound and Vibration, 266(2), 217-235, 1999.
28. **Wahab, M.M.A.** *Effect of Modal Curvatures on Damage Detection Using Model Updating.* s.l. : Mechanical Systems and Signal Processing, 15(2), 439-445, 2001.
29. **Yao, Zhang, Longqi Wang, Zhihai Xiang.** *Damage Detection by Mode Shape Squares from a Passing Vehicle.* s.l. : Journal of Sound and Vibration 331(2012)291–307, 2011.
30. **Hamey, Cole S., et al.** *Experimental Damage Identification of Carbon/Epoxy Composite Beams Using Curvature Mode Shapes.* s.l. : Structural Health Monitoring 2004 3: 333 , 2004.
31. **Cornwell, P., Doebling, S.W. and Farrar, C.R.** *Application of the Strain Energy Damage Detection Method to Plate-like Structures.* s.l. : Journal of Sound and Vibration, 224(2), 359-374, 1999.
32. **Stubbs, N. and Kim, J.T.** *Model-uncertainty Impact and Damage - Detection Accuracy in Plate Girder.* s.l. : Journal of Structural Engineering, 121(10), 1409-1417, 1995.
33. **Stubbs, N. and Kim, J.T.** *Improve Damage Identification Method Based on Modal Information.* s.l. : Journal of Sound and Vibration, 252(2), 223-238, 2002.
34. **Shi, Z.Y. and Law, S.S.** *Structural Damage Localization from Modal Strain Energy Change.* s.l. : Journal of Sound and Vibration v.218, n.5, pp. 825-844, 1998.

35. **Kiriakidis, A.C. and Chen, H.R.** . *Stiffness Evaluation and Damage Detection of Ceramic Candle Filters*. s.l. : Journal of Engineering Mechanics, 126(3), 308-319, 2000.
36. **Farhat, C. and Hemez, F.M.** *Updating finite element dynamic models using an element-by-element sensitivity methodology*. s.l. : AIAA Journal, 31(9), 1702–1711., 1993.
37. **Brown, G.W., Farhat, C. and Hemez, F.M.** *Extending sensitivity-based updating to lightly damped structures*. s.l. : AIAA Journal, 35(8), 1369–1377, 1997.
38. **Chen, H.P. ve Bicanics, N.** *Assessment of damage in continuum structures based on incomplete modal information*. s.l. : Computers and Structures, 74, 559-570, 2000.
39. **Jianhua, Zhao and Ling, Zhang.** *A method for structural damage identification using residual force vector and mode shape expansion*. s.l. : Multimedia Technology (ICMT), 2011 International Conference, 2011.
40. Wikipedia. [Online] [Cited: 4 December 2011.] http://en.wikipedia.org/wiki/Artificial_neural_network.
41. **Wu, X, Ghaboussi, J and Garrett, J.H.** *Use of Neural Networks in Detection of Structural Damage*. s.l. : Computers and Structures; 42(4):649–59, 1992.
42. **Bakhary, N., Hao, H. and Deeks, A.J.** *Damage detection using artificial neural network with consideration of uncertainties*. s.l. : Engineering Structures 29 (11), 2806–2815, 2007.
43. **Rosenblueth, E.** *Point estimates for probability moments*. s.l. : Proceedings of the National Academy of Science 72(10):3812–4, 1975.
44. **Yam, L.H., Yan, Y.J. and Jiang, J.S.** *Vibration-based damage detection for composite structures using wavelet transform and neural network identification*. s.l. : Composite Structures 60, 403–412, 2003.
45. **Marwala, T. and Hunt, H.E.M.** *Fault identification using finite element models and neural networks*. s.l. : Mechanical Systems and Signal Processing, 13(3), 475–490., 1999.
46. **Klugs, W.S. , Cummings, M.R. and Spencer, C.A.** *Concepts of Genetics*. s.l. : Pearson, Prentice Hall, 1983.

47. **Deb, K.** *Genetic Algorithms in Search and Optimisation: The Technique and Applications*. s.l. : Presented at the International Workshop on Soft Computing and Intelligent Systems, 1998.
48. **Miller, B. and Goldberg, D.** *Genetic Algorithms, tournament selection, and the affects of noise*. s.l. : Complex Systems, 9(3):193-212, 1995.
49. **Meruane, V. and Heylen, W.** *An hybrid real genetic algorithm to detect structural damage using modal properties*. s.l. : Mechanical Systems and Signal Processing (submitted after revision)., 2009.
50. **Michalewicz, Z.** *Genetic Algorithms + Data Structures = Evolution Programs*. s.l. : Springer-Verlag, 1994.
51. **Chou, J.H. and Ghaboussi, J.** *Genetic Algorithm in Structural Damage Detection*. s.l. : Computers & Structures 79(14) 1335-1353, 2001.
52. **Ostachowicz, W., Krawczuk, M. and Cartmell, M.** *The location of a concentrated mass on rectangular plates from measurements of natural vibrations*. s.l. : Computers and Structures, 80, 1419–1428, 2002.
53. **Blevins, R.D.** *Formulas for Natural Frequency and Mode Shape*. s.l. : Krieger Publishing Company, Melbourne, Florida., 1995.
54. **MSC.** *PATRAN 2008-r1 User's Guide*. s.l. : MSC, 2008.
55. MATLAB. [Online] MathWorks. [Cited: 24 January 2012.] <http://www.mathworks.com/>.
56. Optimization Toolbox. [Online] MathWorks. [Cited: 24 January 2012.] <http://www.mathworks.com/products/optimization/>.
57. **Huijian, Li, Changjun, He ve Xioaozhan, Yin.** *Structure damages detection based on genetic algorithm with experimental validation*. Piscataway NJ : Second International Conference on Innovative Computing, Information and Control ICICIC'07, pages 76–76, 5-7 September 2007.
58. Mathworks. [Online] [Cited: 30 December 2010.] <http://www.mathworks.com/help/toolbox/optim/ug/brnoxzl.html#brnpeek>.

59. *Mathworks.* [Online] [Cited: 30 December 2010.]
<http://www.mathworks.com/help/toolbox/optim/ug/brnoxzl.html#brnox01>.
60. *Mathworks.* [Online] [Cited: 30 December 2010.]
<http://www.mathworks.com/help/toolbox/optim/ug/brnoxzl.html#brnpd5f>.
61. *Mathworks.* [Online] [Cited: 30 December 2011.]
<http://www.mathworks.com/help/toolbox/optim/ug/brnoxzl.html#bsgppl4>.
62. *Wikipedia.* [Online] [Cited: 30 December 2011.]
http://en.wikipedia.org/wiki/Hessian_matrix.
63. *Mathworks.* [Online] [Cited: 30 December 2011.]
<http://www.mathworks.com/help/toolbox/optim/ug/bsapd3i.html#bsapedt>.
64. **Jiang, Lijun.** *Vibration-based Structural Damage Identification Enhancement via Piezoelectric Circuitry Network and Active Feedback Control.* s.l. : ProQuest, 2007.
65. **Cook, R. D., et al.** *Concept and Application of Finite Element Analysis.* New York : John Wiley and Sons Inc., 2002.
66. **MSC.** *MSC-Nastran-2004-Reference-Manual.* s.l. : MSC, 2004.
67. **Qiao, Pizhong, et al.** *Curvature mode shape-based damage detection in composite laminated plates.* s.l. : Composite Structures 80(3) 409-428, 2007.
68. **Park, N.G.** *Identification of Damage on a Substructure with Measured Frequency Response Functions.* s.l. : Journal of Mechanical Science and Technology 19(10) 1891-1901, 2005.
69. **Shi, Z.Y., Law, S.S. and Zhang, L.M.** *Damage localization by directly using incomplete mode shapes.* s.l. : Journal of Engineering Mechanics 126(11), 1173-1179, 2000.
70. **Lee, Y.S. and Chung, M.J.** *A Study on Crack Detection Using Eigenfrequency Test Data.* s.l. : Computers&Structures 77(3) 327-342, 2000.
71. **Yang, Q.W. and Liu, J.K.** *Structural Damage Identification Based on Residual Force Vector.* s.l. : Journal of Sound and Vibration, 305:298-307, 2007.

72. **Friswell, M.I., Penny, J.E.T. and Wilson, D.A.L.** *Using Vibration Data and statistical measures to locate damage in structure.* s.l. : Modal analysis: The international journal of analytical and experimental modal analysis, vol. 9, No. 4, pp. 239-254, 1994.

APPENDIX A

A.1. Genetic Algorithm (GA) Performance Trials for the Saw-cut Type Damage created on the 6th Element with 30% Severity

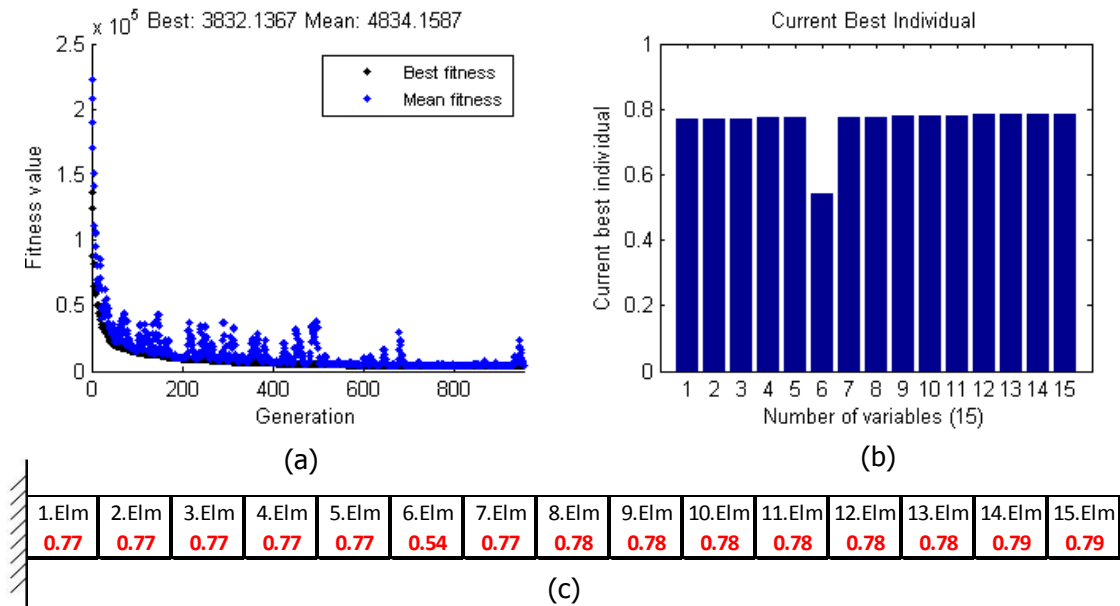


Figure A.1.1 GA results for 30% damage on the 6th element for Trial Run 1

(a) History of convergence (b) Identified damage location and severity

(c) Numerical result of identified state

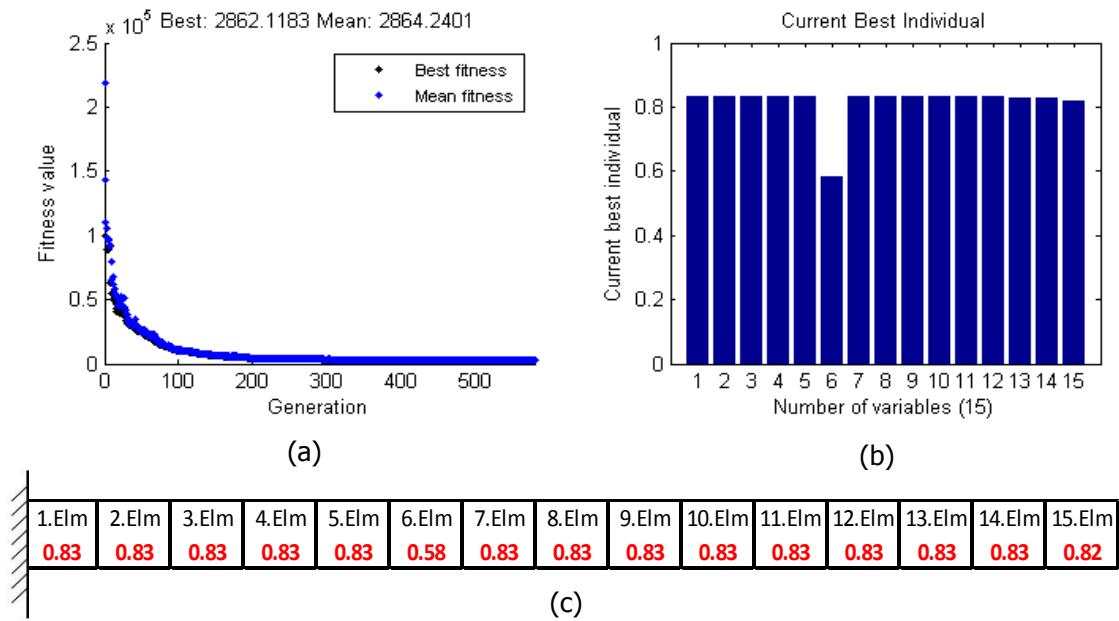


Figure A.1.2. GA results for 30% damage on the 6th element for Trial Run 2

(a) History of convergence (b) Identified damage location and severity

(c) Numerical result of identified state

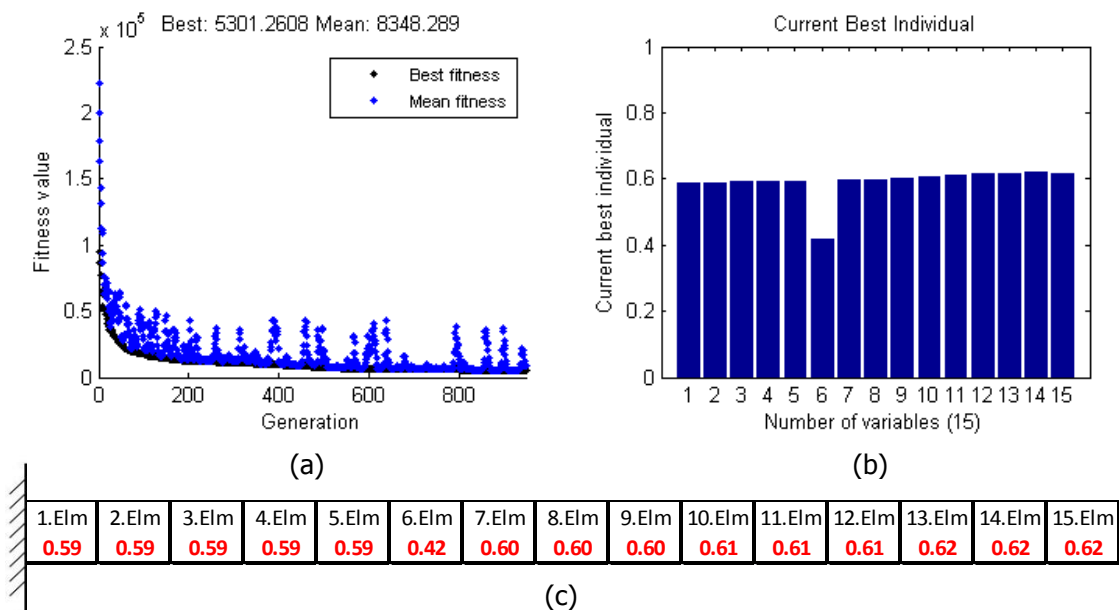


Figure A.1.3. GA results for 30% damage on the 6th element for Trial Run 3

(a) History of convergence (b) Identified damage location and severity

(c) Numerical result of identified state

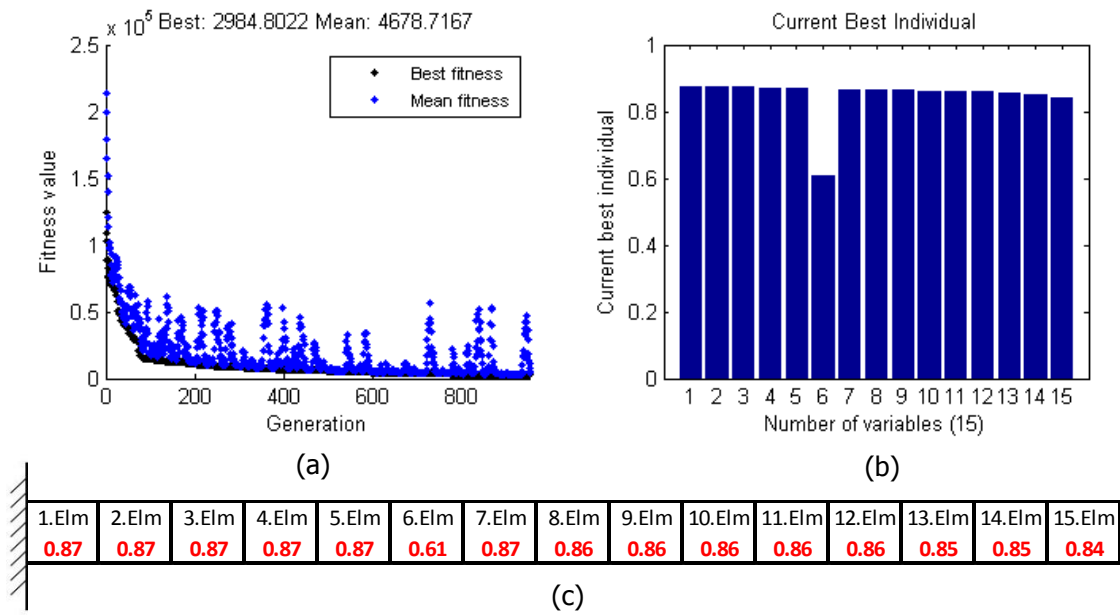


Figure A.1.4. GA results for 30% damage on the 6th element for Trial Run 4

(a) History of convergence (b) Identified damage location and severity

(c) Numerical result of identified state

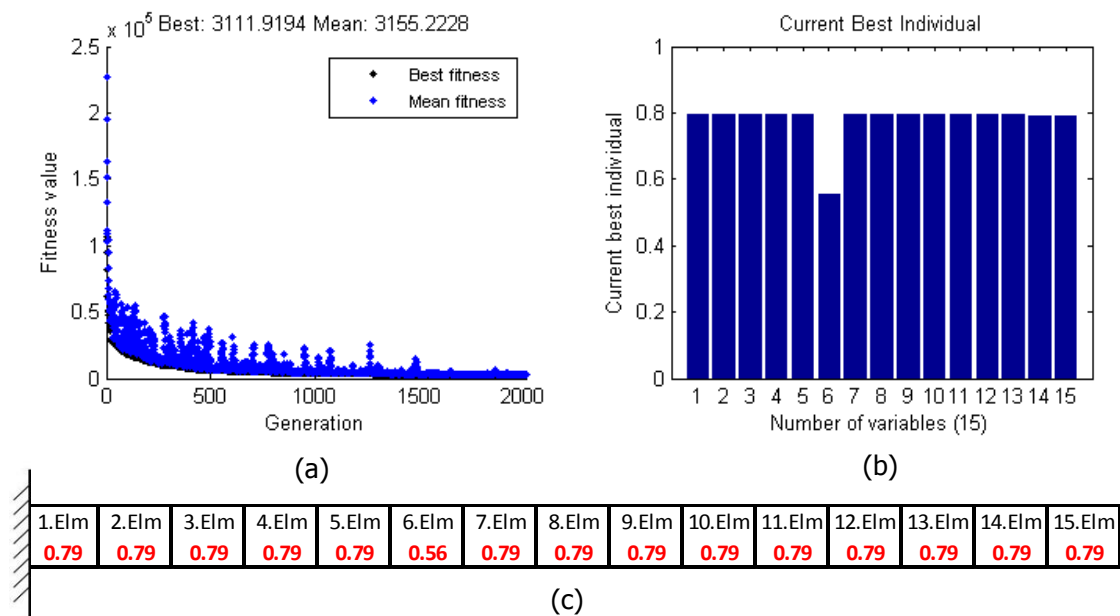


Figure A.1.5. GA results for 30% damage on the 6th element for Trial Run 5

(a) History of convergence (b) Identified damage location and severity

(c) Numerical result of identified state

A.2. FMINCON Performances for various initial guesses

A.2.1 FMINCON Performances for the cases having Initial Guesses from 0.4 to 0.8 by an increment of 0.1

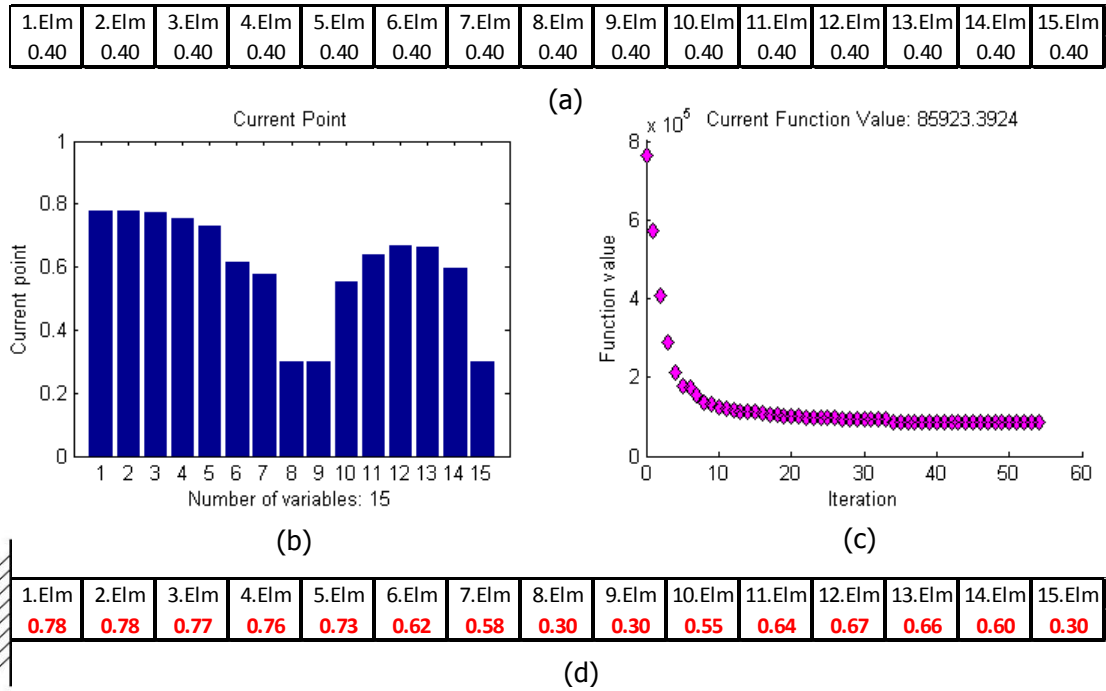


Figure A.2.1.1. FMINCON results for 10% damage on the 6th element (a) Initial guesses for the associated variable (b) Identified damage location and severity (c) History of Convergence (d) Numerical result of identified state

1.Elm	2.Elm	3.Elm	4.Elm	5.Elm	6.Elm	7.Elm	8.Elm	9.Elm	10.Elm	11.Elm	12.Elm	13.Elm	14.Elm	15.Elm
0.70	0.70	0.70	0.70	0.70	0.70	0.70	0.70	0.70	0.70	0.70	0.70	0.70	0.70	0.70

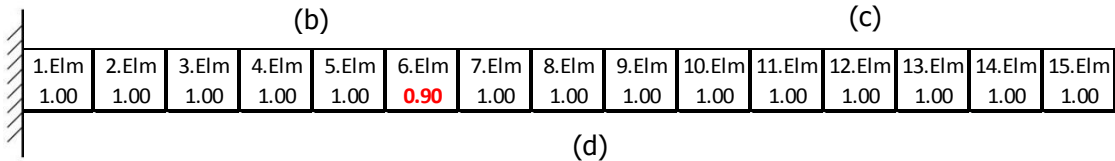
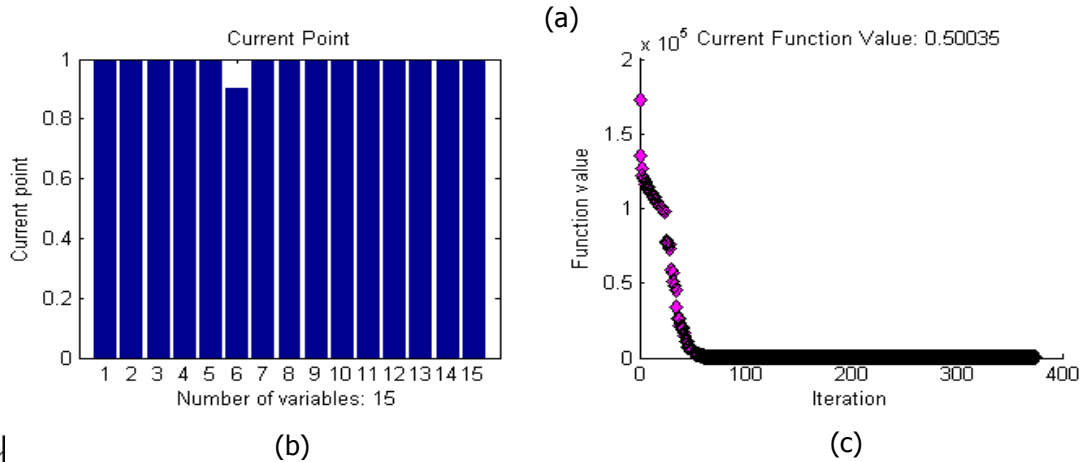


Figure A.2.1.4. FMINCON results for 10% damage on the 6th element (a) Initial guesses for the associated variable (b) Identified damage location and severity (c) History of Convergence (d) Numerical result of identified state

1.Elm	2.Elm	3.Elm	4.Elm	5.Elm	6.Elm	7.Elm	8.Elm	9.Elm	10.Elm	11.Elm	12.Elm	13.Elm	14.Elm	15.Elm
0.80	0.80	0.80	0.80	0.80	0.80	0.80	0.80	0.80	0.80	0.80	0.80	0.80	0.80	0.80

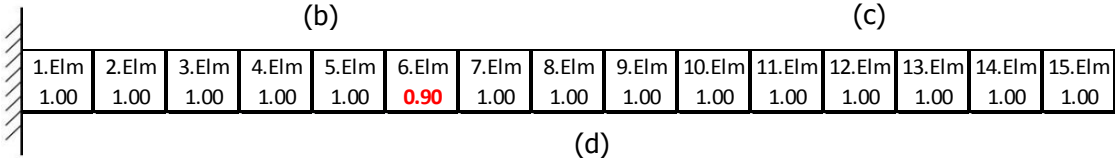
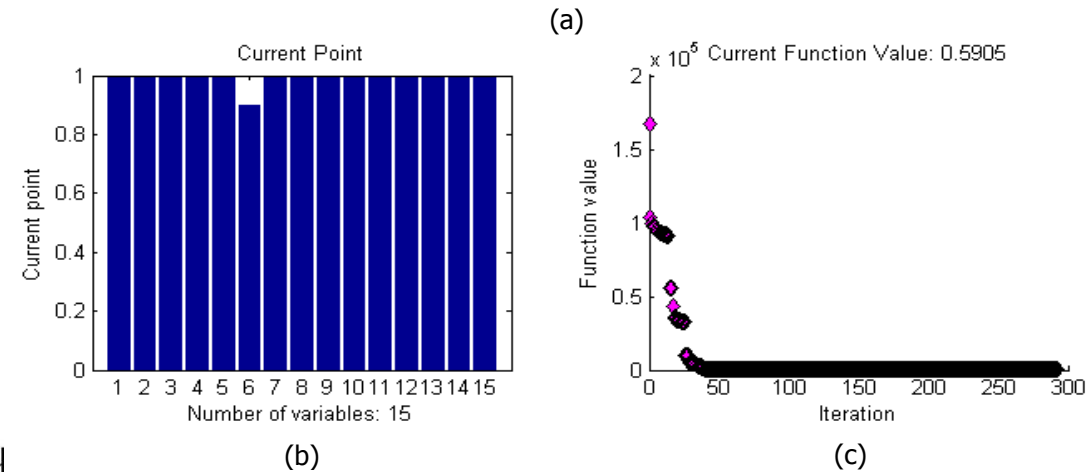


Figure A.2.1.5. FMINCON results for 10% damage on the 6th element (a) Initial guesses for the associated variable (b) Identified damage location and severity (c) History of Convergence (d) Numerical result of identified state

A.2.2 FMINCON Performances for the cases having Randomly Generated Initial Guesses between 0.3 and 1.0

1.Elm	2.Elm	3.Elm	4.Elm	5.Elm	6.Elm	7.Elm	8.Elm	9.Elm	10.Elm	11.Elm	12.Elm	13.Elm	14.Elm	15.Elm
0.39	0.96	0.97	0.70	0.34	0.46	0.55	0.87	0.31	0.33	0.42	0.75	0.81	0.75	0.62

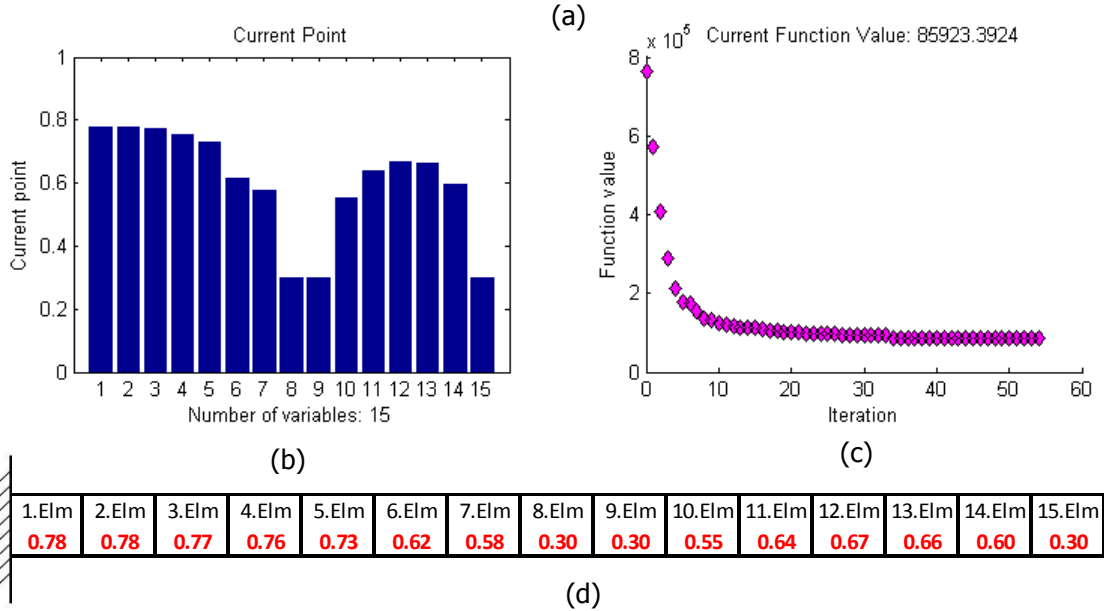
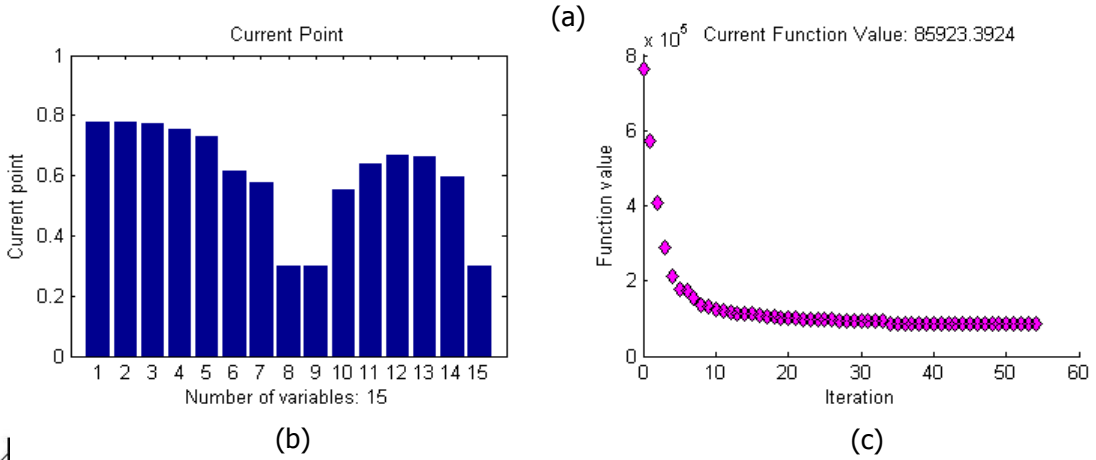


Figure A.2.2.1. FMINCON results for 10% damage on the 6th element (a) Initial guesses for the associated variable (b) Identified damage location and severity (c) History of Convergence (d) Numerical result of identified state

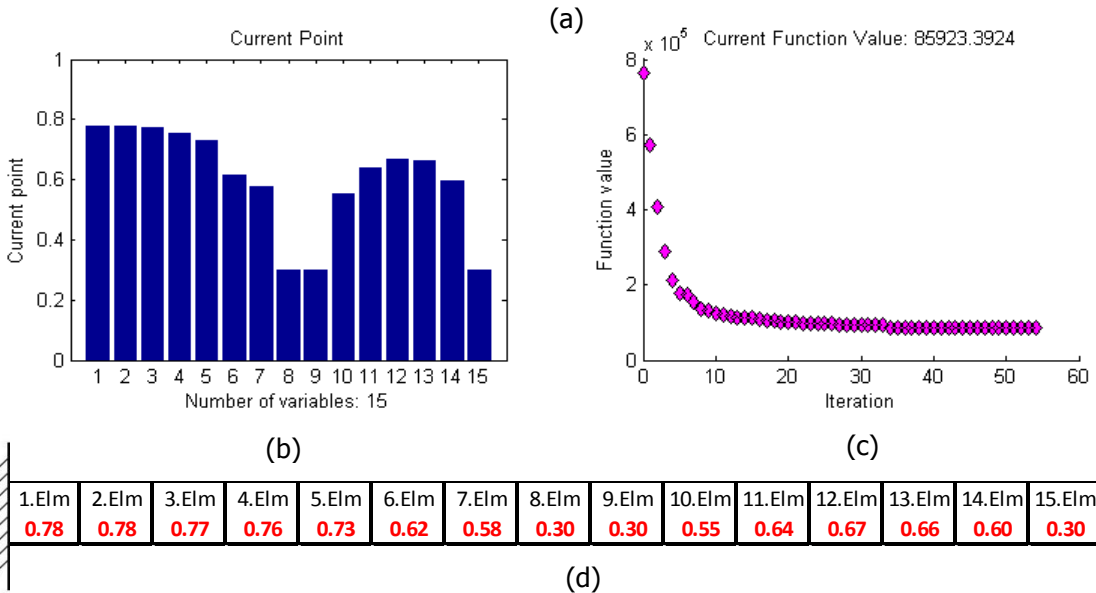
1.Elm	2.Elm	3.Elm	4.Elm	5.Elm	6.Elm	7.Elm	8.Elm	9.Elm	10.Elm	11.Elm	12.Elm	13.Elm	14.Elm	15.Elm
0.68	0.51	0.82	0.43	0.78	0.43	0.56	0.74	0.85	0.36	0.95	0.84	0.64	0.61	0.61



1.Elm	2.Elm	3.Elm	4.Elm	5.Elm	6.Elm	7.Elm	8.Elm	9.Elm	10.Elm	11.Elm	12.Elm	13.Elm	14.Elm	15.Elm
0.78	0.78	0.77	0.76	0.73	0.62	0.58	0.30	0.30	0.55	0.64	0.67	0.66	0.60	0.30

Figure A.2.2.2. FMINCON results for 10% damage on the 6th element (a) Initial guesses for the associated variable (b) Identified damage location and severity (c) History of Convergence (d) Numerical result of identified state

1.Elm	2.Elm	3.Elm	4.Elm	5.Elm	6.Elm	7.Elm	8.Elm	9.Elm	10.Elm	11.Elm	12.Elm	13.Elm	14.Elm	15.Elm
0.51	0.66	0.66	0.87	0.86	0.75	0.57	0.87	0.67	0.55	0.96	0.91	0.69	0.74	0.71



1.Elm	2.Elm	3.Elm	4.Elm	5.Elm	6.Elm	7.Elm	8.Elm	9.Elm	10.Elm	11.Elm	12.Elm	13.Elm	14.Elm	15.Elm
0.78	0.78	0.77	0.76	0.73	0.62	0.58	0.30	0.30	0.55	0.64	0.67	0.66	0.60	0.30

Figure A.2.2.3. FMINCON results for 10% damage on the 6th element (a) Initial guesses for the associated variable (b) Identified damage location and severity (c) History of Convergence (d) Numerical result of identified state

1.Elm	2.Elm	3.Elm	4.Elm	5.Elm	6.Elm	7.Elm	8.Elm	9.Elm	10.Elm	11.Elm	12.Elm	13.Elm	14.Elm	15.Elm
0.45	0.51	0.63	0.46	0.89	0.44	0.46	0.42	0.46	0.60	0.52	0.95	0.60	0.43	0.93

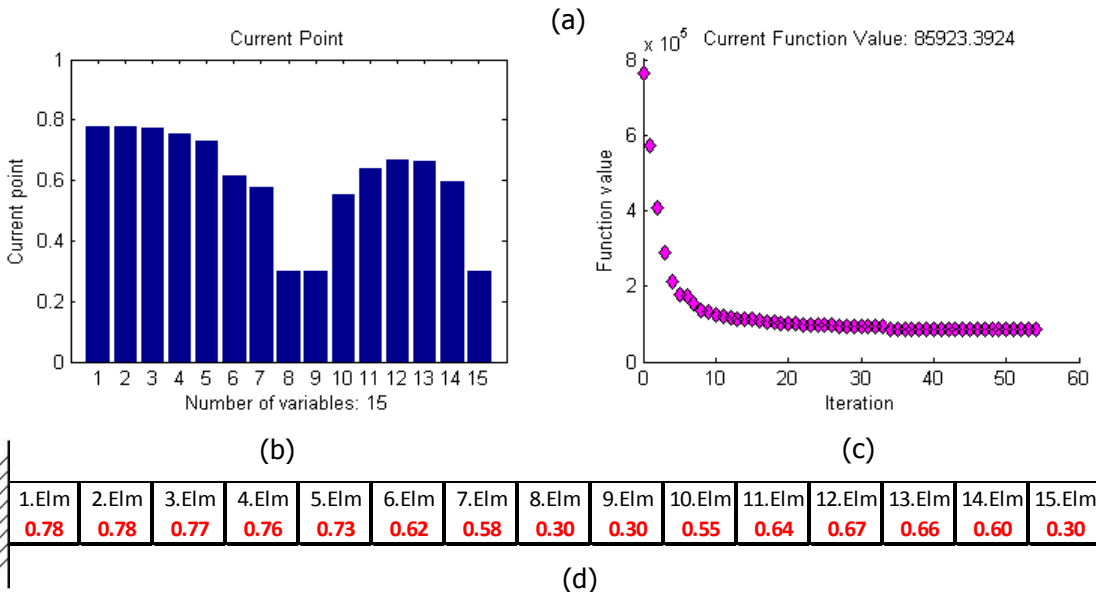


Figure A.2.2.4. FMINCON results for 10% damage on the 6th element (a) Initial guesses for the associated variable (b) Identified damage location and severity (c) History of Convergence (d) Numerical result of identified state

1.Elm	2.Elm	3.Elm	4.Elm	5.Elm	6.Elm	7.Elm	8.Elm	9.Elm	10.Elm	11.Elm	12.Elm	13.Elm	14.Elm	15.Elm
0.99	0.61	0.38	0.48	0.59	0.72	0.48	0.72	0.80	0.46	0.38	0.51	0.52	0.60	0.66

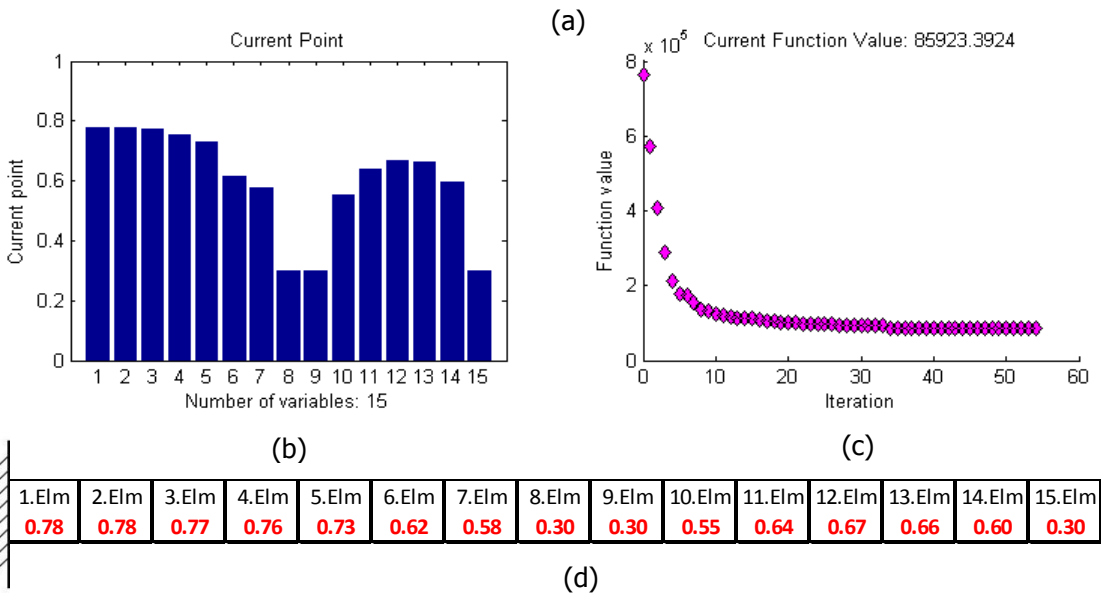


Figure A.2.2.5. FMINCON results for 10% damage on the 6th element (a) Initial guesses for the associated variable (b) Identified damage location and severity (c) History of Convergence (d) Numerical result of identified state